Die approbierte Originalversion dieser Diplom-/Masterarbeit ist in der Hauptbibliothek der Technischen Universität Wien aufgestellt und zugänglich.
http://www.ub.tuwien.ac.at

The approved original version of this diploma or master thesis is available at the main library of the Vienna University of Technology.
http://www.ub.tuwien.ac.at/eng

Diplomarbeit

Control Based Analysis of a Gas Dosing System for Stationary Gas Engines

Regelungstechnische Untersuchung eines Gasdosiersystems für stationäre Gasmotoren

ausgeführt zum Zwecke der Erlangung des akademischen Grades eines Diplom-Ingenieurs
unter der Leitung von

Univ.Prof. Dr.techn. Stefan Jakubek
Institut für Mechanik und Mechatronik
E325 A5

eingereicht an der Technischen Universität Wien

Fakultät für Maschinenwesen und Betriebswissenschaften

von

Johannes Unger
Matr.Nr.: 0526365
Sonnwendgasse 34/32
1100 Wien

Wien, am 26. Jänner 2011

Johannes Unger

Eidesstattliche Erklärung

Ich erkläre an Eides statt, dass ich meine Diplomarbeit nach den anerkannten Grundsätzen für wissenschaftliche Abhandlungen selbständig ausgeführt habe und alle verwendeten Hilfsmittel, insbesondere die zugrunde gelegte Literatur genannt habe.

Weiters erkläre ich, dass ich dieses Diplomarbeitsthema bisher weder im In- noch im Ausland (einer Beurteilerin / einem Beurteiler zur Begutachtung) in irgendeiner Form als Prüfungsarbeit vorgelegt habe und dass diese Arbeit mit der vom Begutachter beurteilten Arbeit übereinstimmt.

Statement of Affirmation

Herewith I affirm that I have written this thesis on my own. I did not enlist unlawful assistance of someone else. Cited sources of literature are perceptibly marked and listed at the end of this thesis. The work was not submitted previously in same or similar form to another examination committee and was not yet published.

Wien, am 26. Jänner 2011

Johannes Unger

Acknowledgements

I want to thank my parents, Walter and Mathilde Unger, who enabled my studies at the Vienna University of Technology and my brother Lukas Unger, who supported me in the correction of this work.

I want to thank Prof. Dr. Stefan Jakubek and Dr. Peter Dolovai for the offer to work on this project and for the outstanding support, which made it possible to finish the work in such a short time period.

Furthermore I want to thank Prof. Dr. Andreas Werner, who was secondary reader of this work.

Johannes Unger

Kurzfassung

Abgasemissionen bei Verbrennungsmotoren spielen heute eine immer bedeutendere Rolle. Um den Anforderungen der ständig sinkenden Emissionsgrenzen gerecht zu werden, benötigt man innovative Systeme, die eine möglichst genaue und schnelle Einhaltung der geforderten Emissionsgrenzen möglich machen. In dieser Arbeit soll für einen stationären Großgasmotor ein aktives Gasmischsystem entwickelt und die regelungstechnischen Möglichkeiten untersucht werden. Im Zuge der Literaturrecherchen wurde das Gasdosiersystem auf die einfachen Komponenten eines Venturi-Mischers und einer Drosselklappe für die Manipulation des Gasmassenstromes festgelegt und diese modelliert. Bei der Modellierung stellen insbesondere die impliziten Modellgleichungen, sowie die algebraischen Schleifen eine Herausforderung dar. Bei der regelungstechnischen Untersuchung wurde zwischen Reglern mit und ohne Lambda-Wert Rückführung unterschieden. Es wird gezeigt, dass auch einfachere Regelalgorithmen durchaus nennenswerte Ergebnisse liefern können. Da es sich bei dieser Arbeit um eine rein theoretische Untersuchung handelt, konnten die Ergebnisse nicht an einem Versuchsstand validiert werden.

Abstract

Today, the topic of exhaust emissions of combustion engines plays a significant role. In order to fulfill standards of emission limits, innovative systems, which are able to comply with restrictions in a fast and robust way, are needed. In this work an active gas dosing system for a stationary gas engine is developed and different control strategies are analyzed, in order to show the different possibilities of the control of such systems. The literature survey showed that a venturi mixer and a butterfly valve for the manipulation of the gas mass flow meet the specifications. Therefore they are chosen to be the main parts of the gas dosing system. Problems with the modeling of the parts of the gas dosing system, especially implicit equations as well as algebraic loops, had to be solved. The control based investigation is subdivided into controllers with and without lambda-value feedback. It is shown that also the simple approaches to the control strategies can have appreciable results. Since this work is only theoretical, the results could not be validated on a test bench.

Contents

1 Introduction **1**

1.1 Motivation 1

1.2 Purpose of this Work 2

1.3 Literature Survey 2

1.3.1 Gas Dosing Systems 2

1.3.2 Flow Measurement 3

1.3.3 Gas Quality Measurement 4

1.3.4 Gas Mixing 4

1.3.5 Control of Butterfly Valves 6

1.3.6 Control 6

1.3.7 Bi-Fuel Systems 7

1.3.8 Conclusion of the Literature Survey 7

2 General Equations and Fluid Characteristics **9**

2.1 First Law of Thermodynamics 9

2.2 Equation of Continuity 9

2.3 Ideal Gas Equation 10

2.4 Isentropic State Change 11

2.5 Static and Total State Variables 11

2.6 Mass Flow Rate 12

2.7 Mach Number 12

2.8 Air and Gas Characteristics 13

2.8.1 Air Characteristics 13

2.8.2 Natural Gas Characteristics 14
2.8.3 Biogas Characteristics 14
2.9 Stoichiometric Combustion 15
2.10 Assumptions and General Guidelines 16

3 Model of the Gas Dosing System 17

3.1 Overview of the Gas Dosing System Model 17
3.2 Venturi Mixer Geometry 19
3.3 Air Filter 20
3.4 Butterfly Valve 21
3.5 Air, Gas and Mixture Reservoir 25
3.6 Venturi Mixer 26
3.6.1 Mixture Mass Flow Across Venturi Mixer 28
3.6.2 Throat Pressure 30
3.6.3 Gas Mass Flow Across Annular Passage 35
3.6.4 Concentration Vector 35
3.6.5 Mixture Temperature 37
3.6.6 Mixture Characteristics 37
3.7 Engine Model 39
3.8 Engine Dead Time 40
3.9 Matlab Implementation 42

4 Control Strategies of the Gas Dosing System 44

4.1 Linearization 44
4.2 Model Reduction 45
4.3 Controller Implementation 46
4.4 Gain-Scheduling 46
4.5 Feedforward Controller 48
4.6 Calorific Value and Stoichiometric Air Requirement 48
4.7 Controller 49

4.7.1 Performance Reference - Static Venturi Mixer 49
4.7.2 Ratio Control Strategy 49
4.7.3 Mass Flow Control Strategy 50
4.7.4 Smith Predictor Control Strategy 51
4.7.5 Cascade Control Strategy 52
4.7.6 Combined Control Strategy 53
4.7.7 More Combinations of Control Strategies 54

5 Results and Performance 55

5.1 Limits of the System 55
5.2 Result and Performance at a Load Change 56
5.3 Result and Performance at a Supply Pipe Pressure Disturbance 61
5.4 Result and Performance at a Supply Pipe Temperature Disturbance 65
5.5 Result and Performance at a Calorific Value Disturbance 70
5.6 Influence of the Linearized Engine Model on the Controller 75
5.7 Influence of the Speed Controller on the Controller 77
5.8 Result and Performance at a Lambda Set Point Change 78

6 Conclusion and Suggestions for Future Work 82

A Nomenclature 89

B Simulink Model 97

List of Figures

1.1 Gas Carburetor Designs 5

(a) Gas Carburetor from [36] 5

(b) Gas Carburetor from [40] 5

2.1 Principle Layout for the Definition of the First Law of Thermodynamics [55] 10

2.2 Flow Rate Function $\beta(\Pi)$ 13

3.1 Overview of the Model and Causal Relation of the Components 17

3.2 Venturi Mixer Geometry 19

3.3 Scheme of the Air-Filter Block 20

3.4 Flow Cross Sectional Area Across the Shaft Angle 22

3.5 Stepper Motor Transfer Function 23

3.6 Scheme of the Butterfly Valve Block 24

3.7 Scheme of the Reservoir Model 26

3.8 Scheme of the Venturi Mixer 27

3.9 Overview of the Venturi Mixer Model 27

3.10 Scheme of the Mixture Mass Flow Block 28

3.11 Scheme of the Throat Pressure Model 30

3.12 Scheme of the System Border of the Energy Equation 31

3.13 Influence of the Throat Pressure p_m on the Energy Equation Error Output by Varying p_m from 0.9 to 1.1bar 34

3.14 Absolute Value Difference of the Iteration and the Exact Solved Value . . . 34

3.15 Scheme of the Gas Mass Flow Into the Venturi Mixer Block 35

3.16 Scheme of the Concentration Vector Block 36

3.17 Scheme of the Mixture Temperature Block 37

3.18 Scheme of the Mixture Characteristics Block 37

3.19 Scheme of the Engine Model 40

4.1 Scheme of the Controller Implementation 46

4.2 Principle of Ratio Control 50

4.3 Scheme of the Ratio Controller 50

4.4 Scheme of the Mass Flow Controller 51

4.5 Scheme of the Smith Predictor Controller 52

4.6 Scheme of the Cascade Controller 52

4.7 Scheme of the Combined Controller 54

5.1 Result of a Load Change from $300kW$ to $360kW$ 56

5.2 Result of a Load Rejection from $360kW$ to $300kW$ 58

5.3 Result of a Load Change from $540kW$ to $600kW$ 59

5.4 Result of a Load Rejection from $600kW$ to $540kW$ 60

5.5 Result of a Pressure Disturbance of $\Delta p_{G0} = 50mbar$ at a Load of $P_{el} = 300kW$ 62

5.6 Result of a Pressure Disturbance of $\Delta p_{G0} = -50mbar$ at a Load of $P_{el} = 300kW$ 63

5.7 Result of a Pressure Disturbance of $\Delta p_{G0} = 50mbar$ at a Load of $P_{el} = 600kW$ 64

5.8 Result of a Pressure Disturbance of $\Delta p_{G0} = -50mbar$ at a Load of $P_{el} = 600kW$ 64

5.9 Result of a Temperature Disturbance of $\Delta T_{G0} = 60K$ at a Load of $P_{el} = 300kW$ 66

5.10 Result of a Temperature Disturbance of $\Delta T_{G0} = -40K$ at a Load of $P_{el} = 300kW$ 67

5.11 Result of a Temperature Disturbance of $\Delta T_{G0} = 60K$ at a Load of $P_{el} = 600kW$ 68

5.12 Result of a Temperature Disturbance of $\Delta T_{G0} = -40K$ at a Load of $P_{el} = 600kW$ 69

5.13 Result of a Calorific Value Disturbance of $\Delta H_i = 8MJ/kg$ at a Load of $P_{el} = 300kW$ 70

5.14 Result of a Calorific Value Disturbance of $\Delta H_i = -8MJ/kg$ at a Load of $P_{el} = 300kW$ 72

5.15 Result of a Calorific Value Disturbance of $\Delta H_i = 8MJ/kg$ at a Load of $P_{el} = 600kW$ 73

5.16 Result of a Calorific Value Disturbance of $\Delta H_i = -8MJ/kg$ at a Load of $P_{el} = 600kW$ 74

5.17 Influence of the Linearized Engine Model at a Load Change from $300kW$ to $360kW$ 76

5.18 Influence of the Linearized Engine Model at a Load Change from $540kW$ to $600kW$ 76

5.19 Speed Controller Influence of a Load Rejection at the Higher Load Level . . 77

5.20 Result of a Lambda Set Point Change from 1.7 to 1.5 at a Load of $P_{el} = 300kW$ 78

5.21 Result of a Lambda Set Point Change from 1.7 to 1.9 at a Load of $P_{el} = 300kW$ 79

5.22 Result of a Lambda Set Point Change from 1.7 to 1.5 at a Load of $P_{el} = 600kW$ 80

5.23 Result of a Lambda Set Point Change from 1.7 to 1.9 at a Load of $P_{el} = 600kW$ 81

B.1 Simulink Model Overview - Part 1 98

B.2 Simulink Model Overview - Part 2 99

B.3 Simulink Model Overview - Part 3 100

B.4 Simulink Model Overview - Part 4 101

B.5 Gas Dosing System Model Block - Part 1 102

B.6 Gas Dosing System Model Block - Part 2 103

B.7 Venturi Mixer Simulink Model Block 104

List of Tables

2.1 Universal Constants 13

2.2 Air Characteristics 14

2.3 Natural Gas Characteristics 14

2.4 Biogas Characteristics 15

2.5 Assumptions and General Guidelines 16

3.1 Geometry Values of the Venturi Mixer 19

3.2 Air Filter Values 21

3.3 Stepper Motor Values 22

3.4 Butterfly Valve Values 24

3.5 Reservoir Values 25

3.6 Sequence of the Calculations of the Venturi Mixer Submodels 28

3.7 Mixture Mass Flow Across Venturi Mixer Values 30

3.8 Throat Pressure Values 33

3.9 Gas Mass Flow Across Annular Passage Values 36

3.10 Concentration Vector Values 38

3.11 Mixture Temperature Values 38

3.12 Mixture Characteristics Values 38

3.13 Engine Values 41

4.1 Options used for the Linearization 45

4.2 Linearization Combinations 45

4.3 Controller Structures used in the Combined Control Strategy 54

Chapter 1

Introduction

In this chapter an introduction is given. Section 1.1 gives a short overview of the problem, section 1.2 defines the purposes of this work and section 1.3 summarizes the result of the literature survey.

1.1 Motivation

A stationary gas engine is an easy and uncomplicated way to generate electrical and thermal energy from the raw material gas (e.g. natural gas or biogas). Its emissions are partly lower than those of the liquid fuels and the storage of the gas is not needed due to local gas grids. Because of the liberalization of the gas market, the gas quality as well as the pressure in the gas grid is more subject to change than in the past.

Conventionally, static gas dosing systems are used for gas engines. These systems are normally based on the venturi effect and the air/fuel-ratio (AFR) is defined by the geometry of the mixer. The pressure difference between the throat of the venturi and the gas pipe must be regulated by a zero pressure regulator, which in general is expensive due to the small pressure tolerances which are accepted. Disturbances in the gas grid therefore have a very adverse influence on static gas dosing systems, because the steady state value of the AFR will be different to the adjusted AFR. This circumstance will lead to a different steady state lambda value in operation and therefore to higher emissions.

Also the increasingly restrictive regulations on emission limits increase the relevance of active gas dosing systems for gas engines. Such modern gas dosing systems should be able to compensate changing operation conditions such as changes in load and rotational speed as well as changes in the gas quality and other disturbances in the gas grid. Another requirement on modern gas dosing systems is to generate different air-fuel ratios for different operation points like starting, idling, partial load and full load. In general, static venturi-based systems are not suitable for such purposes.

1.2 Purpose of this Work

The purpose of this work is to develop a strategy for fulfilling the increasing requirements on the air path system of a gas engine by an active gas dosing system. A theoretical model of an active gas dosing system is developed and different control strategies are designed in order to find out which maximum performance can be reached and at which point the general limit of such systems is to be found. The control system should be able to compensate pressure and temperature fluctuations as well as calorific value differences in the gas grid. Finally the different control strategies should be compared with each other.

1.3 Literature Survey

The aim of this literature survey is to get an overview of gas dosing systems and gas mixing strategies that are currently in use, because the field of active gas dosing systems for gas engines is not very developed yet. Furthermore, ideas about the model and which control strategy is qualified for active gas dosing systems should emanate from this survey.

In section 1.3.1, the implemented active gas dosing systems on the market are summarized and described. The following sections look closely at the parts used in the systems. Section 1.3.2 gives an overview of possible techniques of flow measurements, section 1.3.3 deals with the problem of gas quality measurements, section 1.3.4 summarizes alternative gas mixing devices for this application, section 1.3.5 describes the control of butterfly valves and section 1.3.6 summarizes the used control strategies for AFR control. In order to give an idea of advanced possibilities of an active gas dosing system, section 1.3.7 describes Bi-Fuel Systems. The conclusion of the literature survey is then given in section 1.3.8.

1.3.1 Gas Dosing Systems

Active gas dosing systems are available from different suppliers/manufacturers. All these systems differ a little from each other. Heinzmann[1] offers a gas dosing system which is able to control the AFR using a butterfly valve and a venturi mixer [5]. The system is able to switch between a lambda control with an external set point and an integrated lambda control with a characteristic diagram which targets the lambda value, rotational speed and load of the engine. The system uses pressure and temperature sensors at the entries and pressure sensors at the outlet of the system in order to increase performance. The range of the pressure disturbance, which can be compensated, is specified at $200mbar$. Continental Controls[2] offers a gas dosing system [17] which uses a poppet valve instead of a butterfly valve. The control strategy is based on two feedforward control loops. The first control loop controls the gap of the poppet valve and the second one controls the pressure in the gas

[1] Heinzmann GMBH&CoKG, http://www.heinzmann.com/
[2] Continental Controls Corporation, http://www.continentalcontrols.com/

pipe. The calculation of the set point pressure for the second control loop is based on the measurement of the oxygen ratio in the exhaust. Gill[3] offers a standalone control system [4], which uses a proportional-integral controller (PI-controller) for the lambda control. Additional, an actuating element can be ordered from this company. The input values are the position of the throttle of the engine or the signal of a manifold temperature sensor (MAT sensor) as well as a universal exhaust gas oxygen sensor (UEGO sensor) signal. The last company mentioned is Altronic[4]. This company was taken over by Hoerbiger[5] in 2009. Altronic offers a control system for stoichiometric as well as lean-burn carbureted engines [3], which is based on a closed loop system with a feedback of an oxygen sensor. The control variable is therefore the oxygen ratio in the exhaust. The gas dosing valve in this gas dosing system can be a butterfly valve or a plunger-style valve.

1.3.2 Flow Measurement

The knowledge of the mass flows across the gas dosing system is important for the accuracy of a gas dosing system. Conventional gas dosing systems like the one from Heinzmann [5] calculate the mass flows based on the pressure difference across butterfly valve and venturi mixer. This calculation is very close to the real value if the mass flow is within a specified range. Outside this range, e.g. at very high or low mass flows, the error is not negligible any more, which restricts the range of operation for the gas dosing system. Therefore, active mass flow measurements can increase the accuracy with the disadvantage of higher costs for the gas dosing system. In the following section, three measurement methods and one patent are mentioned which are different from the conventional measurement systems.

The first measurement method is based on the reflection of particles in the mass flow [48]. In detail, two parallel laser beams are aligned in a row in the flow direction. When a particle hits the first laser beam, the laser beam is reflected by the particle and the reflection is detected by a detector. This detector sends an output signal to the electronics of the sensor. When the same particle hits the second laser beam and is detected by the second detector, the electronics can calculate the flow velocity because of the time delay between the two detections. In the calculation, filter algorithms are implemented in order to filter all half detected particles or other disturbances. The measurement can therefore be seen as correct. An advantage of this measurement method is that magnetic disturbances from the ambiance have no effect on the output.

The second measurement method is based on ultra sonic [47]. The time delay of the echo between transducer and detector is proportional to the mass flow of the fluid. This measurement method is already well developed. The third and cheapest method of mass flow measurement is the hot wire measurement method [56]. This method is also already

[3] Gill Instruments Ltd., http://www.gill.co.uk/
[4] Altronic Inc., http://www.altronicinc.com/
[5] Hoerbiger Holding AG, http://www.hoerbiger.com/

well-developed and is used in the mass flow measurement into the cylinder of an engine. The patented measurement method [49] measures the dynamic torque of the plate of a butterfly valve. By identifying the correlation between the mass flow across the valve and the dynamic torque considering the aperture of the valve, the mass flow can be measured by measuring the dynamic torque.

Elster Instromet[6] offers an ultrasonic sensor which can be used for gas dosing systems [14].

1.3.3 Gas Quality Measurement

A gas-phase chromatograph is used to measure the gas quality, e.g. Methane mass fraction of natural gas, but it is very expensive and has a long cycle time and is thus not suitable for the control of gas dosing systems. Therefore, cheaper and faster devices are in development. At this point three methods, which could reach mass production status in the foreseeable future or are already available, should be mentioned. One method is to measure the gas quality with a microchip sensor, which is based on the thermal conductivity of a fluid [42, 43]. The second method is an infrared-based method [19]. Gases own the property to absorb a special range of wavelengths from the light. The third method is based on the speed of sound of the gas [52]. The speed of sound depends on the molecular weight of the gas, which can be used to identify the gas quality by measuring the speed of sound of the gas.

A combination of the three above-mentioned methods is used in the prototype Gas-Lab-Q1 [41]. Besides the Methane mass fraction this prototype also measures the calorific value and other characteristic values of a gas. Other sensors are offered by ABB[7] [7], Trolex[8] [11], Elster Instroment [9], Bluesens[9] [8] and GfG[10] [10]. The disadvantage of some of these sensors is that a reference gas is needed. The typical response time is between $10 - 15sec$ and $2 - 3min$.

1.3.4 Gas Mixing

The conventional way of gas mixing in the application of gas dosing systems is to use static venturi based systems. As described before, this has different disadvantages. In order to avoid these disadvantages, the search for new design approaches would have been the main point of this part of the literature survey. But in fact, no new technologies could be found which are useful and innovative enough to be used for this development of a gas dosing system. In the following there are different publications related to the topic. Each publication has at least one fact which can be used as lead or inspiration for the design of

[6] Elster-Instromet GmbH, http://www.elster-instromet.com/
[7] ABB Automation GmbH, http://www.abb.com/
[8] Trolex Ltd, http://www.trolex.com/
[9] Bluesens Gas Sensors GmbH, http://www.bluesens.com/
[10] GfG Gesellschaft für Gerätebau mbH, http://www.gasmessung.de/

a gas dosing system.

[37] investigates the discharge coefficient of a venturi mixer by computational fluid dynamics (CFD) analysis. The venturi mixer model is related to small engine carburetors whose fuel inlet is constructed as a fuel tube in the throat. The model is described very well. For the calculation of the mass flow across the venturi, the mass flow equation (see equation (2.11)) is used and corrected by experimentally determined coefficients. An important information is that stationary conditions were assumed in the simulation. The conclusion which can be reached for the application of gas dosing systems is that a dynamic model of the venturi mixer is not necessary if the mass flow is corrected. In the case of a multiple-gas gas dosing system, which means a series of venturi mixers, the assumption of ideal gases can be violated and non-ideal gas equations must be used. A mathematical formulation of a venturi used for non ideal gas is given in [38].

An venturi mixer that is already available is the Continental Controls VM-350 [6], which has the feature of a butterfly plate right in front of the gas inlet into the throat in order to damp dynamics in the gas pressure. The basic idea is to be able to calibrate the venturi mixers in case of a dual bank engine. RMG[11] offers static venturi mixers [15] as well as venturi mixers with variable annular passage [16], which is moved by an electrical actor. [39] patented a venturi mixer with variable annular passage as well as variable zeppelin (middle venturi part). [36] and [40] present alternative gas mixer designs which can be used in general for low calorific value gases. Figure 1.1 shows the designs of these systems.

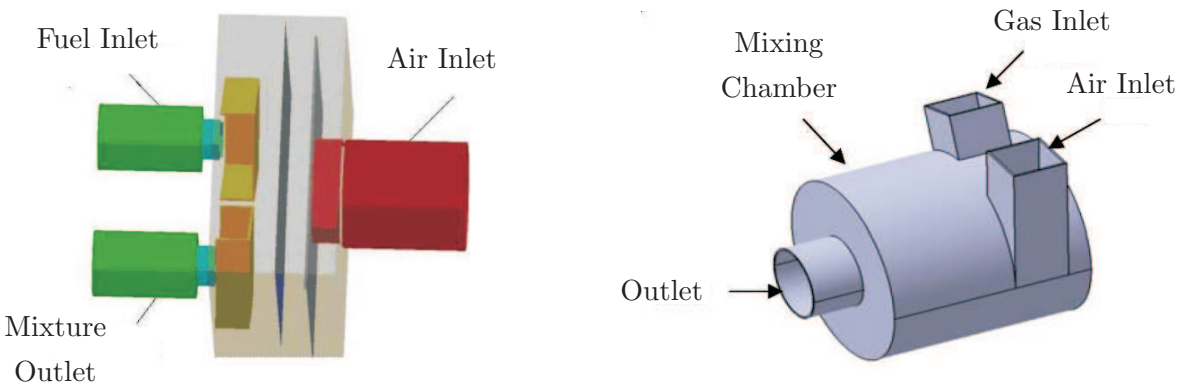

(a) Gas Carburetor from [36]

(b) Gas Carburetor from [40]

Figure 1.1: Gas Carburetor Designs

It can be concluded that for a control based analysis of a gas dosing system, the general equations given in the literature are satisfactory. Good sources are [21, 22, 23, 24, 50, 54, 55].

[11] RMG Regel + Messtechnik GmbH, http://www.rmg.de/

1.3.5 Control of Butterfly Valves

Each active gas dosing system needs an actor in order to react to disturbances as well as to changes in the operation point. In this section, alternatives to the conventionally used butterfly valves should be investigated. Butterfly valves in general are cheap and the aperture can open/close very fast. These properties make the butterfly valve a very interesting component for gas dosing systems. There are no good reasons to replace them by advanced systems. In the following part, publications about the control and the problems of the control of butterfly valves are mentioned. The master thesis [45] deals with the problem of the control of a butterfly valve used as a throttle valve for a Volvo car engine. The butterfly valve is modeled as a linear system, but non-linearities such as dead-zone, spring packages and friction are compensated with an identified model of those non-linearities. The controller is designed in the State-Space (SS) representation as a Gain-Scheduling controller, which uses a State-Observer (SO). [46] investigates the model-based position control of a butterfly valve. The base of the control loop synthesis is a mathematical model which results from an analytical approach, whose parameters are identified by parameter identification. A PI-controller is finally used, which, compared to a PIDT1-structure, has better performance. [44] demonstrates how a control strategy can compensate the delay of an actor of a butterfly valve in order to increase the reaction time of the engine. A side result is that the intake manifold pressure and the torque of the engine are proportional. Equations for the mass flow across as well as for the design of different valve types are mentioned in [13] and [12].

1.3.6 Control

The aim of this section is to get an overview of implemented control strategies in the field of gas dosing systems as well as AFR control. In the field of gas engines, the number of publications is very small. No publication deals with the topic under investigation, with the exception of one patent. Most publications about AFR control are about diesel engines. In the following, the patent is mentioned, followed by different publications which partly fit with the investigation of AFR control of lean burn stationary gas engines. The patent [28] includes a characteristic diagram of the pressure difference across the venturi mixer, depending on the operation point of the engine. This pressure difference is the set point for the engine control system. The engine control system tries to reach the set point pressure difference by opening/closing the aperture of the gas dosing valve. Therefore, the pressure difference across the venturi mixer is the control variable. [31] presents an AFR control system for a gasoline lean burn engine. The controller used is a linear parameter varying (LPV) gain scheduling controller, whose switching criteria is the variable dead time of the system. The dead time is therefore discussed in more detail. The manipulated variable is the fuel mass flow and the control variable is the AFR. [30] investigates the influence of an aging oxygen sensor on the AFR control system. An internal model controller structure

is used, whose internal model is corrected by an adaptive law. An output error model structure is used as the base for the adaptive algorithm. The patent [29] describes a mass flow control system using a cylindrical hollow slide valve to control the gas mass flow. The valve is controlled by a control unit which uses the pressure difference across the valve to calculate the mass flow. An advanced AFR control system for stationary lean-burn gas engines for co-generation has been carried out in [53]. The AFR is controlled by the fluctuation of the rotational speed of the engine.

1.3.7 Bi-Fuel Systems

The term "Bi-Fuel" can be understood in two different ways - on the one hand as systems which can be operated with two different fuels, e.g. gasoline and CNG, on the other hand as systems, which use a mixture of multiple fuels, e.g. diesel and natural gas. This section will be restricted to the second variant. An extended experimental investigation of the effect of a dual fuel (diesel and natural gas) mode engine on the efficiency and the pollutant emissions has been done in [25]. One advantage of natural gas is the high auto-ignition temperature, which can be used to keep the compression ratio at a high level in the case of diesel engines. It is shown that the dual fuel mode is a promising technique to control the NO as well as the soot emissions by adding natural gas into the intake air of an existing direct injection diesel engine. There are just slight modifications required on the engine structure in order to change a diesel engine into a dual fuel engine. An investigation into the effects of the engine parameters on performance and emissions using the same dual fuel mode engine as described in the publication before is done in [26]. In general the same results as in [25] can be presented. An already available Bi-Fuel system is offered by Altronic [1]. The system changes a diesel engine into a dual fuel diesel natural gas engine during operation without a decrease in the power of the engine. The results are lower emissions and lower operational costs. The control system considers information about the pressures and temperatures in the gas supply pipe as well as in the manifolds of the engine and information about the engine vibrations. Another patented system mixes lean gas, e.g. landfill gas (LFG), with rich gas, e.g. natural gas, in order to uphold the calorific value of the mixture [27]. The advantage of this system is that the lean gas can be used to generate energy, e.g. with a stationary gas engine, instead of being burned with a gas flare.

1.3.8 Conclusion of the Literature Survey

The conclusion of the literature survey should summarize the most important points for the theoretical investigation of a gas dosing system. Resulting from [37], a dynamic model of the venturi mixer is not necessary and the equations known from the standard literature are sufficient. Furthermore, no special mass flow sensor is needed if the mass flow, calculated from the pressure difference across the venturi, gets corrected/calibrated in the practical

use. The measurement of the calorific value or the Methane mass fraction in the gas supply pipe is not yet feasible for the implementation at gas dosing systems, which follows from section 1.3.3. A different approach will be shown in a later section.

From section 1.3.5 it can be concluded that a butterfly valve is still the easiest way to manipulate mass flows in the field of engines because of the fastest response time. Resulting from [46], a PI-structure will lead to the best performance in the position control of the butterfly valve. The best control strategy for the whole gas dosing system follows then from section 1.3.6it is a gain-scheduled controller with the use of an internal model in order to consider the dead-time of the system.

Chapter 2

General Equations and Fluid Characteristics

The components of the model and the model itself use the laws of the fields Thermodynamics and Fluid Mechanics. Recurring equations, e.g. mass flow equation and energy balance, are mentioned in summarized form in this chapter, in order to give a good overview about the used equations. In the following sections, quantities that refer to the upstream portion are indicated with a subscript "u", whereas quantities that refer to the downstream portion are indicated with a subscript "d". Furthermore the basic characteristics of the fluids used in this investigation are mentioned and summarized. The nomenclature of all variables is explained in appendix A. Unless stated otherwise in the relevant position, the used units are SI-units.

2.1 First Law of Thermodynamics

The first law of thermodynamics represents the principle of conversation of energy. That means that energy cannot be created or destroyed. For stationary flow processes, the first law of thermodynamics can be written in the following form [54]:

$$\dot{Q} + P_t = \dot{m}_d \left(h_d + \frac{{v_d}^2}{2} \right) - \dot{m}_u \left(h_u + \frac{{v_u}^2}{2} \right) + \frac{dU}{dt}. \tag{2.1}$$

In this form, the gravity influence on the fluid is neglected. Figure 2.1 shows the single variables in a principle layout of the system boundary.

2.2 Equation of Continuity

The mass balance for the system in figure 2.1 follows with

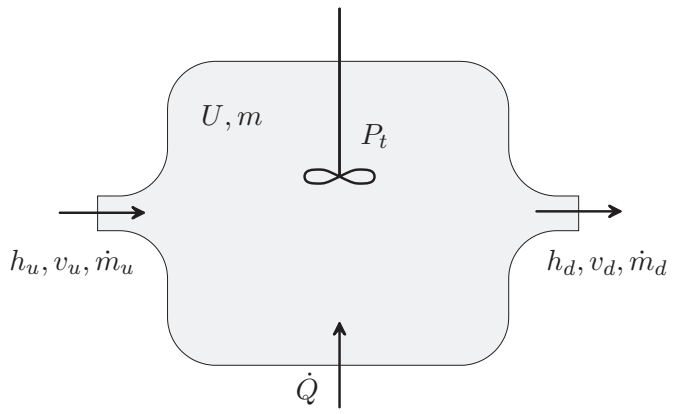

Figure 2.1: Principle Layout for the Definition of the First Law of Thermodynamics [55]

$$\frac{dm}{dt} = \dot{m}_u - \dot{m}_d. \tag{2.2}$$

For stationary systems $\frac{dm}{dt}$ is equal to 0, which leads to the equation of continuity

$$\dot{m} = A_u \, \rho_u \, v_u = A_d \, \rho_d \, v_d. \tag{2.3}$$

The equations above assume the validity of the classical mechanics and therefore the change of mass into energy can be ruled out.

2.3 Ideal Gas Equation

In the model, the gases are assumed to be ideal gases. These assumptions are justified for the pressures and temperatures appearing in this work. Therefore the ideal gas equation

$$p = \rho \, R_s \, T \tag{2.4}$$

is used. Other simplifications resulting from this assumption are the calorific state equations

$$\begin{aligned} u_d &= c_v \, (T_d - T_u) + u_u \\ h_d &= c_p \, (T_d - T_u) + h_u, \end{aligned} \tag{2.5}$$

which can also be used for the present system [54]. For bigger temperature changes, the assumption of constant gas properties might not hold.

2.4 Isentropic State Change

Based on the assumption of high-flow velocities and short distances, the system is assumed to be adiabatic, because of a negligible heat exchange at the wall. Only the reservoirs (section 3.5) include a heat exchanger, based on the energy equation and a defined heat flow rate. Therefore, the ratio of specific heats κ is important, which is the relationship between the isobaric and the isochoric specific heat capacity. The relationship expressed in an equation is written as

$$\kappa = \frac{c_p}{c_v} = \frac{c_p}{c_p - R_s} \geq 1 \tag{2.6}$$

[54], which leads furthermore to the isentropic state equations

$$\begin{aligned} p\,v^{\kappa} &= const. \\ T\,v^{\kappa-1} &= const. \\ T\,p^{\frac{1-\kappa}{\kappa}} &= const.\ . \end{aligned} \tag{2.7}$$

2.5 Static and Total State Variables

In many applications, the difference between flowing and non-flowing fluids plays a role which cannot be neglected. In such cases it is distinguished between static and total state variables. A static state variable is equivalent to the potential energy of the total energy of the fluid. The flow velocity does not affect the value of the static state variable. Adiabatic isentropic deceleration of the fluid into the static condition leads to the total state variable of the fluid. For low velocities the difference between static and total state variables is very small and it can be assumed that static and total state variables are equal. In the following, the equations for the transformation of the static to the total state variables are given.

Transformation from static to total pressure [55]:

$$p_t = \left(\frac{v^2}{2\,c_p\,T} + 1 \right)^{\frac{\kappa}{\kappa-1}} p \tag{2.8}$$

Transformation from static to total temperature [55]:

$$T_t = \left(\frac{v^2}{2\,c_p\,T} + 1 \right) T \tag{2.9}$$

The fluid velocity v in equation (2.8) and (2.9) can be calculated with

$$v = \frac{\dot{m}}{\rho\,A} \tag{2.10}$$

The calculation of the static state variables from the total state variables is more difficult and can be read up in [55].

2.6 Mass Flow Rate

The mass flow across an orifice with known pressure difference is determined by the following equation, which is well known in the standard literature (see section 1.3.4). The derivation of the equation can be found in [22].

$$\dot{m} = A_{eff} \sqrt{\frac{2\kappa}{\kappa - 1}} \frac{p_{u,t}}{\sqrt{R_s\, T_{u,t}}} \beta\left(\Pi\right), \tag{2.11}$$

where

$$\Pi = \frac{p_{u,t}}{p_d}, \tag{2.12}$$

and

$$\beta\left(\Pi\right) = \begin{cases} \sqrt{\Pi^{-\frac{2}{\kappa}} - \Pi^{-\frac{\kappa+1}{\kappa}}} & \Pi \leq \frac{\kappa+1}{2}^{\frac{\kappa}{\kappa-1}} \\ \sqrt{\frac{\kappa-1}{2}\left(\frac{2}{\kappa+1}\right)^{\frac{\kappa+1}{\kappa-1}}} & \Pi > \frac{\kappa+1}{2}^{\frac{\kappa}{\kappa-1}} \end{cases} . \tag{2.13}$$

The flow through the orifice is assumed as an isentropic and adiabatic throttling. The total state of the fluid upstream gets throttled and accelerated to the throat pressure and temperature. The difference between the set throat pressure and the pressure downstream of the orifice therefore defines the loss across the orifice. In many cases the pressure at the throat is assumed to be the same as downstream of the orifice while any losses are considered upstream. The total temperature up- and downstream of the orifice is the same, because of the assumption of an adiabatic system.

The factor β is called the *Flow Rate Function (FRF)* and it depends on the pressure ratio, until the velocity of the fluid reaches the speed of sound level at the throat. Then β does not change any more and stays constant. In figure 2.2, β is shown over the pressure ratio. κ in the figure is chosen as $\kappa = 1.4$.

2.7 Mach Number

The Mach Number (MN) is a very important value for the characterization of fluid flows, because many properties depend on it. The Mach number is defined as

$$M = \frac{v}{a} \quad \text{where} \quad a = \sqrt{\kappa\, \frac{p}{\rho}} = \sqrt{\kappa\, R_s\, T} \tag{2.14}$$

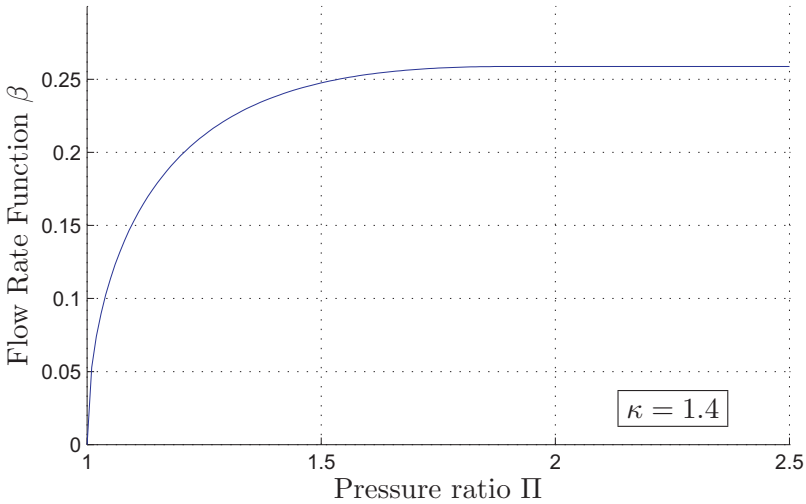

Figure 2.2: Flow Rate Function $\beta(\Pi)$

which is called the speed of sound of the fluid.

2.8 Air and Gas Characteristics

All equations given so far are dependent on fluid characteristics. The values of κ, c_p, R_s,... are subject to experiments and must be measured. These values for air and general values for the calculation are shown in table 2.1 and can be found in almost every chemistry or thermodynamics book, e.g. [24, 54].

Universal gas constant:	$\mathcal{R} = 8.314472\ J/molK$
Avogadro constant:	$\mathcal{N}_G = 6.02214179 \cdot 10^{23}\ 1/mol$

Table 2.1: Universal Constants

The characteristic values for gas are more subject to change and therefore not generally fixed values. In this case a range of the values can be given, but for practical use the values must be adjusted.

2.8.1 Air Characteristics

The air characteristic in the atmosphere is in general the same in the whole world, but air pressure and air temperature are subject to change. Assuming just small changes, the air characteristics can be seen as constant, because these changes have no big influence on the values. In table 2.2 the characteristic values of the air are summarized.

Ratio of specific heats:	$\kappa_{air} = 1.4$
Isobaric specific heat capacity:	$c_{p,air} = 1007\ J/kgK$
Isochoric specific heat capacity:	$c_{v,air} = 718\ J/kgK$
Specific gas constant:	$R_{s,air} = 287\ J/kgK$
Density:	$\rho_{air} = 1.2041\ kg/m^3$
Air composition:	
Nitrogen:	75.51 $mass\%$
Oxygen:	23.16 $mass\%$
Inert gases:	1.28 $mass\%$
Carbon dioxide:	0.05 $mass\%$

Table 2.2: Air Characteristics

2.8.2 Natural Gas Characteristics

Natural gas is normally obtained from the local gas grid. The gas will be regulated from the gas grid pressure, which can be up to $16bar$, to the connection pressure of around $100-200mbar$. Calorific value and gas supply pressure are subject to change, as described in section 1.1. In the literature the values of the gas characteristics are given in a broad range. In order to use realistic values, the values used in [35] are taken. The values used here as well as the ranges of the characteristic values of natural gas are summarized in table 2.3.

Ratio of specific heats:	$\kappa_{gas} = 1.32$
Isobaric specific heat capacity:	$c_{p,gas} = 2143.6\ J/kgK$
Isochoric specific heat capacity:	$c_{v,gas} = 1623.9\ J/kgK$
Specific gas constant:	$R_{s,gas} = 519.65\ J/kgK$
Density:	$\rho_{gas} = 0.7287\ kg/m^3$ $(0.700 - 0.840\ kg/m^3)$
Calorific value:	$H_{i,gas} = 40\ MJ/kg$ $(32.4 - 45\ MJ/kg)$
Natural gas composition (L - H):	
Methane:	95 $mass\%$ $(85 - 98\ mass\%)$
Alkane:	3 $mass\%$ $(4 - 1\ mass\%)$
Inert gases:	2 $mass\%$ $(11 - 1\ mass\%)$

Table 2.3: Natural Gas Characteristics

2.8.3 Biogas Characteristics

Biogas is one of the most interesting fuels in the field of renewable energy. Biological waste is used to produce a gas which includes Methane. This gas can be used to operate a gas engine. Depending on the waste, the mass fraction of Methane in the gas is different. [34]

describes the aerosis in the biogas process in great detail. Also models for the calculation of the gas characteristics are given. The dependence of the gas characteristics on the waste is very big, which leads to the fact that no general ranges of biogas can be found in the literature. The result from [34] is used to estimate the characteristic values of biogas. These values are summarized in table 2.4.

Ratio of specific heats:	$\kappa_{biogas} = 1.12$
Isobaric specific heat capacity:	$c_{p,biogas} = 3842\ J/kgK$
Isochoric specific heat capacity:	$c_{v,biogas} = 3430.35\ J/kgK$
Specific gas constant:	$R_{s,biogas} = 411.64\ J/kgK$
Density:	$\rho_{biogas} = 1.2\ kg/m^3$
Calorific value:	$H_{i,biogas} = 17.5\ MJ/kg\ (14.4 - 27\ MJ/kg)$
Biogas composition:	
Methane:	$60\ mass\%\ (50 - 75\ mass\%)$
Other gases:	$40\ mass\%\ (50 - 25\ mass\%)$

Table 2.4: Biogas Characteristics

2.9 Stoichiometric Combustion

For low emissions it is necessary that the air/fuel ratio is equal to the set point. Stationary gas engines are commonly operated with $\lambda = 1.7$. The λ value is calculated with

$$\lambda = \frac{\dot{m}_{air}}{\dot{m}_{air,st}}, \tag{2.15}$$

where $\dot{m}_{air,st}$ is the air needed for a complete combustion of the fuel. For natural gas, whose main component is Methane, the combustion equation can be approximated with

$$CH_4 + 2\,O_2 \rightarrow CO_2 + 2\,H_2O. \tag{2.16}$$

This equation gives the amounts of Methane and Oxygen needed for the stoichiometric combustion. The atom masses of the components can be looked up in the periodic table of the elements in order to build the needed molar masses [24]

$$\begin{aligned} H &= 1.00794u \approx 1u \\ C &= 12.011u \approx 12u \\ O &= 15.9994u \approx 16u. \end{aligned} \tag{2.17}$$

u in equation (2.17) and (2.18) means the atomic mass. The molar masses then lead to

$$\begin{aligned} CH_4 &= 16u \quad \rightarrow \quad \mathcal{M}_{CH_4} = 16\ kg/kmol \\ O_2 &= 32u \quad \rightarrow \quad \mathcal{M}_{O_2} = 32\ kg/kmol \\ \text{air} &= 29u \quad \rightarrow \quad \mathcal{M}_{air} = 29\ kg/kmol. \end{aligned} \tag{2.18}$$

For the complete combustion of $1mol\ CH_4$, $2mol$ of O_2 are needed, which is equal to $16g$ of CH_4 and $64g$ of O_2, following from equation (2.18). For $1kg$ of Methane, therefore $x\,kg$ of Oxygen are needed, as shown in the following equation.

$$x = \frac{1kg}{\underbrace{16 \cdot 10^{-3}kg}_{1mol\ CH_4}} \cdot \underbrace{2 \cdot 32 \cdot 10^{-3}kg}_{2mol\ O_2} \approx 4kg\,O_2/kg\,CH_4, \tag{2.19}$$

The stoichiometric air requirement $L_{st,Methane}$ for $1kg$ of Methane follows with the before assumed percentage of Oxygen in the air (23.16%), to

$$L_{st,Methane} = \frac{100}{23.16} \cdot 4 \approx 17.3\,kg\,air/kg\,CH_4. \tag{2.20}$$

The needed air for a complete combustion of the fuel can thus be calculated with

$$\dot{m}_{air,st} = \dot{m}_{gas}\,x_{gas}\,L_{st,Methane}, \tag{2.21}$$

where x_{gas} is the mass fraction of CH_4 in the gas, if $\dot{m}_{gas}$ is not pure Methane.

2.10 Assumptions and General Guidelines

Every model is based on assumptions, which lead to simplified conditions that are sufficient for the problem under investigation. In order to keep the overview of these assumptions, they are summarized in table 2.5. Furthermore, all general guidelines used in this work are also formulated in the following table.

- All calculations assume ideal gas
- The components are adiabatic except for the reservoirs
- Constant fluid characteristics

Table 2.5: Assumptions and General Guidelines

Chapter 3

Model of the Gas Dosing System

In this section, the model of an active gas dosing system is developed and modeled. Firstly, an overview of the gas dosing system as well as the components which are included in the model is given. Secondly, a summary of the geometry of the implemented venturi mixer follows the overview. Thirdly, a detailed description of the different components follows the geometry of the venturi mixer section. At the end of this chapter the challenges in the implementation in Matlab Simulink are mentioned.

3.1 Overview of the Gas Dosing System Model

Active gas dosing systems can be seen as supplementary parts of an engine, which can replace an existing system without changing anything in the established system. This circumstance is one basic point in this investigation. Figure 3.1 schematically shows an overview of the system to be modeled.

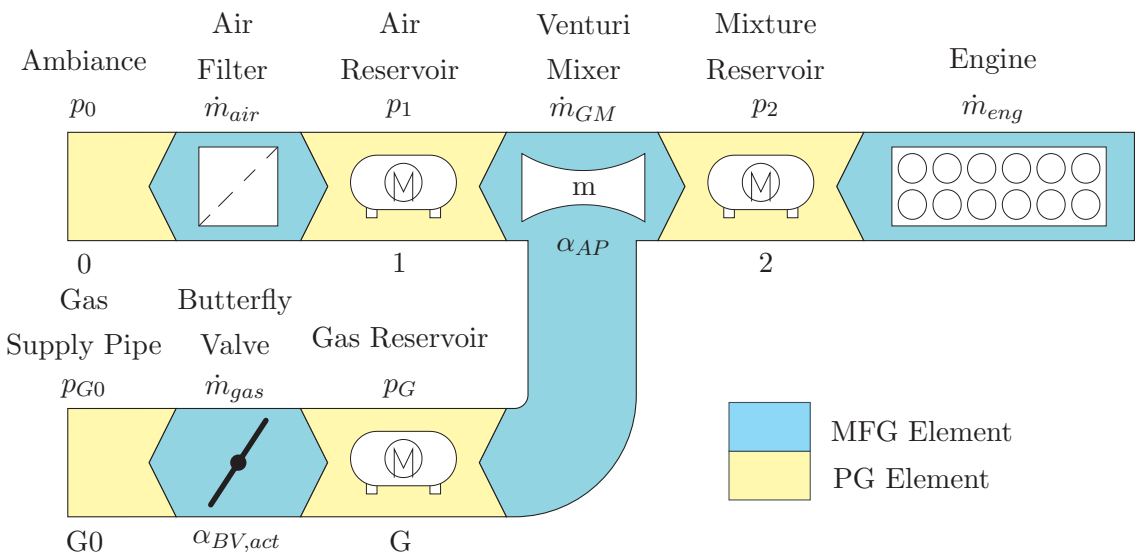

Figure 3.1: Overview of the Model and Causal Relation of the Components

The flow direction is from the left to right side of the figure, while the following description of the different model components will be from the right to the left side. The variables below the names of the components are given for better orientation. The numbers/letters below the symbols of the components in the figure define the states of the model. Downstream and upstream is therefore explicitly defined and will be used in the following paragraph for the explanation. The colors of the single parts in the figure define mass flow giving (MFG) or pressure giving (PG) elements, whose purpose is described in more detail in section 3.9.

The engine is the end of the air path, which means that at this point the input variables must be defined for the model. In reality, at this point, the input into the engine would be the mass flow of the mixture of air and gas. This value is therefore defined as the input variable of the gas dosing system model. The model of the engine is described in section 3.7, which is a provided model in the form of a Matlab S-Function. Upstream of the engine, a mixture reservoir (see section 3.5) is modeled in order to consider the possibility of emptying the intake manifold of the engine. The mass flow into the engine reduces the pressure in the mixture reservoir, which is followed by a pressure difference across the venturi mixer. This pressure difference generates a mass flow across the venturi mixer (see section 3.6.1), which leads to a pressure drop in the throat of the venturi (see section 3.6.2) as well as in the air reservoir. A schematic figure of the venturi mixer is depicted in figure 3.2. The reduced pressure in the throat is followed by a pressure difference between gas reservoir and the throat, which leads to a gas mass flow into the throat (see section 3.6.3). The pressure drop in the air and the gas reservoirs leads to a pressure difference between the atmosphere and the air reservoir as well as the gas supply pipe and the gas reservoir. These pressure differences generate the air mass flow across the air filter and the gas mass flow across the butterfly valve. Both atmosphere and gas supply pipe are the other end of the model, which means that the variables from these sections must be defined in order to close the system.

This is basically the function of the model of the gas dosing system, whose components are built with the knowledge of the literature survey in section 1.3. Besides these components, a model for the mixture temperature in the throat (see section 3.6.5), a model for the concentration vector in the throat (see section 3.6.4) and a model for the mixture characteristics (see section 3.6.6) are developed.

The ultimate aim is to be able to design a controller for the lambda value of the engine by using the knowledge gained from the model. In order to control the gas mass flow, two ways are prepared in the model. The primary approach is the use of the butterfly valve, by controlling the angle of the plate of the butterfly valve. The secondary approach is the gap of the annular passage. The main focus will be on the butterfly valve, though.

In the following section, the geometry of the venturi mixer is described, followed by detailed descriptions of the models.

3.2 Venturi Mixer Geometry

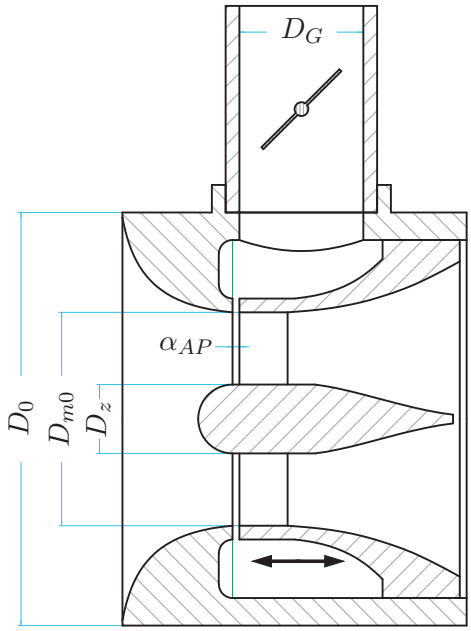

Figure 3.2: Venturi Mixer Geometry

An essential topic in the design of a gas dosing system is the geometry of the venturi mixer. The geometry of the venturi has a great influence on the throat pressure, which is furthermore limited by the Mach number. In order to offer a gas dosing system for the whole power range of the engine, the throat must be big enough to provide the needed mixture mass flow. This work is based on a theoretical approach, which implies that no built apparatus is available and therefore the geometry of the venturi mixer must be approximated for the used engine. In order to use realistic values, data from Woodward[1] [20], RMG [15, 16] and Heinzmann [18] were compared and used for the estimation. In figure 3.2, the schematic layout of the used geometry is depicted. The approximated values are summarized in table 3.1.

Nominal diameter:	$\emptyset D_0 = 300mm$
Throat diameter:	$\emptyset D_{m0} = 155mm$
Zeppelin diameter:	$\emptyset D_z = 50mm$
Gas supply pipe diameter:	$\emptyset D_G = 126mm$
Gap of the annular passage:	$\alpha_{AP} = 1mm$

Table 3.1: Geometry Values of the Venturi Mixer

The cross sectional area (CSA) of the annular passage is calculated with $A_{AP}{=}D_{m0}\,\pi\,\alpha_{AP}$. The throat cross sectional area is calculated with $A_m = A_{m0} - A_z$ where $A_i = \frac{1}{4}\,D_i^2\,\pi$. α_{AP} gives a reference for a set point, but is modeled variably in the Simulink model.

[1] Woodward Governor Company, http://www.woodward.com/

3.3 Air Filter

Each engine needs air for the combustion, which is normally drawn from the ambiance. Air from the ambiance can be polluted, which has negative effects on the intake pipes as well as on the abrasion of the wall of the combustion chamber. In order to avoid these effects, an air filter is used. Especially in polluted air conditions (e.g. power generators at construction sites), a careful selection of the right air filter is important. Dirty particles in the air will be caught and saved in the air filter, thus changing the streaming conditions through the air filter after some time of usage.

This pollution causes a significant pressure drop across the air filter, which can cause a higher fraction of fuel in the air-fuel mixture and lead to higher emissions. In the simulation model, an air filter is modeled to regard this pressure drop across the air filter as well as to take the losses across the venturi mixer into account.

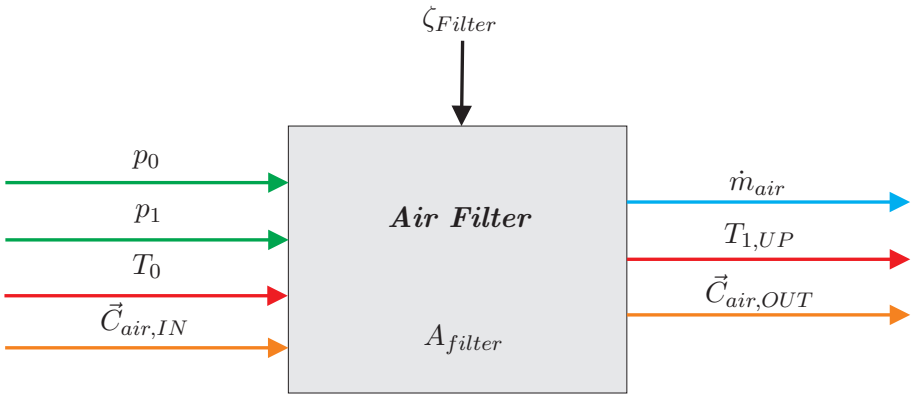

Figure 3.3: Scheme of the Air-Filter Block

In figure 3.3, the general layout of the Simulink model block can be seen. For the model of the air filter, different approaches can be used. In this case a very simple approach is used, because the purpose of an air filter is just to regard the pressure drop between the atmosphere and the gas dosing system intake manifold. The defined values for the model are summarized in table 3.2.

In the model, equation (3.1) is used for the calculation of the pressure drop, which is well known from the standard literature on fluid mechanics.

$$\Delta p_{filter} = p_0 - p_1 = \frac{1}{2}\,\zeta_{filter}\,\rho_0\,v_{filter}^2. \tag{3.1}$$

In the equation, ζ_{filter} is the variable resistance coefficient, which can be used to simulate the pollution of the air filter. The middle velocity across the filter is defined by the cross sectional area of the filter, which is a constant and has to be given by the apparatus. The middle velocity is therefore given with equation (3.2).

Inputs	
Ambient pressure:	$p_0 = 101325\ Pa = 1.01325\ bar$
Ambient temperature:	$T_0 = 294\ K = 21\ °C$
Air reservoir pressure:	p_1
Concentration vector from the ambiance:	$\vec{C}_{air,IN}$
Outputs	
Mass flow of the air across the filter:	$\dot{m}_{air}$
Output temperature of the air filter:	$T_{1,UP}$
Concentration vector from the air filter:	$\vec{C}_{air,OUT}$
Parameters	
Pollution coefficient:	$\zeta_{filter} = 135$
Filter CSA:	$A_{filter} = 0.6\ m^2$

Table 3.2: Air Filter Values

$$v_{filter} = \frac{\dot{m}_{air}}{\rho_0\, A_{filter}} \tag{3.2}$$

In order to minimize the losses across the air filter, the middle velocity should be small. With the assumption of small velocities and an adiabatic body of the filter, the temperature across the filter does not change. This allows the calculation of the density of the air with the ambient conditions.

$$\rho_0 = \frac{p_0}{R_{s,air}\, T_0} \tag{3.3}$$

In the simulation model, the air filter is modeled as an MFG element. The conversion of equation (3.1) gives an equation for $\dot{m}_{air}$. This equation is implemented in the simulation block for calculating the mass flow of the air, which is implied in the overview figure 3.1.

3.4 Butterfly Valve

The butterfly valve, as mentioned in section 3.1, is the main actor of the active gas dosing system to be modeled. The pros and cons of using a butterfly valve are discussed in section 1.3.5. A butterfly valve consists of an actor and a butterfly plate, which is rotated in order to open/close the valve. The flow cross-sectional area is a function of the angle of the shaft of the butterfly plate, which is shown in equation (3.4) [55].

$$A_{BV}\left(\alpha_{BV,act}\right) = A_G\left(1 - \frac{cos\left(\alpha_{BV,act} + \alpha_{BV,0}\right)}{cos\left(\alpha_{BV,0}\right)}\right), \tag{3.4}$$

where $\alpha_{BV,0}$ is the initial angle of the plate, if the butterfly plate is bigger than the diameter of the pipe. The angle $\alpha_{BV,act}$ starts to be counted from the closed butterfly valve. The behavior of this equation is nonlinear, which requires a linearization in order to control the mass flow through the butterfly valve. Figure 3.4 shows the nonlinearity of the equation.

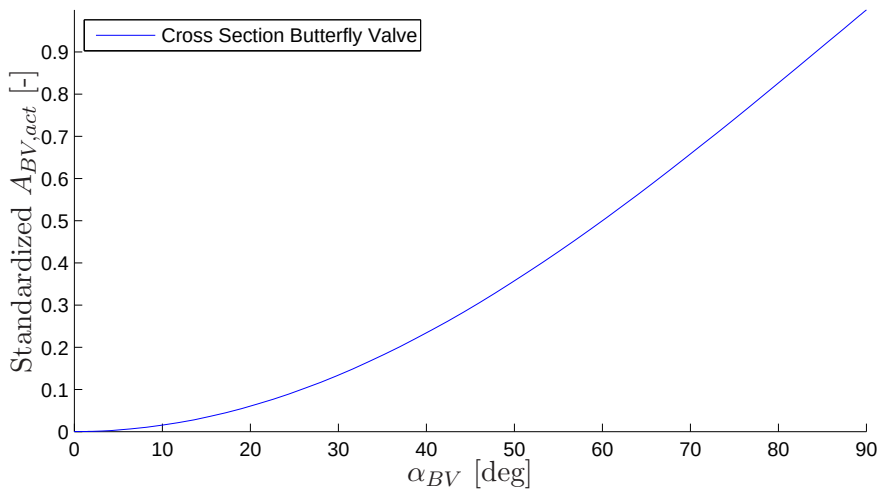

Figure 3.4: Flow Cross Sectional Area Across the Shaft Angle

The rotation of the shaft is done by an actor. In reality, these actors have a minimal delay between the input signal and the reached final value. For a realistic simulation, a Stepper Motor model from Hoerbiger is used. The model of the actor has a transfer function, which is shown in figure 3.5.

The main input and output of the Stepper Motor model is summarized in table 3.3. It is implemented as a simple linear time-invariant (LTI) system block in Matlab Simulink.

Input	
Angle set point in degree:	α_{BV}
Output	
Angle of the stepper motor:	$\alpha_{BV,act}$

Table 3.3: Stepper Motor Values

It is not only the angle of the shaft that is responsible for the mass flow across the butterfly valve. In fact, the main reason and therefore the relevant value for the gas mass flow is the pressure difference. Another factor that has influence on the gas mass flow, though to

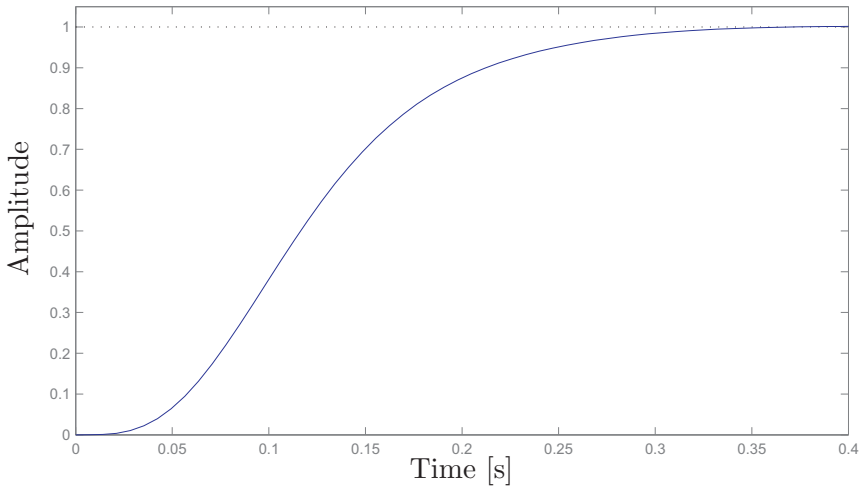

Figure 3.5: Stepper Motor Transfer Function

smaller extent, is the temperature of the gas. The reduced over pressure in the gas grid in general is around $100 - 200mbar$ to the atmosphere pressure. The gas mass flow across the butterfly valve therefore follows with equation (2.11) to

$$\dot{m}_{gas} = A_{BV}\left(\alpha_{BV,act}\right)\sqrt{\frac{2\kappa_{gas}}{\kappa_{gas}-1}}\frac{p_{G0,t}}{\sqrt{R_{s,gas}\,T_{G0,t}}}\,\beta\left(\frac{p_{G0,t}}{p_G}\right), \tag{3.5}$$

where β is the FRF equation (2.13). The total states of the pressure and the temperature are considered with equation (2.8) and (2.9). The needed gas mass flow for the calculation of the total states is taken into account by a feedback of the gas mass flow. A direct feedback is impossible due to algebraic loops in the simulation. The problem of the algebraic loop is solved by using a first-order lag element (PT1-element), shown in equation (3.6).

$$G\left(s\right) = \frac{1}{0.1\,s\,+\,1} \tag{3.6}$$

It is assumed that temperature effects of the butterfly valve can be neglected, which means constant temperature of the gas upstream and downstream of the butterfly valve. The assumption of an adiabatic system, in combination with the energy equation, can be used to prove this simplification.

In figure 3.6 all inputs and outputs of the simulation model block can be seen, as well as the parameters which are used for the calibration. In order to give a good overview, all the values used in the simulation are summarized in table 3.4.

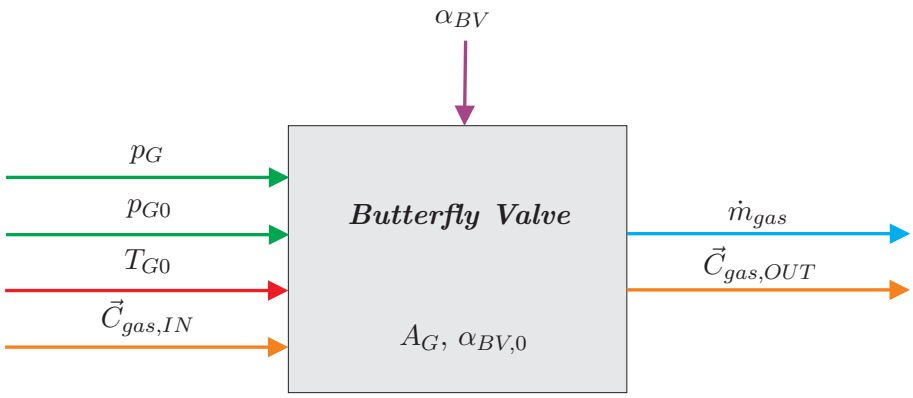

Figure 3.6: Scheme of the Butterfly Valve Block

Inputs	
Pressure in the gas reservoir:	p_G
Gas supply pipe pressure:	$p_{G0} \approx 111325\ Pa = 1.11325\ bar$
Gas supply pipe temperature:	$T_{G0} \approx 294\ K = 21\ °\mathrm{C}$
Gas concentration vector from the gas supply pipe:	$\vec{C}_{gas,IN}$
Set angle of the butterfly valve plate:	α_{BV} (degrees)
Outputs	
Gas mass flow across the butterfly valve:	$\dot{m}_{gas}$
Gas temperature upstream of the butterfly valve:	$T_{G,up}$
Gas concentration vector into the gas reservoir:	$\vec{C}_{gas,OUT}$
Parameters	
CSA of the gas supply pipe:	$A_G = 124.7\ cm^2\ (D_G = 126mm)$
Initial angle of the butterfly plate:	$\alpha_{BV,0} = 0$

Table 3.4: Butterfly Valve Values

3.5 Air, Gas and Mixture Reservoir

In the air path the different components (e.g. super charger, compressors, carburetor,...) are connected by pipes, which also influence the whole dynamics of the system. This dynamics cannot be neglected automatically. Because of this, the spaces between the components of the gas dosing system are added to the model and are also modeled. As seen in the previous sections, pressures are needed for the MFG model parts. Because of that, the reservoirs between the model parts are modeled as PG elements. The meaning of MFG and PG elements, as well as another advantage of this, is described in section 3.9.

The models of the different reservoirs, like gas-, air- and mixture reservoir are all the same. The only differences are the values of the parameters. The reservoirs also offer the possibility to simulate the emptying of the reservoir, which means that the time delay from an appearing output mass flow change to the input mass flow change can be varied by changing the volume of the reservoir. Table 3.5 shows the used parameter values.

Inputs	
Mass flow into the reservoir:	$\dot{m}_{IN}$
Mass flow from the reservoir:	$\dot{m}_{OUT}$
Temperature into the reservoir:	T_{IN}
Concentration vector into the reservoir:	$\vec{C}_{IN}$
Outputs	
Pressure in the reservoir:	p_R
Temperature in the reservoir:	T_R
Concentration vector from the reservoir:	$\vec{C}_{OUT}$
Parameters	
Heat flow across the wall of the reservoir:	$\dot{Q} = 0\ W$
Volume of the air reservoir:	$V_R = 0.07069\ m^3$
Volume of the gas reservoir:	$V_R = 0.000623449\ m^3$
Volume of the mixture reservoir:	$V_R = 0.07069\ m^3$
Mass of the reservoir wall:	$m_{Wall} = 7.8\ kg$ (Aluminum)
Heat capacity of the reservoir wall:	$c_{Wall} = 896\ J/kgK$ (Aluminum)

Table 3.5: Reservoir Values

Basically, the mass inside a reservoir defines the pressure if temperature and fluid characteristics are known, as shown in equation (3.7).

$$p_R = \frac{m_R\, R_s\, T_R}{V_R} \tag{3.7}$$

The fluid is assumed to be an ideal gas for the pressures and temperatures appearing in the system. The mass inside the reservoir can be calculated by integration of equation (2.2). The temperature at the output can be calculated with the energy equation and the assumption of the lumped parameter approach [23], which actually means that the output temperature is equal to the reservoir temperature. The following equation is based on the energy equation, but transformed in order to calculate the change of the reservoir temperature [55].

$$\dot{T}_{R,t} = \frac{1}{c_{v,R}\, m_R + c_{Wall}\, m_{Wall}} \left[\dot{m}_{IN} \left(c_p\, T_{IN,t} - c_{v,R}\, T_{R,t} \right) - \dot{m}_{OUT} \left(R_s\, T_{R,t} \right) - \dot{Q} \right] \tag{3.8}$$

Integration of equation (3.8) yields the output temperature of the reservoir. The implemented heat flow $\dot{Q}$ can be used to cool or heat the fluid through the wall of the reservoir. The inputs and outputs of the simulation block are summarized in figure 3.7.

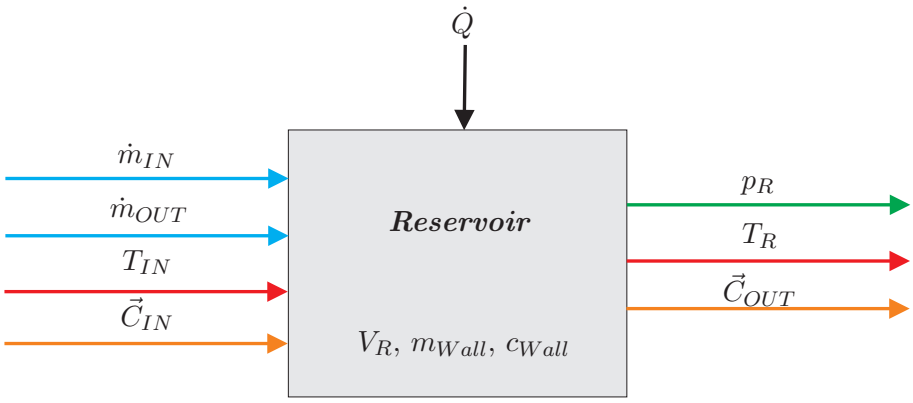

Figure 3.7: Scheme of the Reservoir Model

3.6 Venturi Mixer

The venturi mixer is the main part of a gas dosing system. It is the part where the gas is mixed with the air. Figure 3.8 shows an overview of this part.

Venturi mixers use the principle of the venturi effect to mix gas into the air mass flow. The venturi effect denotes the static pressure drop and the acceleration of a fluid velocity at a constricted section of a pipe. In a venturi mixer, the constricted area is called the throat of the venturi or simply throat. This point is the smallest cross sectional area in the mixer. At the circumference of the throat, an annular passage (AP) connects the air pipe with the gas reservoir, which is just the pipe between the butterfly valve and the venturi mixer. The pressure in the gas reservoir is higher than the pressure at the throat. Therefore gas flows into the throat and gets mixed with the air. The amount of gas flowing into the throat is defined by the pressure difference between the gas reservoir and the throat and can be controlled by the butterfly valve as well as basically by the geometry of the

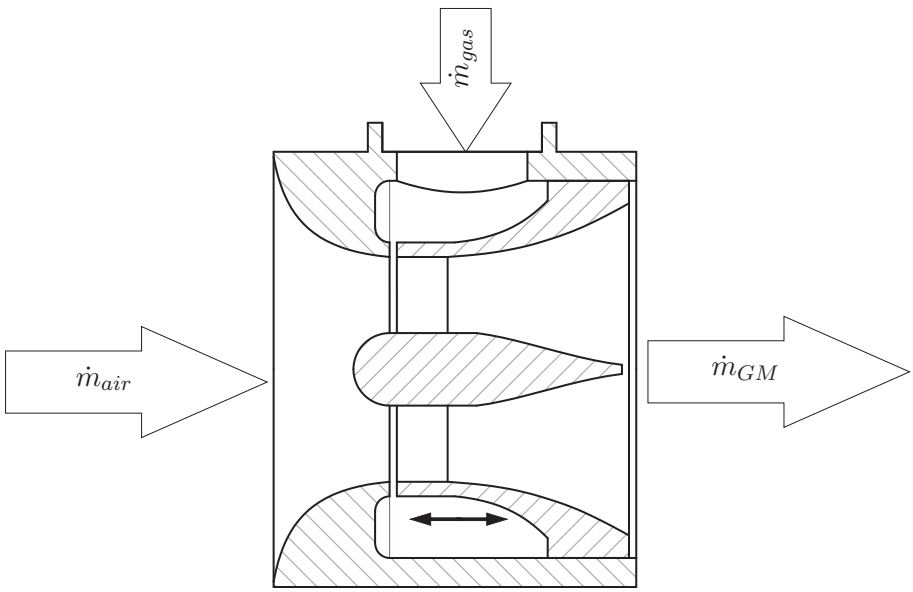

Figure 3.8: Scheme of the Venturi Mixer

venturi. As described before, the butterfly valve is the main actor of the system, but the annular passage, especially the gap of the annular passage, can be used for regulation, as it is also adjustable. This can be a secondary actor of the gas dosing system. Figure 3.9 summarizes the inputs and outputs of the venturi mixer simulation block.

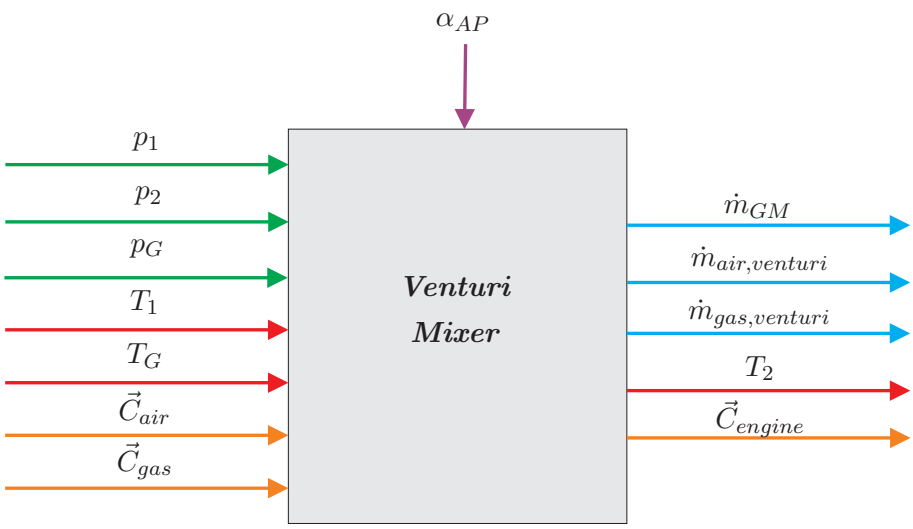

Figure 3.9: Overview of the Venturi Mixer Model

The venturi mixer model itself is divided into six submodels, which use the inputs and outputs depicted in figure 3.9. The descriptions of the submodels appear in the order of their calculations (see table 3.6). The variables used in figure 3.9 are explained in the corresponding detailed descriptions.

1. Mixture Mass Flow Across Venturi Mixer Block (section 3.6.1)
2. Throat Pressure Block (section 3.6.2)
3. Gas Mass Flow Across Annular Passage (section 3.6.3)
4. Concentration Vector Block (section 3.6.4)
5. Mixture Temperature Block (section 3.6.5)
6. Mixture Characteristic Block (section 3.6.6)

Table 3.6: Sequence of the Calculations of the Venturi Mixer Submodels

3.6.1 Mixture Mass Flow Across Venturi Mixer

This model is based on the assumption that no Mach number greater than 1 appears in the throat. Furthermore, for the exact calculation of the pressure p_m in the throat, the mass flow across the venturi is needed (see section 3.6.2). This leads to an algebraic loop in the system, which can only be solved by iteration. In order to avoid iterations in a simulation, the mixture mass flow across the venturi cannot be calculated exactly online [55]. Therefore the mixture mass flow value is calculated approximately, which leads to a practical result if the mass flow value is calibrated [37]. For the calculation itself, the pressure difference across the venturi mixer is used with some assumptions. Nevertheless, the calculation of the mixture mass flow across the venturi is not trivial. Because of this reason, for this part of the investigation, the difference of the mixture mass flow and the air mass flow is neglected, because otherwise the system would be undefined. Figure 3.10 shows the overview of the Simulink block used.

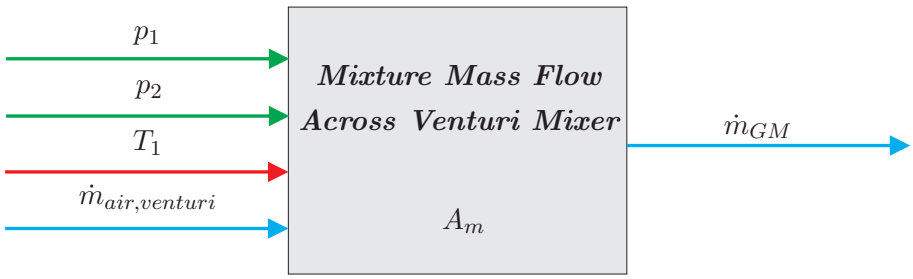

Figure 3.10: Scheme of the Mixture Mass Flow Block

In the simulation, different variants for the calculation of the mixture mass flow are implemented. Variant one is the mixture mass flow calculated with the equations (2.11), (2.12) and (2.13) as well as equation (2.8) and (2.9), in order to regard the total states of the incoming fluid.

$$\dot{m}_{GM} = A_m \sqrt{\frac{2\kappa_{mix}}{\kappa_{mix} - 1}} \frac{p_{1,t}}{\sqrt{R_{s,mix}\, T_{1,t}}} \beta \left(\frac{p_{1,t}}{p_2} \right) \tag{3.9}$$

In order to simplify the calibration process, the mixture characteristics presented in section 3.6.6 are used. In this approximation the assumption is made that the static pressure at the throat can be approximated by the value of the static pressure after the venturi mixer. In the simulation, the steady state value of the mixture mass flow is reached, which justifies the use of the static pressure after the venturi mixer in equation (3.9).

The pressure drop equation, which is also used for the pressure difference at the air filter (equation (3.1)), is used in variant two. It is given in order to give an alternative to equation (3.9).

$$\Delta p_{venturi} = p_1 - p_2 = \frac{1}{2} \zeta_{venturi}\, \rho_1\, v_m^2, \tag{3.10}$$

where

$$v_m = \frac{\dot{m}_{air,venturi}}{\rho_1\, A_m} \tag{3.11}$$

and

$$\rho_1 = \frac{p_1}{R_{s,air}\, T_1}. \tag{3.12}$$

The air mass flow into the venturi used in equation (3.11) is calculated with

$$\dot{m}_{air,venturi} = \dot{m}_{GM} - \dot{m}_{gas,venturi}, \tag{3.13}$$

where the gas mass flow is the feedback value of the gas mass flow across the annular passage as described in section 3.6.3. The air mass flow would lead to an algebraic loop in the simulation and therefore it is delayed with a PT1-element with a time constant of $0.1 sec$ as shown in equation (3.14).

$$G(s) = \frac{1}{0.1\, s + 1}. \tag{3.14}$$

The gas mass flow into the venturi depends on the mixture mass flow calculated in this block. Therefore, strictly speaking, the value of the air mass flow into the venturi lags one time step behind the mixture mass flow; but this has actually no effect on the stationary result of the venturi mixer and can therefore be neglected. In table 3.7 all values of the simulation block are summarized.

Inputs	
Pressure upstream of the venturi mixer:	p_1
Temperature upstream of the venturi mixer:	T_1
Pressure downstream of the venturi mixer:	p_2
Air mass flow into the venturi mixer:	$\dot{m}_{air,venturi}$
Outputs	
Mass flow across the venturi mixer:	$\dot{m}_{GM}$
Parameters	
CSA upstream of the venturi mixer:	$A_1 = 706.9\ cm^2\ (D_1 = 300mm)$
CSA of the Zeppelin:	$A_z = 19.6\ cm^2\ (D_z = 50mm)$
CSA at the throat without Zeppelin:	$A_{m0} = 188.7\ cm^2\ (D_{m0} = 155mm)$
CSA at the throat:	$A_m = A_{m0} - A_z = 169.1\ cm^2$
Pressure loss coefficient of the venturi mixer:	$\zeta_{venturi} = 0.95$

Table 3.7: Mixture Mass Flow Across Venturi Mixer Values

3.6.2 Throat Pressure

The geometry of the venturi defines the pressure p_m in the throat, which is needed for the calculation of the gas mass flow into the venturi, as described in section 3.6.3. The calculation of the throat pressure should be as close as possible to the real throat pressure, in order to minimize the error of the gas mass flow, which is the most important variable for the calculation of the engine power. Figure 3.11 shows an overview of the simulation block. All corresponding variables are summarized in table 3.8.

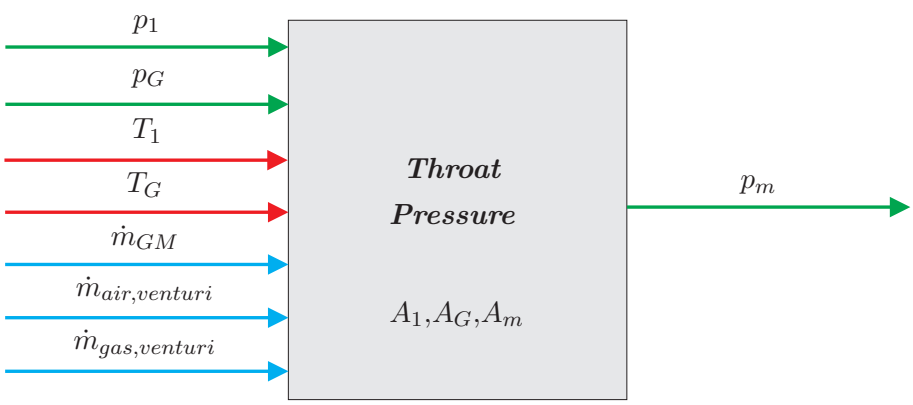

Figure 3.11: Scheme of the Throat Pressure Model

For the calculation of the throat pressure p_m two approaches are investigated. Different approaches mean different variants of the equations for the throat pressure. Variant one is the easiest equation. This equation sets the mixture mass flow equal to the air mass flow

and neglects the gas mass flow into the venturi for the calculation of the throat pressure. Variant one therefore is an energy balance with the borders upstream of the venturi mixer and in the throat. A schematic view of the system boundaries of the energy balance is shown in figure 3.12.

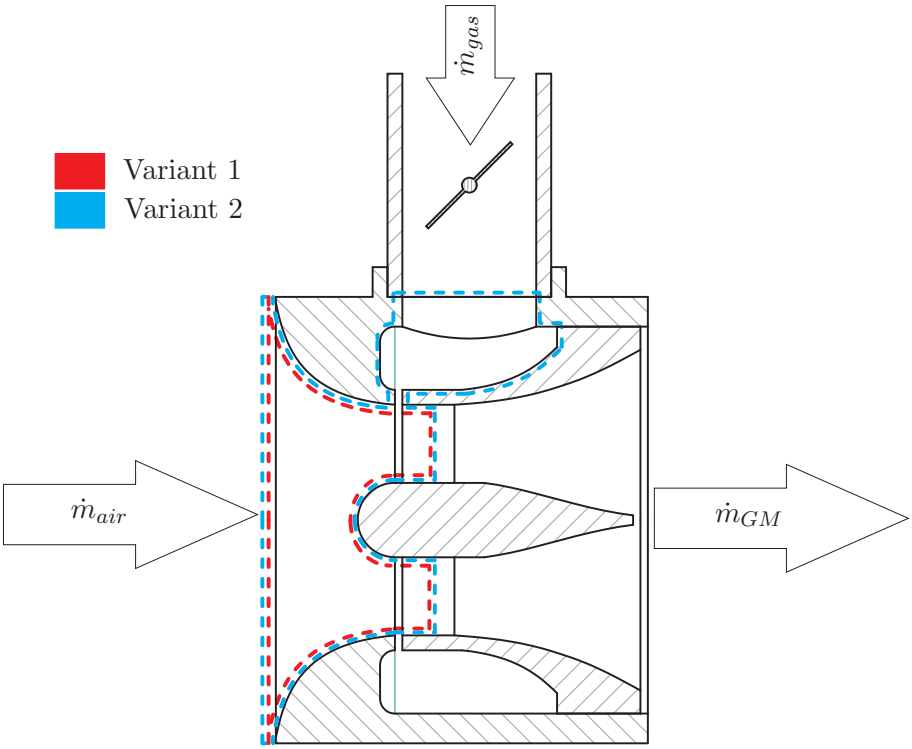

Figure 3.12: Scheme of the System Border of the Energy Equation

The energy equation of variant 1 leads to equation (3.15).

$$\left(\frac{1}{2}\underbrace{\left(\frac{\dot{m}_{GM}\,R_{s,air}\,T_1}{p_1\,A_1}\right)^2}_{v_{air,venturi}^2}+c_{p,air}\,T_1\right)=\left(\frac{1}{2}\underbrace{\left(\frac{\dot{m}_{GM}\,R_{s,air}\,T_m}{p_m\,A_m}\right)^2}_{v_m^2}+c_{p,air}\,T_m\right) \tag{3.15}$$

The throat temperature in this case is calculated by the transformed equation (2.7) to yield the isentropic equation (3.16).

$$T_m = T\left(\frac{p_m}{p}\right)^{\frac{\kappa-1}{\kappa}} \tag{3.16}$$

[54], where $T = T_1$, $p = p_1$ and $\kappa = \kappa_{air}$. Variant two considers the gas mass flow into the venturi. The energy balance of variant two follows to equation (3.17).

$$\dot{m}_{air,venturi}\left(\frac{1}{2}\underbrace{\left(\frac{\dot{m}_{air,venturi}\,R_{s,air}\,T_1}{p_1\,A_1}\right)^2}_{v^2_{air,venturi}}+c_{p,air}\,T_1\right)+$$
$$\dot{m}_{gas,venturi}\left(\frac{1}{2}\underbrace{\left(\frac{\dot{m}_{gas,venturi}\,R_{s,gas}\,T_G}{p_G\,A_G}\right)^2}_{v^2_{gas,venturi}}+c_{p,gas}\,T_G\right)= \tag{3.17}$$
$$\dot{m}_{GM}\left(\frac{1}{2}\underbrace{\left(\frac{\dot{m}_{GM}\,R_{s,mix}\,T_m}{p_m\,A_m}\right)^2}_{v^2_m}+c_{p,mix}\,T_m\right)$$

The throat temperature in variant two is calculated as mixed temperature, which is shown in equation (3.18).

$$T_{m,mix}=\frac{\dot{m}_{air,venturi}\,c_{p,air}\,T_{m,air}\;+\;\dot{m}_{gas,venturi}\,c_{p,gas}\,T_{m,gas}}{\dot{m}_{GM}\,c_{p,mix}}, \tag{3.18}$$

where the throat temperatures $T_{m,air}$ and $T_{m,gas}$ of the components are calculated using equation (3.16). For the calculation of $T_{m,air}$, the same values as for variant 1 can be used. For the temperature of the gas in the throat, the values $T = T_G$, $p = p_G$ and $\kappa = \kappa_{gas}$ are used. This is acceptable because of the assumption of an adiabatic venturi mixer. The mass flow of the air and the mass flow of the gas are also delayed with a PT1-element in order to avoid an algebraic loop. The used transfer function is

$$G\,(s)=\frac{1}{0.1\,s\;+\;1}. \tag{3.19}$$

Thus equations (3.15) and (3.17) are implicit and have to be solved by looking for the root of the equation in every time step. Implicit equations are not advantageous for simulations, because the simulation time lengthens dramatically. This is a challenge for the programming; in order to save simulation time intelligent solving algorithms have to be used.

In the model, three different programming approaches are developed and compared with each other:

- Implicit equation solver with an S-Function environment
- Implicit equation solver with Matlab Simulink Algebraic Constraint Block
- Approximation of the throat pressure by using extrapolation

- The energy equation is modeled in such a way that the output is zero ($E_{in} - E_{out} = 0$) if p_m is equal to the searched value. By analyzing the relation between throat pressure and energy equation error and by varying p_m, a linear correlation can be found (figure 3.13). The slope of the line was identified as -0.9. Dividing the energy equation error value by 0.9 and adding the old value of p_m results in the first approximated value for p_m. Repeating the same procedure two more times results in the final value for p_m.

The advantage of the approximation of the throat pressure by using extrapolation is that in some special cases, which appear randomly, the result is more stable than the exact solution of the Matlab Simulink Algebraic Constraint Block. Using this block for the exact solution, it can happen that the pressure p_m jumps very quickly, because of the numerical stiffness of the system in combination with the numerical solving algorithms. This has a very bad influence on the controller. Furthermore, the iteration is a faster alternative to the exact solution calculated with an S-Function environment, which is also a stable solution in all cases. The approximation approach is therefore used in the simulation, because the error of the throat pressure is negligibly small, as can be seen for a load change of $P_{el} = 50kW$ in figure 3.14.

Inputs	
Pressure upstream of the venturi mixer:	p_1
Temperature upstream of the venturi mixer:	T_1
Pressure in the gas reservoir:	p_G
Temperature in the gas reservoir:	T_G
Mixture mass flow across the venturi mixer:	$\dot{m}_{GM}$
Air mass flow into the venturi mixer:	$\dot{m}_{air,venturi}$
Gas mass flow into the venturi mixer:	$\dot{m}_{gas,venturi}$
Outputs	
Throat pressure:	p_m
Parameters	
CSA upstream of the venturi:	$A_1 = 0.07069\ m^2\ (D_1 = 300mm)$
CSA of the Zeppelin:	$A_z = 0.00196\ m^2\ (D_z = 50mm)$
CSA at the throat without Zeppelin:	$A_{m0} = 0.01887\ m^2\ (D_{m0} = 155mm)$
CSA at the throat:	$A_m = A_{m0} - A_z = 0.01691\ m^2$

Table 3.8: Throat Pressure Values

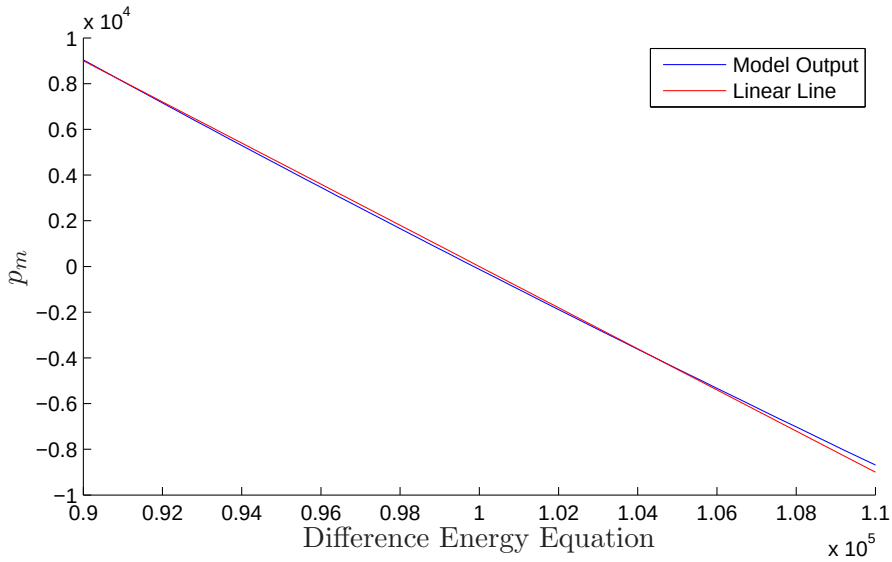

Figure 3.13: Influence of the Throat Pressure p_m on the Energy Equation Error Output by Varying p_m from 0.9 to 1.1bar

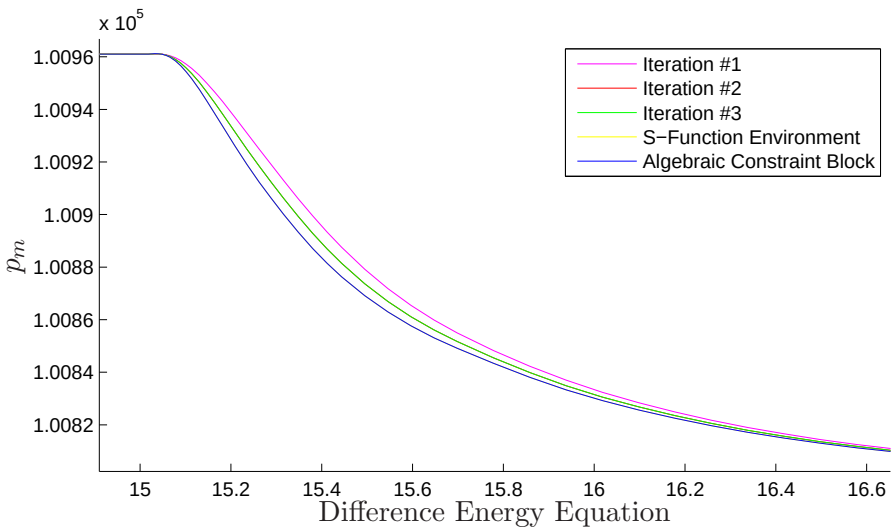

Figure 3.14: Absolute Value Difference of the Iteration and the Exact Solved Value

3.6.3 Gas Mass Flow Across Annular Passage

This section describes the calculation of the gas mass flow from the gas reservoir into the venturi mixer. The mass flow depends on the size of the gap of the annular passage, which is implemented as a secondary control variable. The mass flow is used as a feedback variable for the calculation of the throat pressure. Figure 3.15 shows the overview of the simulation block.

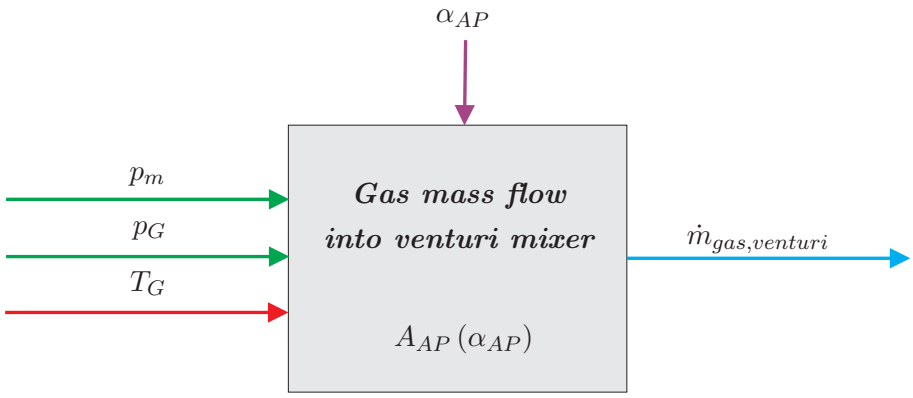

Figure 3.15: Scheme of the Gas Mass Flow Into the Venturi Mixer Block

The gas mass flow into the venturi is calculated with the equations (2.11), (2.12) and (2.13) as well as equation (2.8) and (2.9), in order to take into account the total states of the incoming fluid.

$$\dot{m}_{gas,venturi} = A_{AP}(\alpha_{AP}) \sqrt{\frac{2\kappa_{gas}}{\kappa_{gas}-1}} \frac{p_{G,t}}{\sqrt{R_{s,gas}\, T_{G,t}}} \beta\left(\frac{p_{G,t}}{p_m}\right) \tag{3.20}$$

The annular passage in this equation is the control variable of the gas mass flow into the throat. The total state in this equation is considered with a feedback of the result. The feedback is also a PT1-element, whose transfer function is given in equation (3.21).

$$G(s) = \frac{1}{0.1\, s + 1}. \tag{3.21}$$

The stationary gas mass flow across the butterfly valve and the stationary gas mass flow across the annular passage are the same. For a better overview, the variables of the model are summarized in table 3.9.

3.6.4 Concentration Vector

In section 1.3.7, advanced possibilities of the gas dosing system are mentioned. In order to prepare the system for a mixture of multiple components (e.g. different gases), the whole model provides the usage of a concentration vector, which has the form

Inputs	
Throat pressure of the venturi mixer:	p_m
Pressure in the gas reservoir:	p_G
Temperature in the gas reservoir:	T_G
Outputs	
Gas mass flow into the venturi mixer:	$\dot{m}_{gas,venturi}$
Parameters	
Gap of the annular passage:	α_{AP} (mm)

Table 3.9: Gas Mass Flow Across Annular Passage Values

$$\begin{bmatrix} \text{Oxygen mass fraction} \\ \text{Inert gas mass fraction} \\ \text{Methane mass fraction} \end{bmatrix}. \tag{3.22}$$

In all blocks except this block, the concentration vector is not manipulated and just fed through without any change. The major advantage of this approach is that multiple gas dosing systems can be arranged in a row and at the end one value for the gas mass is given. Another advantage is that at every point of the simulation the concentration of the mixture is known. For this investigation, the concentration vector plays only a minor role. Figure 3.16 shows an overview of the simulation block.

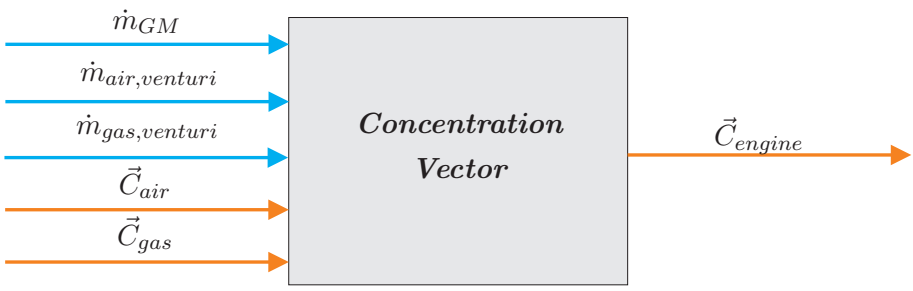

Figure 3.16: Scheme of the Concentration Vector Block

The defined variables of this block are summarized in table 3.10. Depending on the mass fractions of the air and the gas, the final concentration of the mixture is calculated with equation (3.23). It is assumed that at the end of the venturi mixer, the mixture is homogeneous and there is no reaction of the fluids with each other (ideal mixture of the gases) [54].

$$\vec{C}_{engine} = \frac{1}{\dot{m}_{GM}} \left(\vec{C}_{air}\, \dot{m}_{air} + \vec{C}_{gas}\, \dot{m}_{gas} \right) \tag{3.23}$$

3.6.5 Mixture Temperature

The mixture temperature block is used to calculate the output temperature of the mixture of the venturi mixer. The simulation block is shown in figure 3.17 and in table 3.11 all variables are summarized.

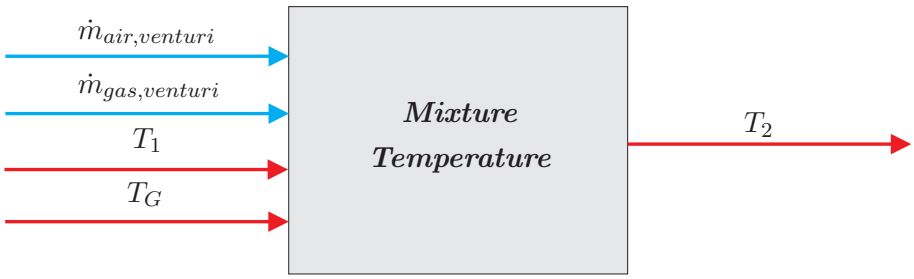

Figure 3.17: Scheme of the Mixture Temperature Block

It is assumed that the mixture temperature of the mixture mass flow only depends on the mass fractions of the air and gas mass flow. The mixture temperature of ideal gases can therefore be calculated with equation (3.24). This simple approach also assumes an adiabatic system.

$$T_2 = \frac{\dot{m}_{air,venturi}\, c_{p,air}\, T_1 \; + \; \dot{m}_{gas,venturi}\, c_{p,gas}\, T_G}{\dot{m}_{air,venturi}\, c_{p,air} \; + \; \dot{m}_{gas,venturi}\, c_{p,gas}} \tag{3.24}$$

3.6.6 Mixture Characteristics

This section shows the calculation of the characteristic values of the air-gas mixture. Depending on the mass fraction of the gas, the characteristic values of the mixture can vary. This has serious influence on the behavior of the venturi mixer. As observed in the other simulation blocks, the characteristic values are dependent on the values of the mass flows, which need the characteristic values for the calculation. In order to avoid this algebraic loop, all the calculations of the characteristic values are delayed with a PT1-element with a time constant of $0.1sec$. Figure 3.18 shows the overview of the mixture characteristic block. Table 3.12 provides the overview of used variables.

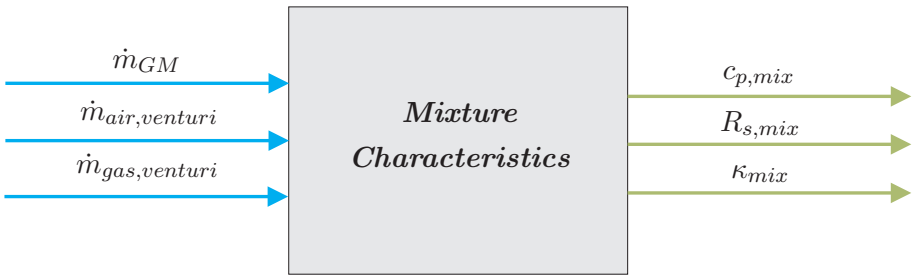

Figure 3.18: Scheme of the Mixture Characteristics Block

Inputs	
Mass flow across the venturi mixer:	$\dot{m}_{GM}$
Air mass flow into the venturi mixer:	$\dot{m}_{air,venturi}$
Gas mass flow into the venturi mixer:	$\dot{m}_{gas,venturi}$
Air concentration vector:	$\vec{C}_{air} = \begin{bmatrix} 0.2316 \\ 0.7684 \\ 0 \end{bmatrix}$
Gas concentration vector:	$\vec{C}_{gas} = \begin{bmatrix} 0 \\ 0.05 \\ 0.95 \end{bmatrix}$
Outputs	
Concentration vector from the venturi mixer:	$\vec{C}_{engine}$

Table 3.10: Concentration Vector Values

Inputs	
Air mass flow into the venturi mixer:	$\dot{m}_{air,venturi}$
Gas mass flow into the venturi mixer:	$\dot{m}_{gas,venturi}$
Air reservoir temperature:	T_1
Gas reservoir temperature:	T_G
Outputs	
Temperature downstream of the venturi mixer:	T_2

Table 3.11: Mixture Temperature Values

Inputs	
Mixture mass flow across the venturi mixer:	$\dot{m}_{GM}$
Air mass flow into the venturi mixer:	$\dot{m}_{air,venturi}$
Gas mass flow into the venturi mixer:	$\dot{m}_{gas,venturi}$
Outputs	
Specific heat capacity of the mixture:	$c_{p,mix}$
Specific gas constant of the mixture:	$R_{s,mix}$
Isentropic coefficient of the mixture:	κ_{mix}

Table 3.12: Mixture Characteristics Values

In the following paragraphs, the calculations of the mixture characteristics are shown. The base for the calculation of the mixture gas constant is the molar mass of the mixture $\mathcal{M}_{mix}$. Equation (3.25) provides an equation for the calculation of $\mathcal{M}_{mix}$.

$$\frac{\dot{m}_{GM}}{\mathcal{M}_{mix}} = \frac{\dot{m}_{gas}}{\mathcal{M}_{gas}} + \frac{\dot{m}_{air}}{\mathcal{M}_{air}}. \tag{3.25}$$

The specific gas constant of the mixture follows then with equation (3.26).

$$R_{s,mix} = \frac{\mathcal{R}}{\mathcal{M}_{mix}} \tag{3.26}$$

For the calculation of the ratio of specific heats, the molar fractions y_i of the components are needed. The molar fractions can be calculated with equation (3.27).

$$\mathcal{M}_{mix} = y_{gas}\,\mathcal{M}_{gas} + y_{air}\,\mathcal{M}_{air} = y_{gas}\,\mathcal{M}_{gas} + (1 - y_{gas})\,\mathcal{M}_{air} \tag{3.27}$$

The calculated molar fractions are used to calculate the ratio of specific heats κ_{mix}, which follows in equation (3.28).

$$\kappa_{mix} = \frac{\sum_i \frac{y_i\,\kappa_i}{\kappa_i - 1}}{\sum_i \frac{y_i}{\kappa_i - 1}} = \frac{\frac{y_{gas}\,\kappa_{gas}}{\kappa_{gas}-1} + \frac{y_{air}\,\kappa_{air}}{\kappa_{air}-1}}{\frac{y_{gas}}{\kappa_{gas}-1} + \frac{y_{air}}{\kappa_{air}-1}}. \tag{3.28}$$

The last unknown characteristic value which is required is the isobaric specific heat capacity $c_{p,mix}$. It is calculated with equation (3.29).

$$c_{p,mix} = \frac{\kappa_{mix}}{\kappa_{mix} - 1} R_{s,mix}. \tag{3.29}$$

3.7 Engine Model

For the simulation of an active gas dosing system, an engine model is required in order to show the influence of the gas dosing system on the engine. The modeling of an engine is not part of this work, so the engine model is implemented as a blackbox S-Function in Matlab Simulink. The engine model simulates a GE[2] Jenbacher $J320\ GS$ gas engine [2] with an electrical power of $1065kW$. The model includes a turbocharger and a recirculation system. The nominal speed of the engine is held by a speed controller (SC) at $n_{set} = 1500rpm$. The generator (GEN) controls the engine load P_{eng} and includes a load reduction function which lowers the engine load if the nominal speed of the engine drops below $1470rpm$. This should help the engine to reach the nominal speed faster after a load change. Furthermore the model uses equation (3.30)

[2]General Electrics (GE), http://www.ge-energy.com/, http://www.gejenbacher.com/

$$P_{eng} = \eta_{eng}\, H_i\, \dot{m}_{eng}\, \frac{1}{1 + \lambda\, L_{st}}, \tag{3.30}$$

with a fixed value $L_{st} = L_{st,eng} = 17.2$ for the calculation of the lambda value of the engine, which means that no combustion model is included in the engine model. This equation is therefore not exactly realistic, but it is a good approximation for the steady state lambda value. The dead time of the lambda value change is not considered and is therefore investigated in section 3.8. The characteristic consumption of the engine is given as $352\,kg/h$ biogas at a calorific value of $5kWh/Nm^3$ and as $176\,kg/h$ natural gas at a calorific value of $10kWh/Nm^3$. The Simulink model block is shown in figure 3.19.

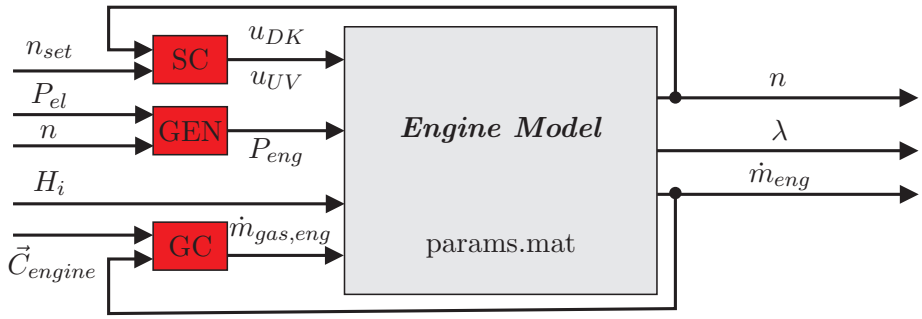

Figure 3.19: Scheme of the Engine Model

The model is able to simulate a load rejection as well as a load change. The input for a load change or rejection can be simulated by changing the input P_{el}. Both engine valves are controlled by the speed controller and are not changed or manipulated. The calorific value H_i of the gas can be changed with the corresponding input into the model. The engine mass flow $\dot{m}_{eng}$, which is an output of the model, describes the complete mass flow into the engine. The input of the gas mass flow $\dot{m}_{gas,eng}$ is calculated with equation (3.31), where the concentration vector $\vec{C}_{engine}$, which is an output of the mixture reservoir, is used.

$$\dot{m}_{gas,eng} = \vec{C}_{engine}\, \dot{m}_{eng} \tag{3.31}$$

For a better overview, all inputs and outputs as well as the parameters of the model are summarized in table 3.13.

3.8 Engine Dead Time

In general, the dead time of the λ-signal is basically dependent on the engine speed. In the case of a stationary gas engine, the engine speed is controlled at the value of $1500rpm$. This is required for the generator which should have, as far as possible, constant rotational speed. The dead time of the changes in the λ-value therefore just depends on the mass

Inputs	
Set point rotational speed:	$n_{set} = 1500rpm$
Aperture engine throttle:	u_{DK}
Aperture recirculation system:	u_{UV}
Electrical load of the engine:	P_{el} $(300kW - 600kW)$
Load of the engine:	P_{eng}
Calorific value of the gas:	H_i $(32MJ/kg - 48MJ/kg)$
Concentration vector from the mixture reservoir:	$\vec{C}_{engine}$
Gas mass flow into the engine:	$\dot{m}_{gas,eng}$
Outputs	
Rotational speed:	n
Lambda value of the engine:	λ
Engine mass flow:	$\dot{m}_{eng}$
Parameters	
Stoichiometric air requirement:	$L_{st,eng} = 17.2$
Engine efficiency:	$\eta_{eng} = 0.353$
Speed Controller:	SC
Gas mass flow Calculation:	GC
Generator (Engine Load Control):	GEN
Parameters of the engine:	*params.mat*

Table 3.13: Engine Values

flow across the engine, which in turn is dependent on the different engine pressures like loading pressure or intermediate pressure. No values of the dead time of the used engine are available, which makes it necessary to look at different approaches to calculating the engine dead time in the following paragraph.

[33] discusses the effect of dead time behavior in more detail. The value of the dead time is given with $T_{dead} = 0.6 - 0.4sec$. [31] specifies the dead time as $T_{dead} = 0.1sec$ and [30] specifies it as $T_{dead} = 0.2sec + \tau_{Lambda-Sensor} \approx 0.25$, where $\tau_{Lambda-Sensor}$ is the time constant of the lambda sensor. All of these values are for different engines. None of the sizes fit the size of the engine which is used in this investigation. [51] gives an equation for the approximation of the dead time (equation (3.32)), which includes the engine rotational speed n, volumes of the manifolds in front of and after the engine V_i, the density of the fluids ρ_i and the mass flows $\dot{m}_i$. This equation has been used for the calculation of the dead time in [32] as well as in this investigation. The dead time is therefore not fixed in the model, but compared to the values above, the range of dead times in equation (3.32) lies between them.

$$T_{dead} = \frac{120}{n} + \frac{\rho_{Mixture} V_{Intake\ Manifold}}{\dot{m}_{Mixture}} + \frac{\rho_{Exhaust} V_{Exhaust\ Manifold}}{\dot{m}_{Exhaust}} \tag{3.32}$$

3.9 Matlab Implementation

In the following paragraphs, the basic points of the implementation in Matlab Simulink will be given. As mentioned in section 3.5, the meaning of Mass Flow Giving (MFG) and Pressure Giving (PG) elements should be explained first. Simulation blocks (SB) which calculate a mass flow are called mass flow giving. Simulation blocks which calculate a pressure are called pressure giving.

The main problem of the system is that ultimately the complete model structure depends basically on the engine mass flow $\dot{m}_{eng}$. This makes the complete system extremely stiff in the numerical meaning. In order to solve the problem, an MFG SB and a PG SB are placed. This can also be seen in figure 3.1, where the colors as well as the forms of the surrounding frame are referring to this structure. With this configuration of the simulation blocks, the numerical stiffness of the system can be reduced and simulation time can be saved. Another advantage of this constellation is that the state variables are given in each part of the simulation.

Another approach to reducing the numerical stiffness is given in [55]. By raising the volumes of the reservoirs, the numerical stiffness of the whole system can also be reduced. A disadvantage of this solution is that the delay of the mass flow in the reservoirs rises with the rising volume. In this case, the values could be held at a realistic level.

Simulation Starting Conditions

In the whole system, many PT1-elements are used. The default initial value of these blocks is zero, which leads to completely wrong initial conditions. In order to minimize the problems at the start of the simulation, the initial conditions, except the initial conditions of the controllers, are set to the steady state conditions at a load of $P_{el} = 300kW$. The start of the simulation at full load (e.g. $P_{el} = 600kW$) can therefore lead to unstable behavior of the whole system. This must be considered for a full load simulation (e.g. usage of a ramp load change with a slope of $10kW/sec$).

Chapter 4

Control Strategies of the Gas Dosing System

In this chapter, the controller design is described. The basic problem of the design is the nonlinear behavior of the model, the dead time of the system and the unmeasurable calorific value. In order to regard non-linearity, linearizations at different operation points are used to design the controllers (see section 4.1). For the implementation (see section 4.3), the principle of Gain-Scheduling is used to switch between the different operation points/controllers (see section 4.4).

The real disturbances of the system are the gas pipe pressure and gas pipe temperature as well as the unmeasurable calorific value of the gas. For the compensation of the pressure and temperature disturbances, static feedforward controllers are used in all control strategies, as explained in section 4.5. The disturbances induced by load changes and load rejections are compensated with the gain-scheduling. The calorific value cannot be compensated by a feedforward strategy, because no online measurement is available. Section 4.6 explains the problem of the calorific value measurement as well as the stoichiometric air requirement, which is closely connected with the calorific value, in more detail.

4.1 Linearization

The linearization of a model can be very complicated if it is to be analytical. In this case, it is advantageous to use the numerical linearization function of the 'Simulink Control Design Toolbox'. This toolbox offers two different linearization methods:

- Block by Block Linearization
- Numerical Perturbation Linearization

On the one hand, the main disadvantage of the block-by-block method is that S-Functions (e.g. the engine model) are not linearizable. On the other hand, the numerical perturbation method is very sensitive and can lead to unstable linearized transfer functions.

Avoiding the disadvantages, both methods are used for linearization of the plant. In order to improve the performance of the methods, the options in table 4.1 are used.

- `SampleTime` is set to 0
- `RateConversionMethod` is set to *tustin*
- `NumericalPertRel` is set to $1 \cdot 10^{-14}$

Table 4.1: Options used for the Linearization

The difficulties of linearizing models with dead time are avoided, because no combustion model or dead time are used in the engine model (see section 3.7 and section 3.8). This leads to a linearization, which is not influenced by these difficulties. In table 4.2 different combinations of linearizations of the model are shown, which are used for the different controller designs.

Inputs	Outputs
$\dot{m}_{gas}$	
α_{BV}	$\dot{m}_{gas}$
α_{AP}	λ
p_{G0}	λ_{BV}
T_{G0}	

Table 4.2: Linearization Combinations

The result of the linearization in Simulink is a transfer function in state-space (SS) representation. The numerical linearization in Simulink does not regard the order of the transfer function, which means that it cannot decide between important and unimportant states. The result is a very high order transfer function, which is higher than 20 in this case. For a reasonable design of the controller, the order must be reduced; thus is described in section 4.2.

4.2 Model Reduction

The linearized transfer functions, with appearing transfer function orders above 20, make a model reduction indispensable. This reduction is needed in order to design controllers

with the assistance of automated tuning algorithms, which are provided in the different Matlab packages (e.g. SISOTOOL).

First, the linearized system must be balanced with the Matlab command `balreal`, in order to get information about the independent states of the linearized model. The model reduction can then be progressed with the Matlab command `modred`. The output of the model can additionally be checked with the command `minreal` in order to cancel pole-zero pairs in the transfer functions. The finally received transfer functions are the base for the controller design. The best reduced model order is found to be 4.

4.3 Controller Implementation

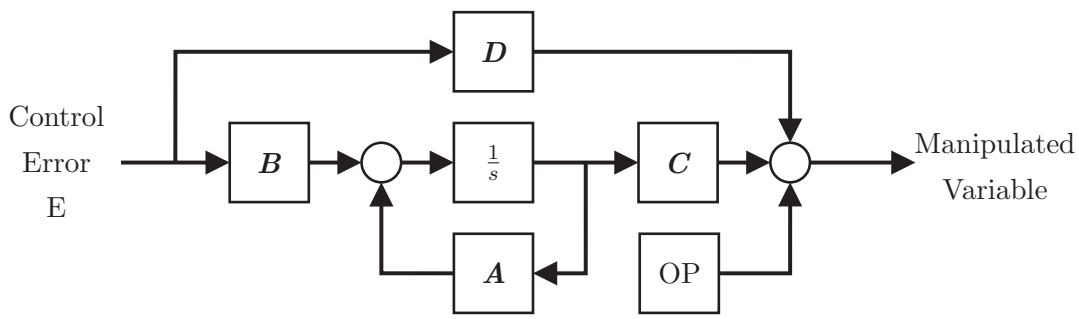

Figure 4.1: Scheme of the Controller Implementation

The easiest way to implement a controller in Simulink is to use the LTI-Model block. In this case, a gain-scheduling controller is used in the implementation, where the controller gains change with the operation point (see section 4.4). The LTI-Model block does not support changing controller transfer functions and therefore a special solution is needed. The easiest way is to generate an LTI-block for each controller and switch the output with a multiport switch block. Another way is to implement the controller as an SS representation. The advantage of the SS representation is that there is no limitation to the controller structure and the output of the linearization need not be converted into SS representation. Another advantage is that matrices can be stored in lookup tables and can be automatically reloaded if the operation point changes, which makes an easy manipulation of the controller values possible. The system is therefore built as shown in figure 4.1. OP in the figure symbolizes the lookup table of the operation point value, which must be added due to linearized SS representation matrices. The important points and problems of lookup tables are described in more detail in section 4.4.

4.4 Gain-Scheduling

A very common way to make linear controllers usable for nonlinear systems is called Gain-Scheduling. Gain-Scheduling uses lookup tables to adjust the controller parameters with

changing operation conditions. Lookup tables are blocks in Simulink which change their output with changing input conditions. The switching criteria can be modified in these blocks, but the biggest problem of using lookup tables cannot be ignored - the point of switching. In the case of the gas dosing system, the operation point is defined by the requested electrical load P_{el} of the generator, which is driven by the gas engine. The output of the lookup tables is therefore dependent on the change of the electrical load of the generator. In the simulation, the load is also the input for the test cycle, which leads to step changes of the controller matrices and furthermore to step changes in the controller gains. In reality the electrical load can change very fast, which makes a solution for the switching problem necessary.

The point under investigation is the sequence of the matrix values over the different operation points. After the design with the SISOTOOL in Matlab, the changes in this sequence can be very big. These changes mainly follow from the linearized transfer functions, which cannot be influenced at the time of the linearization. The stepplot of the linearized model does not show any big differences and the SS representation of the linearized model is a transfer function with an order of 4, which means that a manipulation of the matrix values is almost impossible.

The only way to correct these big differences is to manipulate the matrices of the controllers. This can be done, because the plant does not change as much as one might assume by looking at the matrices. In general, a PI-controller is sufficient for the gas dosing system, which leads to an SS representation order of 1.

After adjusting the matrix values, different approaches for the gain scheduling have been compared in order to find the best performance solution. In the following enumeration, the different methods are described briefly and sorted from the poorest to the best performance:

1. Matrix Delay Method
   - This method uses first order lag elements for the matrix values to damp the step change.
2. Output Interpolation Method
   - This method is a more complex one. Two controllers run parallel and their outputs are interpolated by using a window function.
3. Controller Matrix Interpolation Method
   - This method interpolates the single matrix values. This method is limited by the controller order because of the complexity, but it showed the best performance.

4.5 Feedforward Controller

As mentioned in the introduction of this section, a static feedforward controller is used in all controller strategies for the compensation of the measurable disturbances. The controller gain is basically calculated by the gain of the disturbance transfer function divided by the gain of the plant transfer function. Matlab provides the command `dcgain`, which calculates the static gain of a transfer function. This command is used in this investigation.

4.6 Calorific Value and Stoichiometric Air Requirement

The calorific value or the percentage of Methane in the gas can be measured with a gas-phase chromatograph, but such measurement devices are very expensive and not really practical for *online in the loop* usage. Alternatives [19, 42, 43, 52] for fields like this are still in development, as mentioned in section 1.3.3.

Another possible way to calculate the calorific value of the gas is given with equation (3.30). Transforming this equation yields equation (4.1).

$$H_i = \frac{P_{eng}}{\eta_{eng}\,\dot{m}_{gas}}. \tag{4.1}$$

η_{eng} is the efficiency of the engine, which should be known from the engine characteristics diagram. P_{eng} is the engine power and $\dot{m}_{gas}$ is the gas mass flow into the engine, which are both normally measured.

For a compensation of a calorific value change, this value must be calculated on line. One problem of the calculation is that the gas mass flow $\dot{m}_{gas}$ as well as the engine power P_{eng} are able to change very fast, which leads to a very fast changing calculated calorific value. Assuming that in reality the calorific value is changing very slowly, the calculated calorifc value can be damped with a first-order lag element. The chosen time constant in the simulation is $15sec$, because this time constant has the best damping to steady state performance.

The calculation of the calorific value H_i is actually not necessary for control strategies which control lambda. Control strategies like the ratio control strategy (see section 4.7.2), which do not use a feedback of the engine (e.g. lambda), are need to be updated, because otherwise the stationary control error is not equal to zero.

The important variable in this case is the stoichiometric air requirement of the gas. It is possible to calculate this value exactly if the composition of the gas is known. Assuming that the main component of natural gas is Methane, which has a calorific value of $50MJ/kg$, it follows that natural gas with $80mass\%$ Methane has a calorific value of approximately $40MJ/kg$, when neglecting other burnable substances. Another known value

is the stochimetric air requirement of Methane $L_{st,Methane} = 17.3kg\ air/kg\ CH_4$, a calculation which is shown in section 2.9. Dividing this value by the assumed $80mass\%$ Methane in the gas leads to a stoichiometric air requirement of $L_{st,NG} = 13.84kg\ air/kg\ gas$.

In the model, a lookup table is used for the correlation between calorific value and stoichiometric air requirement. This has the advantage that the stoichiometric air requirement for different ranges of applications can be calibrated. In order to be able to compare the simulation results, the stoichiometric air requirement of the calorific value of $40MJ/kg$ is set to 17.2 with respect to the engine model, where $L_{st,eng} = 17.2$.

4.7 Controller

In the following sections, the different controller designs are described. The performance of the different controllers and their interpretation are shown in section 5.

4.7.1 Performance Reference - Static Venturi Mixer

Each model needs to be validated in order to check how close it comes to reality. For this investigation, no measurements of the performance of static venturi mixers which are commonly used are available. Therefore, the idea is to use the output of the engine to calculate the gas mass flow, which yields the lambda set point of 1.7, and feed it back to the gas mass flow input of the engine. In order to avoid an algebraic loop, the gas mass flow is delayed with the same PT1-element as in equation (3.6). In this assumption, the complete dynamic behavior of a static venturi mixer as well as the pressure and temperature influence of the gas are neglected.

4.7.2 Ratio Control Strategy

The idea of the ratio control strategy is to keep the air/gas ratio constant. With measurements of the mixture mass flow as well as the gas mass flow across the butterfly valve in the gas dosing system, the lambda value of the mixture can be calculated and kept at the set lambda value of 1.7. Figure 4.2 shows an overview of the control principle. FT specifies the measurement devices of the system, FY presents the calculation of the lambda value λ_{BV} with equation (4.2) and C is the controller.

The block diagram of the controller is shown in figure 4.3. The manipulated variable λ_{BV} is calculated with equation (4.2).

$$\lambda_{BV} = \frac{\dot{m}_{GM} - \dot{m}_{gas}}{\dot{m}_{gas}\, L_{st}}, \tag{4.2}$$

where L_{st} is the variable stoichiometric air requirement, as described in section 4.6. $\dot{m}_{GM}$ and $\dot{m}_{gas}$ are the mixture mass flow across the venturi mixer and the gas mass flow across

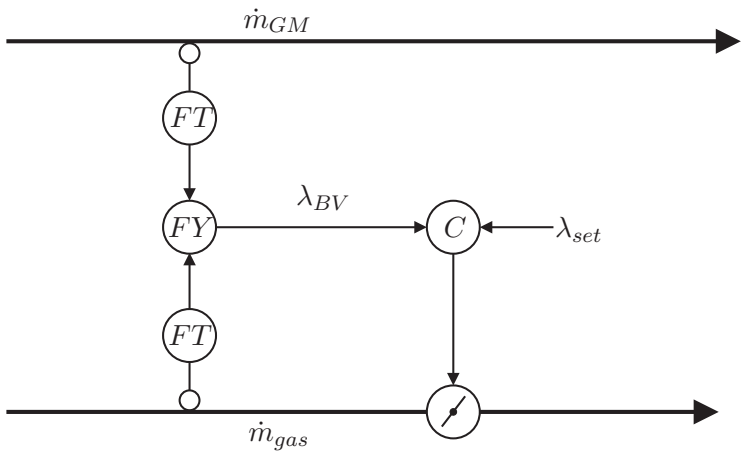

Figure 4.2: Principle of Ratio Control

the butterfly valve respectively.

For this control strategy the block-by-block linearization is used, because there is no S-Function in this part of the plant. The input of the linearization of the plant transfer function G_P is set to α_{BV} and the output is set to λ_{BV}. G_P is used for the controller design as well as for the calculation of the feedforward controller gains. The inputs of the disturbance transfer functions $G_{FC,1}$ and $G_{FC,2}$ are set to p_{G0} and T_{G0} and the output of both is also set to λ_{BV}. Using the SISOTOOL Toolbox of Matlab, the optimal structure of the controller G_C is found to be a PI-structure. *Noise* summarizes all other disturbances as well as the noise in the measurements.

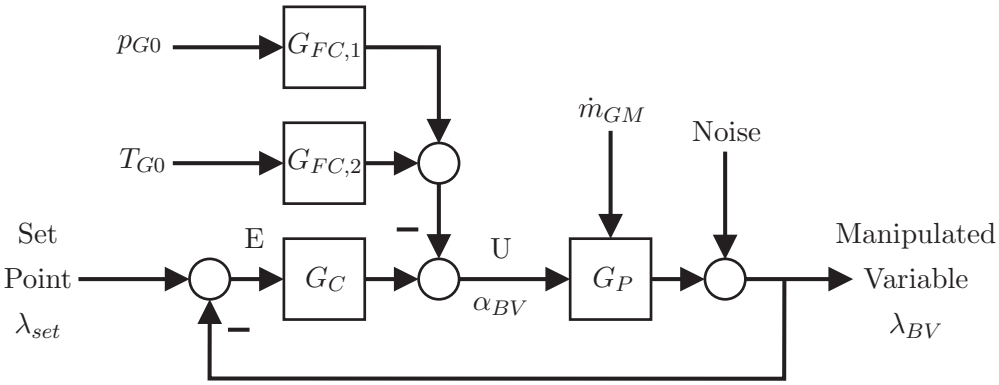

Figure 4.3: Scheme of the Ratio Controller

4.7.3 Mass Flow Control Strategy

The mass flow control strategy is the easiest of all strategies under investigation. The aim of the mass flow control is to control the value of the gas mass flow into the engine, which is a function of the mixture mass flow across the gas dosing system. The block diagram of the controller is shown in figure 4.4.

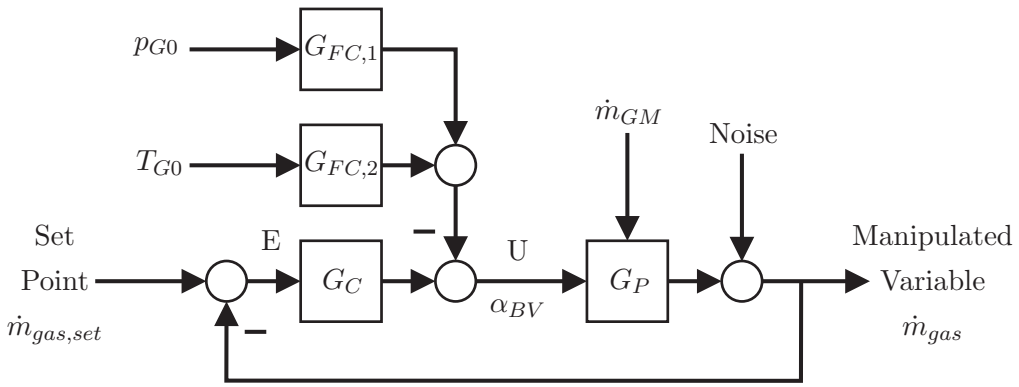

Figure 4.4: Scheme of the Mass Flow Controller

The gas mass flow set point is calculated with

$$\dot{m}_{gas,set} = \frac{\dot{m}_{GM}}{1 + L_{st}\,\lambda_{set}} \tag{4.3}$$

where L_{st} is again the calculated stoichiometric air requirement as described in section 4.6, λ_{set} is the lambda set point and $\dot{m}_{GM}$ is the mixture mass flow.

For the controller design with SISOTOOL, the block-by-block linearization of the plant transfer function G_P with the input α_{BV} and the output $\dot{m}_{gas}$ is used. The plant in this case is only the butterfly valve. The structure of the controller G_C has turned out to be a PI-structure as the structure in the ratio control strategy. The static feedforward controllers $G_{FC,1}$ and $G_{FC,2}$ are calculated with the linearized disturbance transfer functions of the plant by setting the linearization inputs to p_{G0} and T_{G0} and setting the linearization output to $\dot{m}_{gas}$. *Noise* summarizes all other disturbances.

4.7.4 Smith Predictor Control Strategy

The principle of the smith predictor control strategy has been developed for systems with pure dead time, e.g. belt conveyor, in order to raise the performance of such control systems. The lambda value of the gas engine is delayed due to transport delays of the exhaust gas from the cylinder to the oxygen (lambda) sensor as well as to a reaction time of the sensor itself. Figure 4.5 shows the principle block diagram of a smith predictor controller.

The plant in this control strategy includes the engine model, which implies the dead time of the lambda value. The plant is therefore linearized with the numerical perturbation method, with α_{BV} as set input and λ as set output. There are no difficulties with the linearization of the plant, because the dead time of the lambda value is implemented as an external block, which is neglected at the linearization. The resulting plant transfer function G_M, which does not include the lambda dead time is used for the controller design with SISOTOOL. The controller G_C has turned out to be a PI-structure. In figure 4.5, $e^{-s\,T_{dead}}$ symbolizes the pure dead time of the plant, which, together with the plant transfer

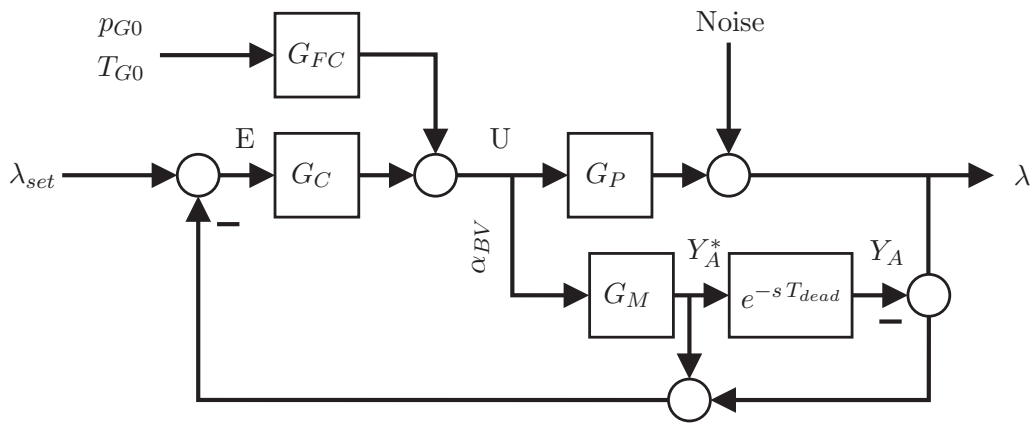

Figure 4.5: Scheme of the Smith Predictor Controller

function G_M, yields the plant transfer function G_P. The static feedforward controller gains are again calculated with the disturbance transfer functions, which are linearized with the inputs p_{G0} and T_{G0} to the output λ. G_{FC} summarizes both feedforward controllers. *Noise* summarizes again all other disturbances (e.g. sensor noise).

The plant model G_M is very important for the performance of the control system. In this case the gas engine model is also speed-controlled, which leads to changing transfer functions when the apertures of the engine valves are different to those of the engine at the linearization point. This is one very big disadvantage of this control scheme when adapting it to the control of a gas dosing system. The influence is described in more detail in section 5.6

4.7.5 Cascade Control Strategy

This control strategy is developed in order to improve the closed-loop disturbance control performance. The controller consists of an outer and an inner loop. It is an advantage if the inner loop plant is faster than the outer loop plant. Figure 4.6 shows the block diagram of a cascade controller.

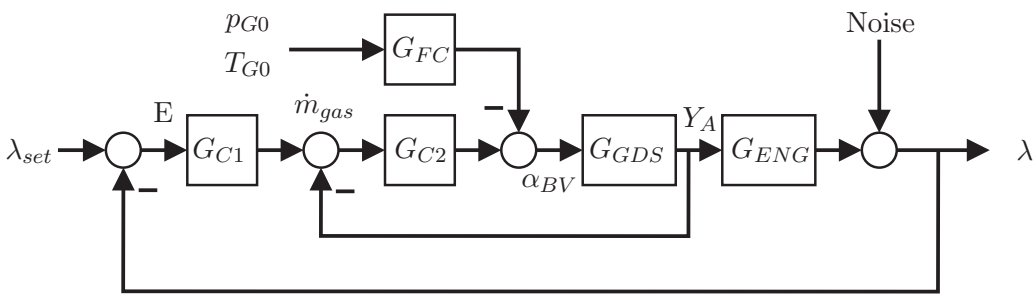

Figure 4.6: Scheme of the Cascade Controller

The control variable of the outer loop is the lambda value, which is controlled by the controller G_{C1} and uses the outer loop plant G_{ENG}, which is the engine. The input of the

engine is the gas mass flow $\dot{m}_{gas}$, which is simultaneously the input for the linearization. The output λ of the outer loop plant is also used as output for the linearization. In this case, the numerical perturbation method is used because of the engine model. The inner loop plant G_{GDS} is therefore the gas dosing system. In this case the block-by-block method is used for the linearization. The input is set to α_{BV} and the output is set to $\dot{m}_{gas}$. The inner loop is controlled by the controller G_{C2}. It is furthermore practical if the inner loop has faster response times than the outer loop, which is the case in this constellation of the plant. The disturbance transfer functions are linearized with the block-by-block method because the disturbances only influence the inner control loop. The used inputs are again p_{G0} and T_{G0} and the used output in this case is $\dot{m}_{gas}$. The linearized disturbance transfer function is again used for the static feedforward controller gain calculation. G_{FC} again summarizes both controllers and *Noise* summarizes all other disturbances.

For the design of the controllers G_{C1} and G_{C2}, two approaches are tried out in SISOTOOL:

- SISOTOOL using the cascade structure
- Separated design of the inner and outer loop using SISOTOOL
    1. Designing the inner loop
    2. Calculating the plant transfer function of the outer loop
    3. Designing the outer loop

A partly stable solution for the stand-alone cascade controller case can only be found with the SISOTOOL cascade structure design. The resulting controller structure is a P-controller for the inner loop and a PI-controller for the outer loop. For the combined control strategy the second method is used in order to optimize the main control loop for the gas mass flow. The resulting controller structure for the separated design is a PI-PI combination, which leads to an unstable controller in the stand-alone case.

4.7.6 Combined Control Strategy

The idea of the combined control strategy is to merge the advantages of the other control strategies described in section 4.7.3-4.7.5. The block diagram of the merged system is depicted in figure 4.7. In this figure, G_{C1}, G_{C2}, G_{FC}, G_{GDS} and G_{ENG} (including the dead time of the lambda value) are the same transfer functions as described in the cascade control strategy section 4.7.5. G_M and $e^{-sT_{dead}}$ are described in the smith predictor control strategy section 4.7.4. G_{C3} is an open loop controller, which calculates the main part of the set point of the gas mass flow of controller G_{C2}. Equation (4.3) is used for this calculation. L_{st} in the equation is fixed to 17.2, which is the basic difference to the mass flow control strategy described in section 4.7.3. In order to give a better overview, table 4.3 summarizes the used controller structures.

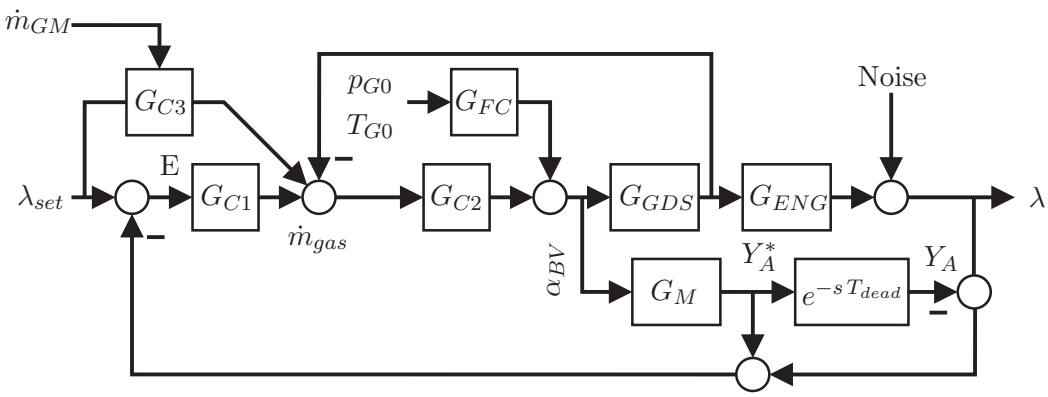

Figure 4.7: Scheme of the Combined Controller

Controller	***Structure***
G_{C1}	PI
G_{C2}	PI
G_{C3}	P

Table 4.3: Controller Structures used in the Combined Control Strategy

4.7.7 More Combinations of Control Strategies

The following two controller combinations are also designed, but the results are not even slightly stable. Therefore, they are only mentioned, but not described in this section. The controller parameters for the controller combinations are used from the previously described controllers.

- Cascade - Smith Predictor Controller
- Mass Flow - Cascade Controller

Chapter 5

Results and Performance

In this chapter, the results of the simulations are presented and the performances of the different controllers are compared. It is shown where the difficulties of the design of the controllers are and which factors are limiting the system. The limits of the system are therefore defined for the control based case as well as for the model of the gas dosing system.

In the following sections, different disturbances of the system are used to show the performance of the different controllers. In these cases they are based on the lower load level $300kW$ and the higher load level $600kW$ to give a better overview of the load range of the system. Later in the chapter, the set point change performance, the influence of the speed controller and of the linearized engine model are discussed.

The first subplots of the result figures show the different disturbances. The second subplots show the lambda values and the third subplots show the $\alpha_{BV,act}$ value. The fourth subplots in some of the result figures show different system values for a deeper understanding of the system. The noise of the oxygen sensor is implemented as a band limited white noise with a range of $\pm 10\%$ of the lambda value, but is not used in the following figures.

5.1 Limits of the System

The limits of the model depend on the stability of the model. As described in section 3.9, the problem is the stiffness of the system. This stiffness also results from the mass flow equation (2.11), where small changes of Π close to 1 create big differences in the mass flow. In the case of low engine load levels, the mixture mass flow across the gas dosing system is small and therefore the pressure ratios Π are close to 1. This leads to very small simulation steps, which furthermore end in an abort of the simulation in Matlab. In order to simulate small engine loads, the geometry of the venturi mixer must be changed, which will raise the flow velocities in the system and also the pressure differences in the system. Therefore, the used engine load P_{el} is limited to $300 - 600kW$ for the given geometry (see

section 3.2).

Another possibility, which is not investigated in this work but should be mentioned, is to change the annular passage by using a second actor. By changing the annular passage, the pressure difference between the throat and the gas reservoir also changes, which leads to a better pressure range for the butterfly valve. The advantage of this is that the gas dosing system can be used for a wider range of engine loads, so that the usage of two different venturi mixers for part load and full load is not necessary.

5.2 Result and Performance at a Load Change

The load change is the most interesting result of this investigation. Load changes appear very often if the engine is used in isolated operation. The used range of the engine is between $300kW$ and $600kW$. For the simulation, therefore, a step input of $60kW$ is used, which is a change of 20% of the load range.

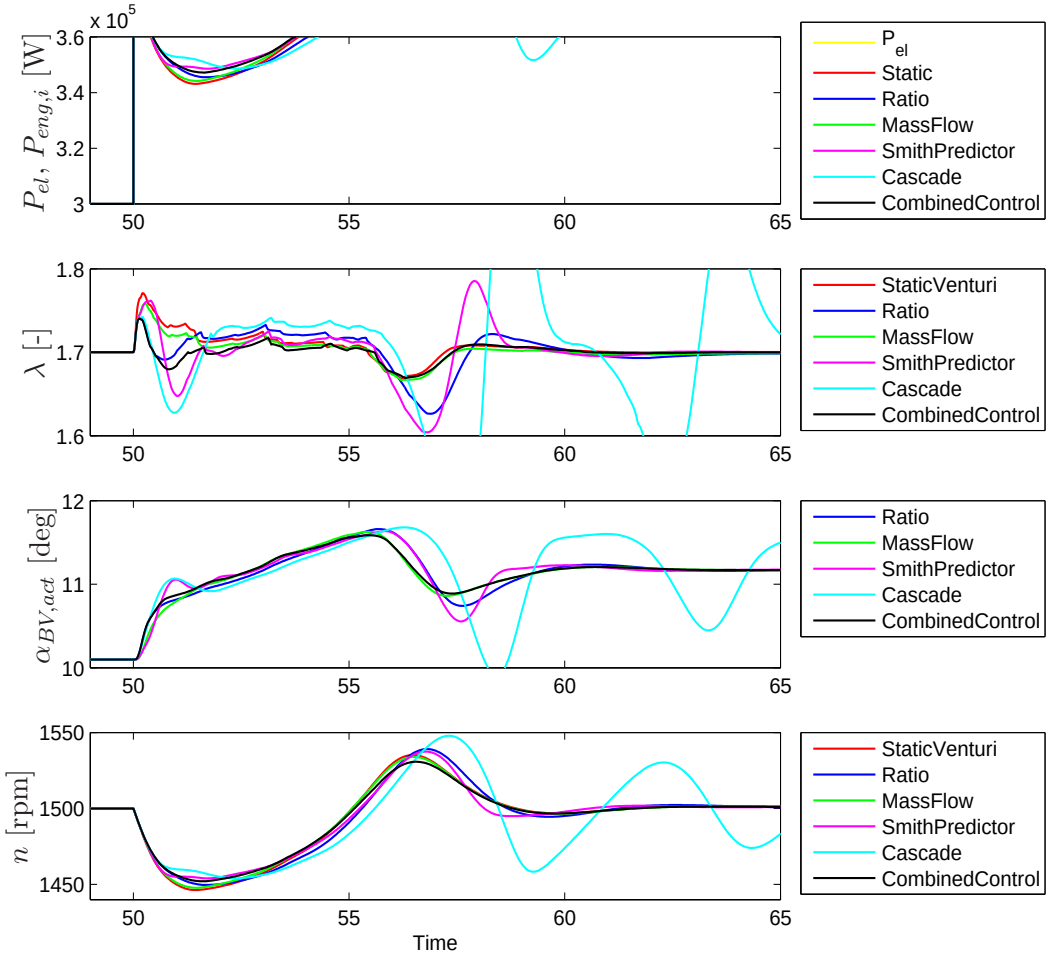

Figure 5.1: Result of a Load Change from $300kW$ to $360kW$

Figure 5.1 shows a step input from $300kW$ to $360kW$. In the first subplot it can be seen that the engine load is reduced, which is due to the above-mentioned influence of the load reduction function in the generator. This appears at almost every bigger load change, because, as can be seen in subplot four, the rotational speed of the engine is underneath the generator load reduction function limit. The smallest load reduction is achieved by the combined controller. It can also be seen that the reference performance (see section 4.7.1), which is the approximation of a static venturi mixer (used names in figures), has a poorer performance than the combined control. The lambda values shown in subplot two give more information about the stability of the controllers. It can be seen that the performance of the cascade control is insufficient and does not lead to a stable state. The mass flow control shows sufficient performance and the combined control shows a even better performance than the static venturi mixer reference. A very interesting point is the performance of the cascade and the smith predictor control compared to the combined control. Although both the cascade and the smith predictor controls show the poorest results in this plot, the combined control has the best one. This can be explained by the linearized engine model in the smith predictor control, which only allows small deviation to the linearized values and the dead time influence on the cascade control, which both lead to instability. The smith predictor controller is not able to compensate the difference of the engine and the linearized engine model, and the cascade control is not able to deal with the dead time. In the combined control, the disadvantage of the smith predictor controller is canceled by the mass flow controller and the disadvantage of the cascade controller is canceled by the smith predictor controller. Therefore the linearized engine model is accurate enough for this usage and the dead time of the system does not influence the cascade control. In the third subplot, the value of the angle of the shaft is plotted. In this plot the influence of the mass flow control on the combined control can be seen very clearly. Another point is that all controllers, except the cascade controller, reach the steady state almost at the same time.

Figure 5.2 shows a load rejection from $360kW$ to $300kW$, where in subplot two as well as in subplot three it can be seen that the smith controller tends to oscillate. Furthermore, the cascade controller seems to stabilize itself slowly. The combined control again has the best performance and has the smallest overshoot in subplot two. The performance of the mass flow control and the ratio controller are almost the same. The complete behavior of the plant changes at a different load level because of the non-linearity of the system. In order to show this behavior, figure 5.3 depicts a load change from $540kW$ to $600kW$.

In comparison with figure 5.1 it can be seen that the load reduction of the generator is in general smaller at the higher load level. The load reduction of the combined control can almost be neglected, in contrast to the static venturi mixer. In subplot two, the higher dynamics at this level, which comes from higher mass flows across the system, can be seen very well at the oscillation of the combined control. The oscillation of the combined control results from the oscillation of the shaft angle, which can be seen in subplot three.

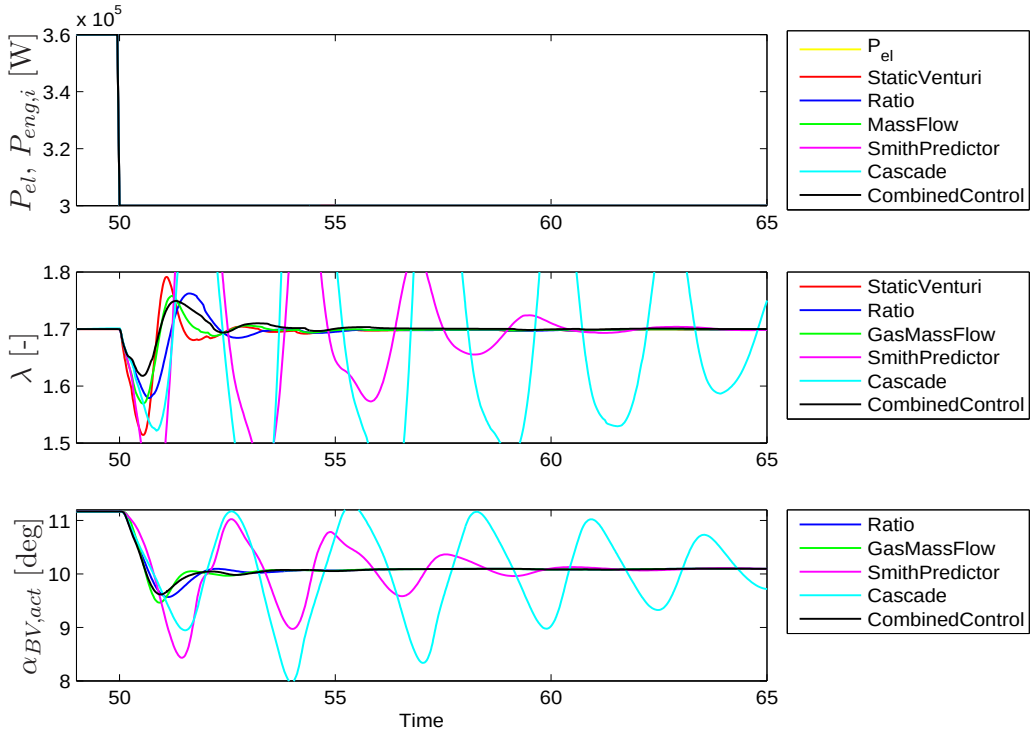

Figure 5.2: Result of a Load Rejection from $360kW$ to $300kW$

The reason for this oscillation can be found in the difference between the engine and the used linearized engine model, which is shown in subplot four. This influence is discussed in more detail in section 5.6. The peak of the ratio controller in subplot three at the time of the input results from the time delay of the calculation of the calorific value (see equation (4.1)).

In figure 5.4 a load rejection from $600kW$ to $540kW$ is depicted. In subplot one, the load reduction of the generator can be seen in case of the smith predictor control. The overshoots of the smith predictor are too high, which leads to insufficient performance. The combined control is not sufficient either. The reason of the oscillation of the combined control can be found in the speed controller, which is described in more detail in section 5.7. Subplot four shows the apertures of the engine valves which are controlled by the speed controller. An oscillating behavior of the valves can be noticed.

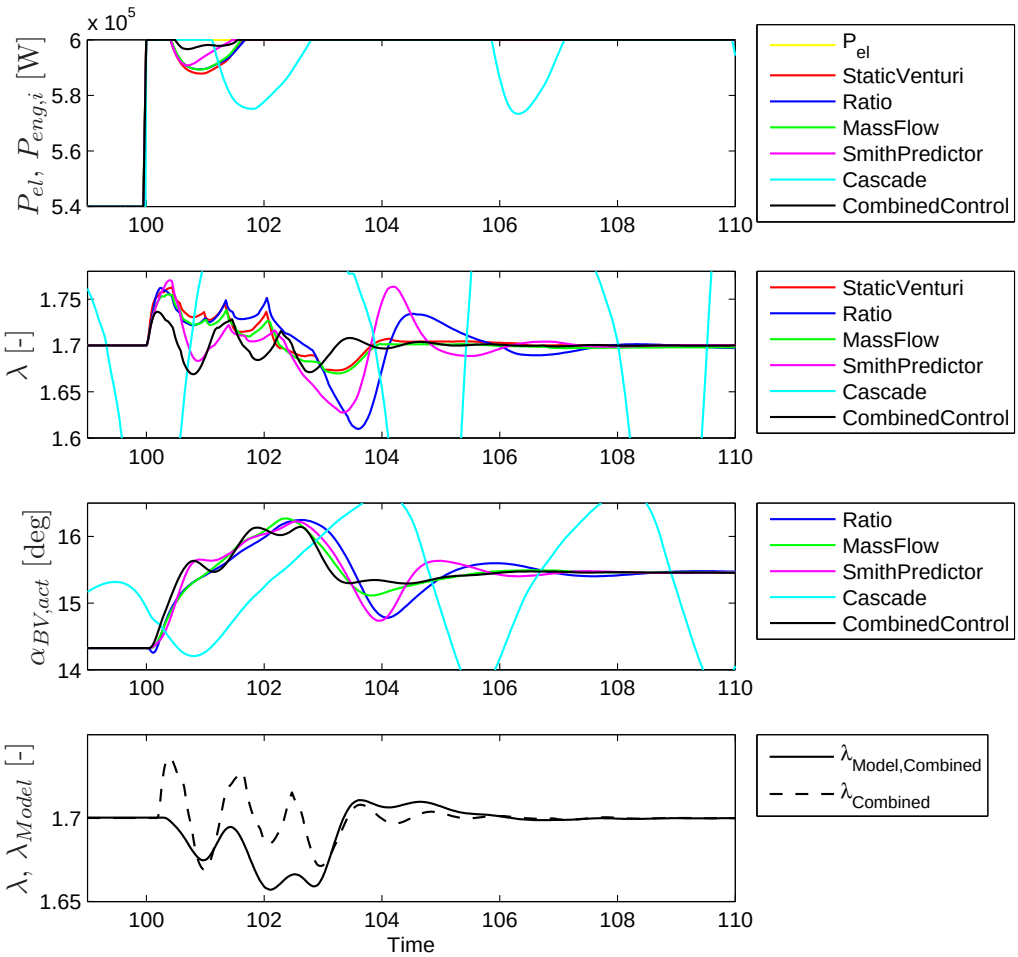

Figure 5.3: Result of a Load Change from $540kW$ to $600kW$

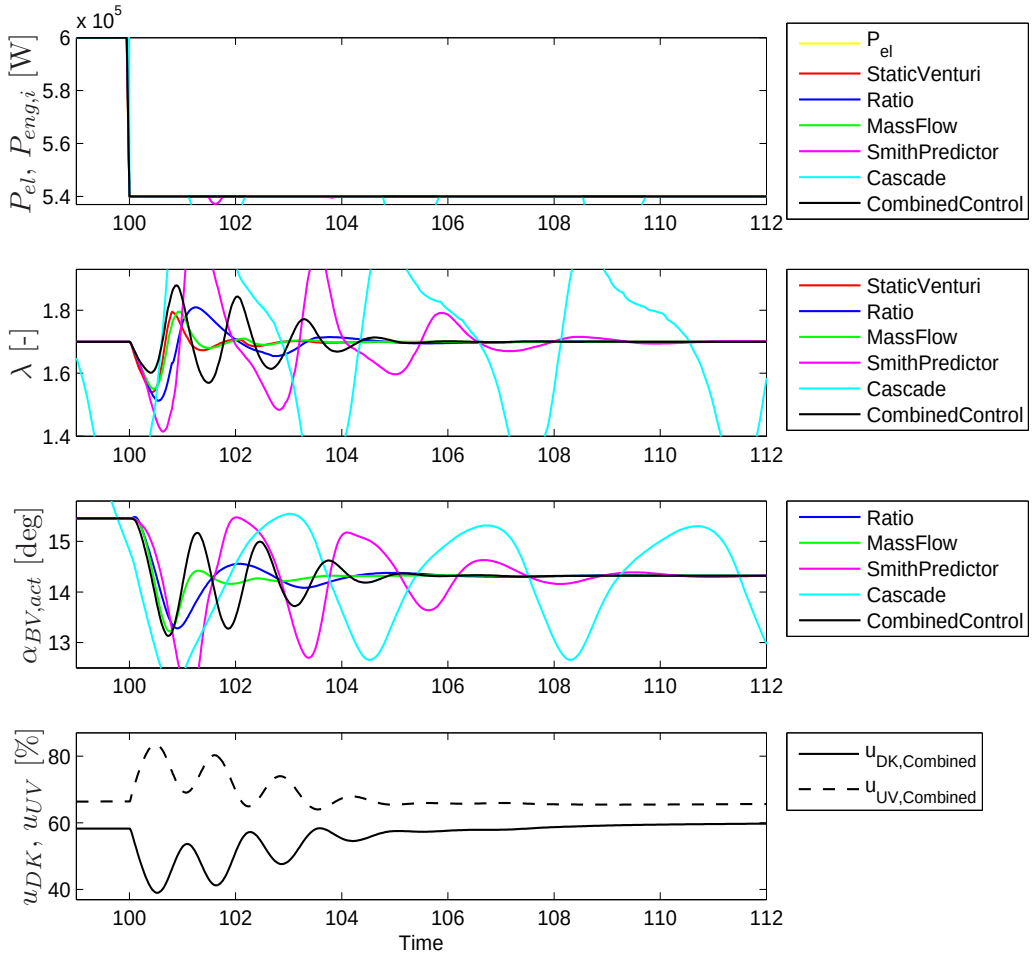

Figure 5.4: Result of a Load Rejection from $600kW$ to $540kW$

5.3 Result and Performance at a Supply Pipe Pressure Disturbance

In this section the performance of the controller by applying a supply pipe pressure disturbance is shown. The pressure in the gas grid can change very fast, which makes a feedforward compensation necessary or at least advantageous. In the following figures, the first subplots of the figures show the pressure disturbance. Δp_{G0} is the difference to the assumed overpressure of $100mbar$. The disturbances chosen are $\pm 50mbar$, which equals 50% of the overpressure. The pressure from the gas grid should be at least within this range.

The cascade control is not able to deal with the pressure difference, which was also the case in the previous section, where the cascade control is unstable in all cases. Because of this reason, the cascade control is not depicted in the following figures. Furthermore the static venturi is not depicted either, because the calculation of the gas mass flow does not regard the pressure of the gas supply pipe, which makes a comparison with the static venturi case unnecessary.

Figure 5.5 shows the result of a pressure disturbance of $50mbar$ at a load of $300kW$. The best performance of the pressure disturbance is provided by the mass flow control. The first peak into the rich range of the lambda value in subplot two comes from the feedforward controller, which is not damped by a PT1-element. This applies for the mass flow as well as the combined control. The smith predictor is too slow; it also has too high overshoots and is therefore not sufficient. The feedforward controller of the ratio controller is damped by a PT1-element with a time constant of $0.4sec$. This causes the smaller overshoot in the shaft angle (subplot three), but also the longer settling time (subplot two). The second peak of the combined control in subplot two is basically caused by the linearized engine model, which is influenced by the undamped feedforward controller of the combined control. Subplot four shows furthermore that the steady state value of the linearized engine model does not reach the set point, which causes the long settling time of the combined control.

The first peak of the system, which is caused by the feedforward controller, shows that the static feed forward controller is not completely optimized. As the static feed forward controller design is described in section 4.5, it can be concluded that an automatic computation is not sufficient.

Figure 5.6 shows a negative disturbance of the gas supply pressure at a load of $300kW$. The influence of the linearized engine model is evident there as well. The mass flow controller has again the best performance of the different controllers. In subplot three, the influence of the feedforward controller can be noticed at the first peak at the time of the disturbance. The peak of the angle shaft can be damped at the expense of the settling time, which can be seen on the ratio controller in subplot two and three. This damping

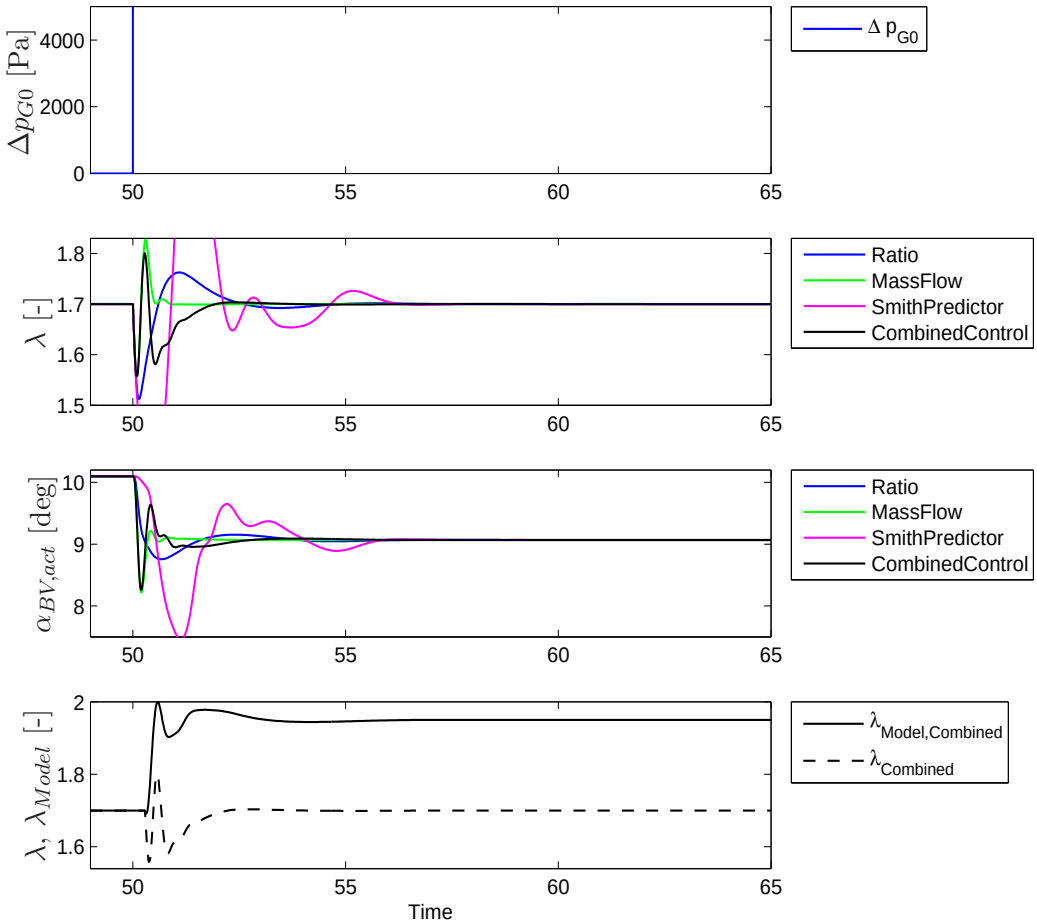

Figure 5.5: Result of a Pressure Disturbance of $\Delta p_{G0} = 50mbar$ at a Load of $P_{el} = 300kW$

of the peaks needs to be adjusted for the special purposes which are requested.

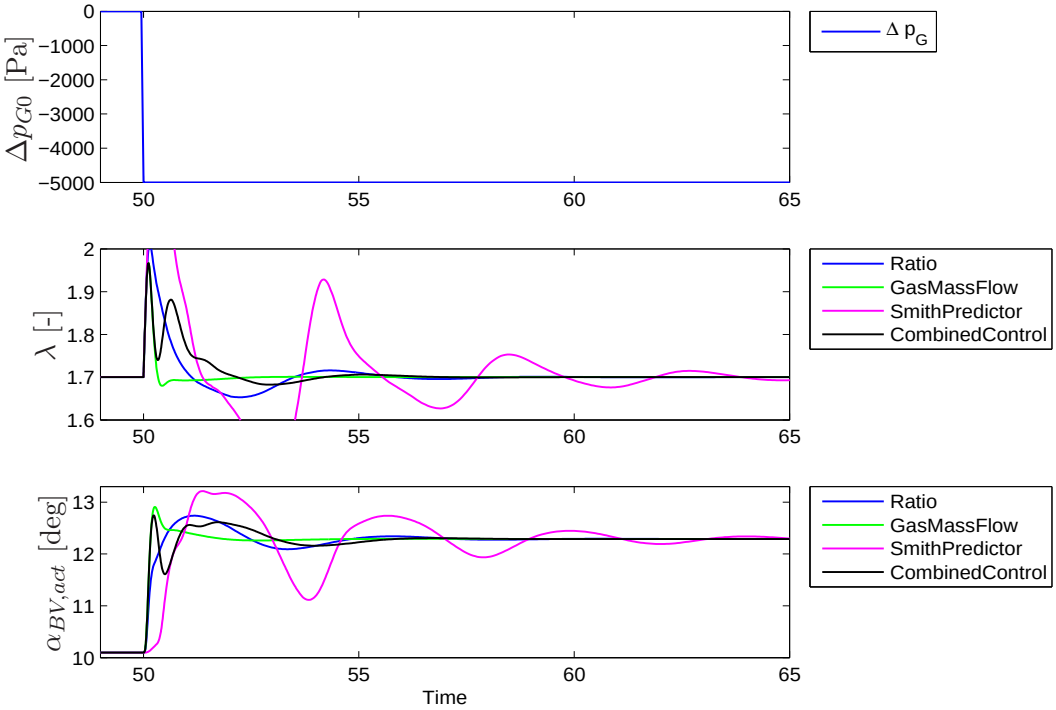

Figure 5.6: Result of a Pressure Disturbance of $\Delta p_{G0} = -50mbar$ at a Load of $P_{el} = 300kW$

Figure 5.7 shows the positive pressure disturbance of $50mbar$ at a load of $600kW$. The dynamics of the lambda value in subplot two are the same as in the load change case. The cause of this dynamics, which generates the oscillations, is also the speed controller as well as the feedforward controller. In subplot three it can be seen that the first peak of the angle of the shaft is bigger than in the case of the lower load level. This shows that the gains of the feedforward controller, as calculated from the linearized transfer functions, are not completely adequate for the model. This demands a careful check of the linearized transfer functions of the system.

Figure 5.8 shows a negative pressure disturbance of $-50mbar$ at a load of $600kW$. In this case it can be seen that the energy content of the mixture is close to the limit which is needed for a sufficient operation of the engine. Furthermore, the angle of the butterfly valve is at a value which makes a fast and precise control more difficult. For the change of the gas mass flow, proportionally bigger angle changes are necessary than those used when the butterfly valve is more closed. Finally, it can be concluded that, the best pressure disturbance compensation is achieved by the mass flow control if the static feedforward gains of the combined control are not adjusted.

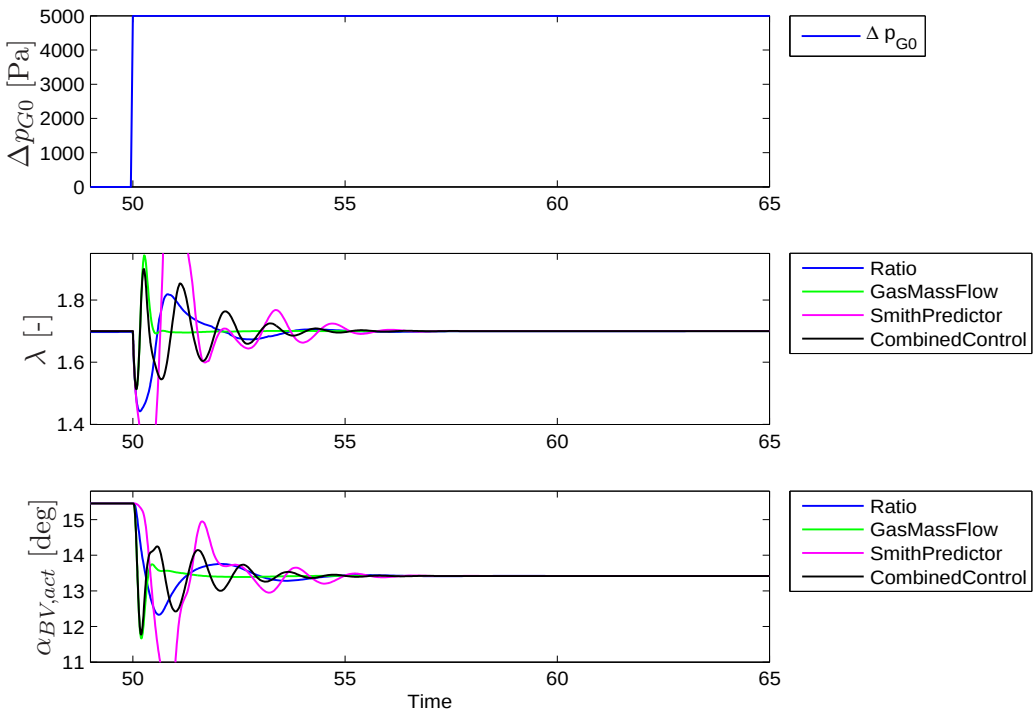

Figure 5.7: Result of a Pressure Disturbance of $\Delta p_{G0} = 50mbar$ at a Load of $P_{el} = 600kW$

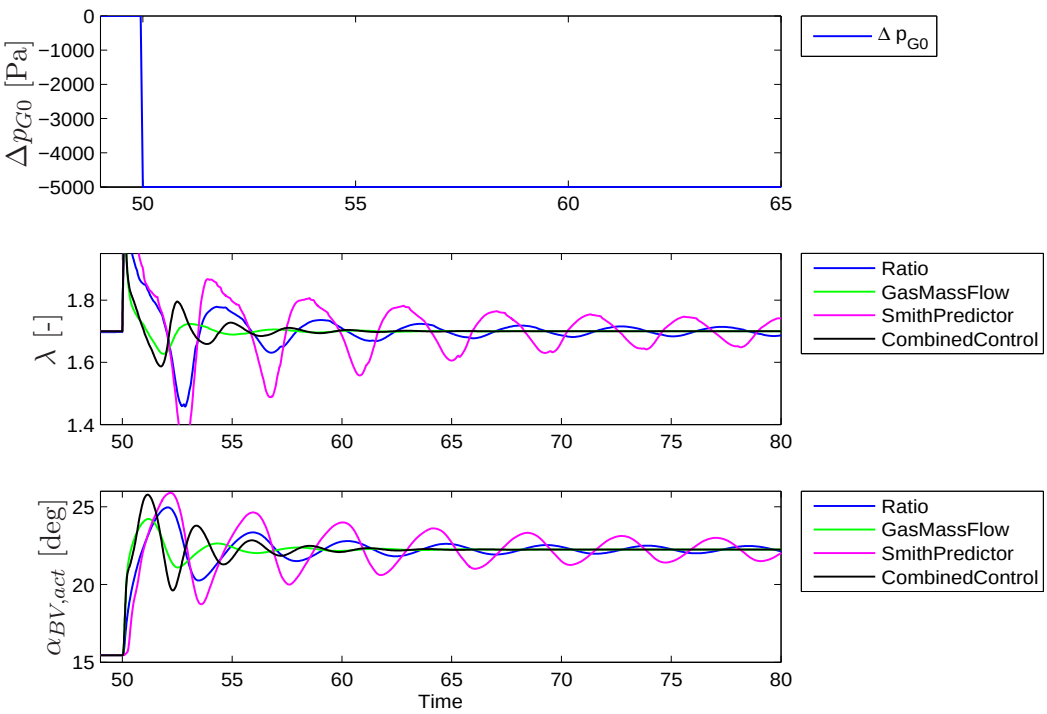

Figure 5.8: Result of a Pressure Disturbance of $\Delta p_{G0} = -50mbar$ at a Load of $P_{el} = 600kW$

5.4 Result and Performance at a Supply Pipe Temperature Disturbance

In this section the performance of the temperature disturbance compensation is shown. The temperature also has an influence on the lambda value and is not negligible. Normally, stationary gas engines are placed in machine houses, where the temperature is almost constant except for small differences over the year. The linearization temperature of the gas is assumed to be $294K$ and the temperature disturbances, which should cover the whole possible range of temperatures, range from $-40K$ to $60K$. These are very extreme values which normally never appear, but the model is able to deal with them. In the following paragraphs, the first subplots are again the disturbance of the assumed stationary temperature value, followed by the second subplot, which is the lambda value. The third subplot shows the angle of the shaft. As in the section before, the static venturi mixer reference is not depicted, as the influence of the temperature disturbance is not considered either. The influence of the temperature effect is also so small that the cascade controller is able to deal with it. Therefore the cascade control is depicted in the figures.

Figure 5.9 shows the result of a $60K$ temperature step at a load of $300kW$. The best performance is again achieved by the mass flow control, which has the advantage of the direct influence of the gas mass flow on the control error. Like the feedforward controller, this accelerates the settling time. Compared with the combined control, the influence of the linearized engine model is again clearly observable. By adjusting the gains of the feedforward controller, the effect of the first peak can also be minimized. All controllers are settled after $3-4sec$, which is quite good for such a big temperature disturbance. Cascade control and smith predictor control are stable, but not sufficient for practical usage because of the oscillation. Figure 5.10 shows a temperature disturbance of $-40K$ at the same load as before. Additionally, subplot four depicts the rotational speed of the engine. In general, the figure is the mirrored picture of figure 5.9. The same effects are noticeable and therefore the figure is not described at this point any more.

Figure 5.11 shows the temperature disturbance of $60K$ at a load of $600kW$. As seen before, the cascade control is not stable at a load of $600kW$ and is therefore not able to deal with the temperature disturbance. The smith predictor is able to deal with the disturbance, but oscillates and is therefore the least useful stable controller. The overshoot of the mass flow as well as the ratio and combined control, in subplot two, is smaller than the overshoot in the lower load level result. This is caused by the smaller dead time of the higher load levels. The combined control oscillates due to the influence of the speed controller, an effect which is described in section 5.6 and can also be seen in subplot four. In Figure 5.12, the case of a temperature disturbance of $-40K$ at a load of $600kW$ is depicted. Subplot four also shows the rotational speed of the engine. Basically, the effects are the same as described in figure 5.11, but again only mirrored. The figure is just depicted for the sake of completeness.

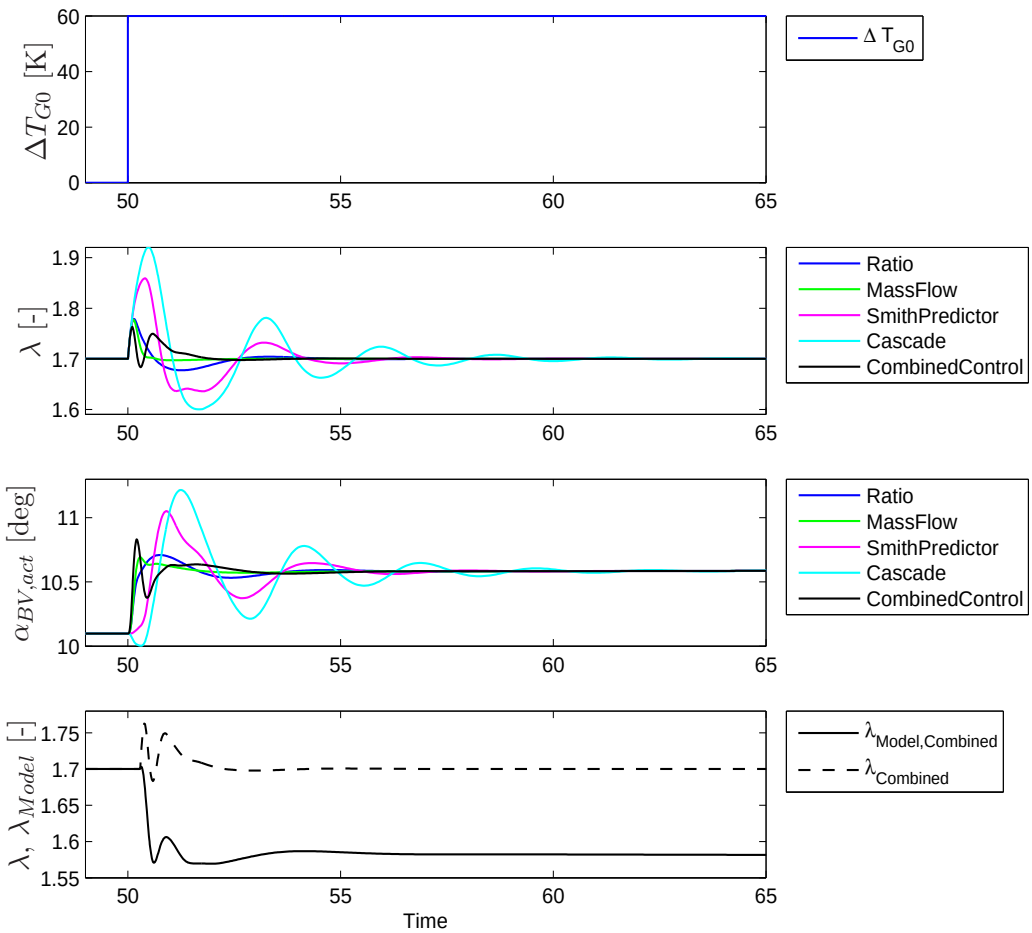

Figure 5.9: Result of a Temperature Disturbance of $\Delta T_{G0} = 60K$ at a Load of $P_{el} = 300kW$

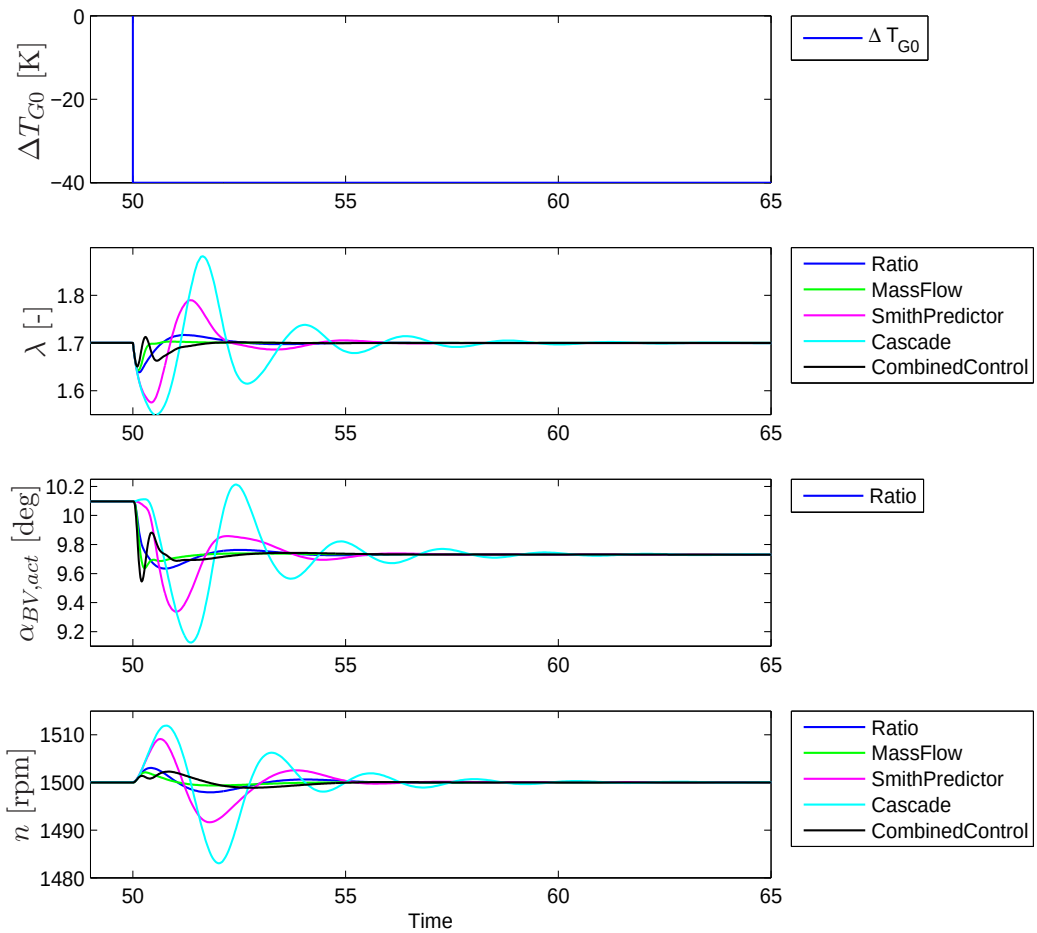

Figure 5.10: Result of a Temperature Disturbance of $\Delta T_{G0} = -40K$ at a Load of $P_{el} = 300kW$

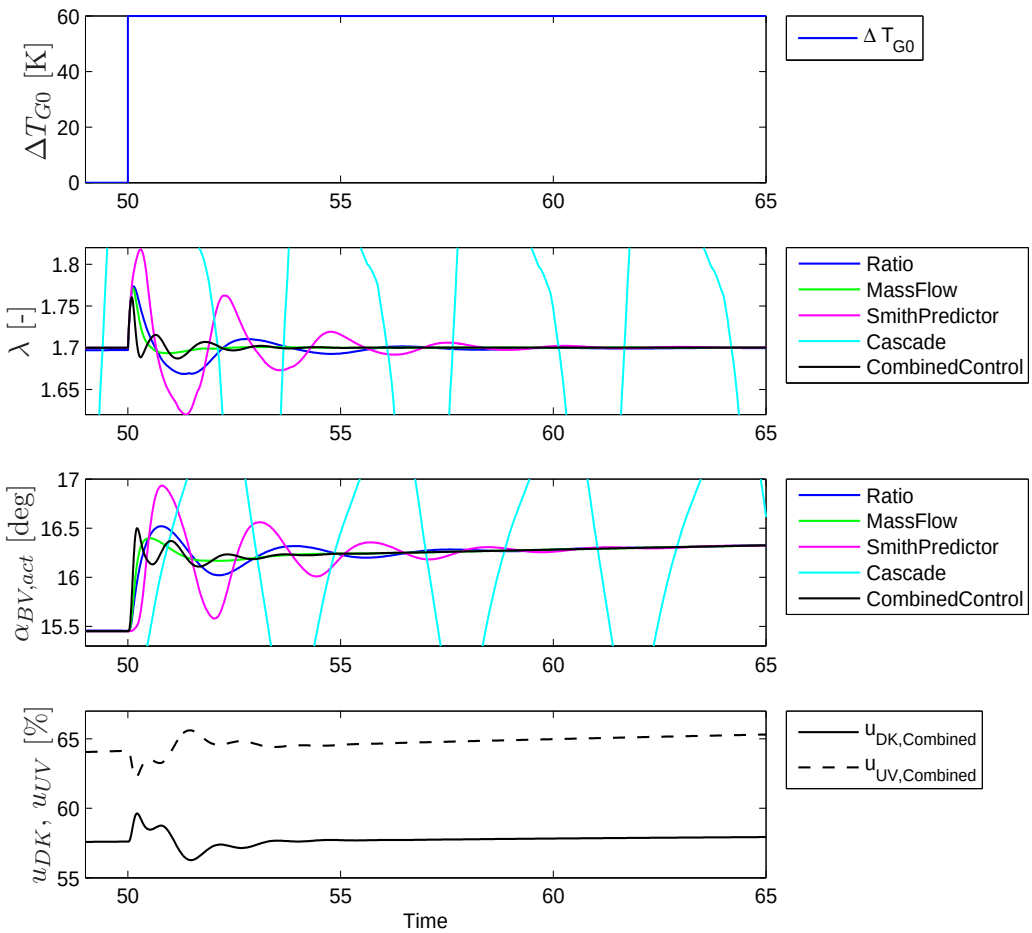

Figure 5.11: Result of a Temperature Disturbance of $\Delta T_{G0} = 60K$ at a Load of $P_{el} = 600kW$

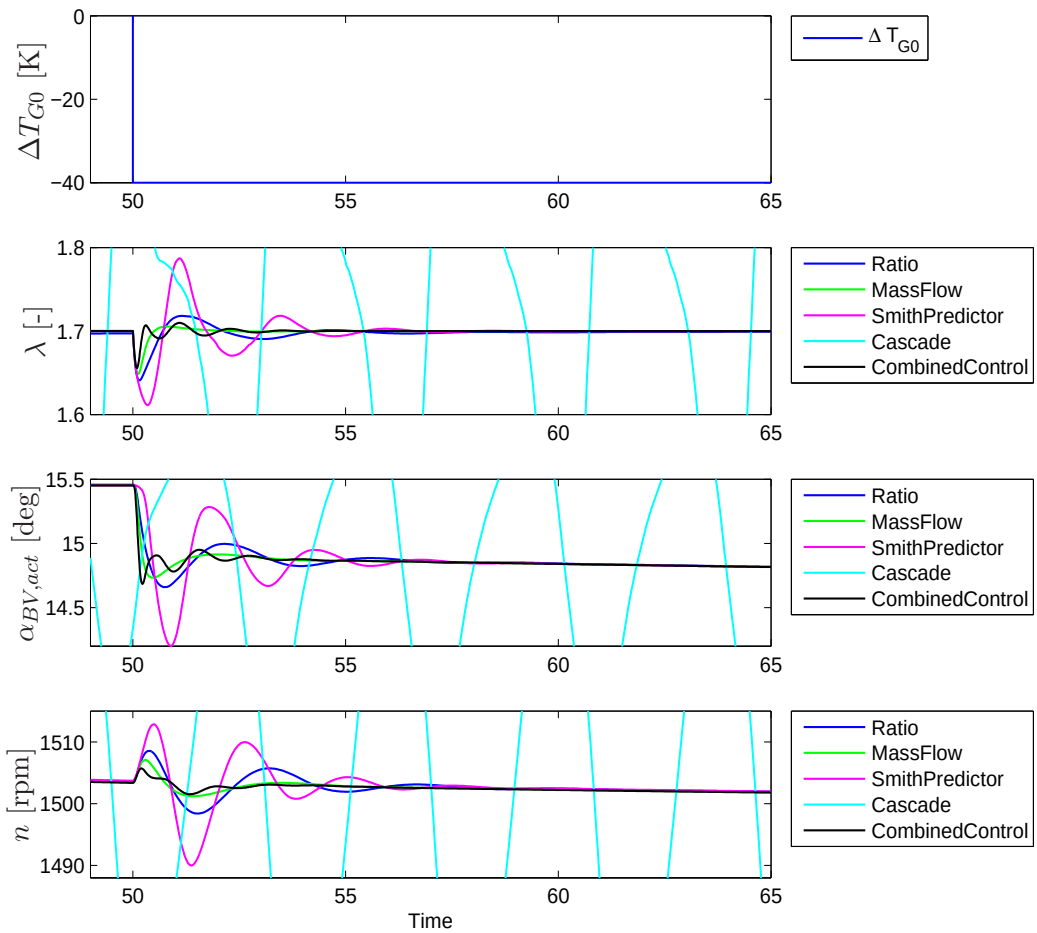

Figure 5.12: Result of a Temperature Disturbance of $\Delta T_{G0} = -40K$ at a Load of $P_{el} = 600kW$

5.5 Result and Performance at a Calorific Value Disturbance

The calorific value disturbance, whose results are shown in this section, is the only disturbance that is not measurable. In the following figures, the disturbance of the calorific value is again shown in the first subplot. The response of the lambda value and the response of the angle of the shaft are depicted in subplots two and three. The range of the calorific value which can occur in natural gas, is defined as $\pm 8MJ/kg$, which is equal to a change of 20% from a calorific value of $40MJ/kg$. However, the changes in the calorific value of natural gas are neither very big nor common. The changes in biogas are more realistic, but the difference of the calorific value between natural gas and biogas is more than 50% of the absolute value of the natural gas. Therefore a change of the geometry would be required, but this is not done in this thesis and might be investigated in a future project.

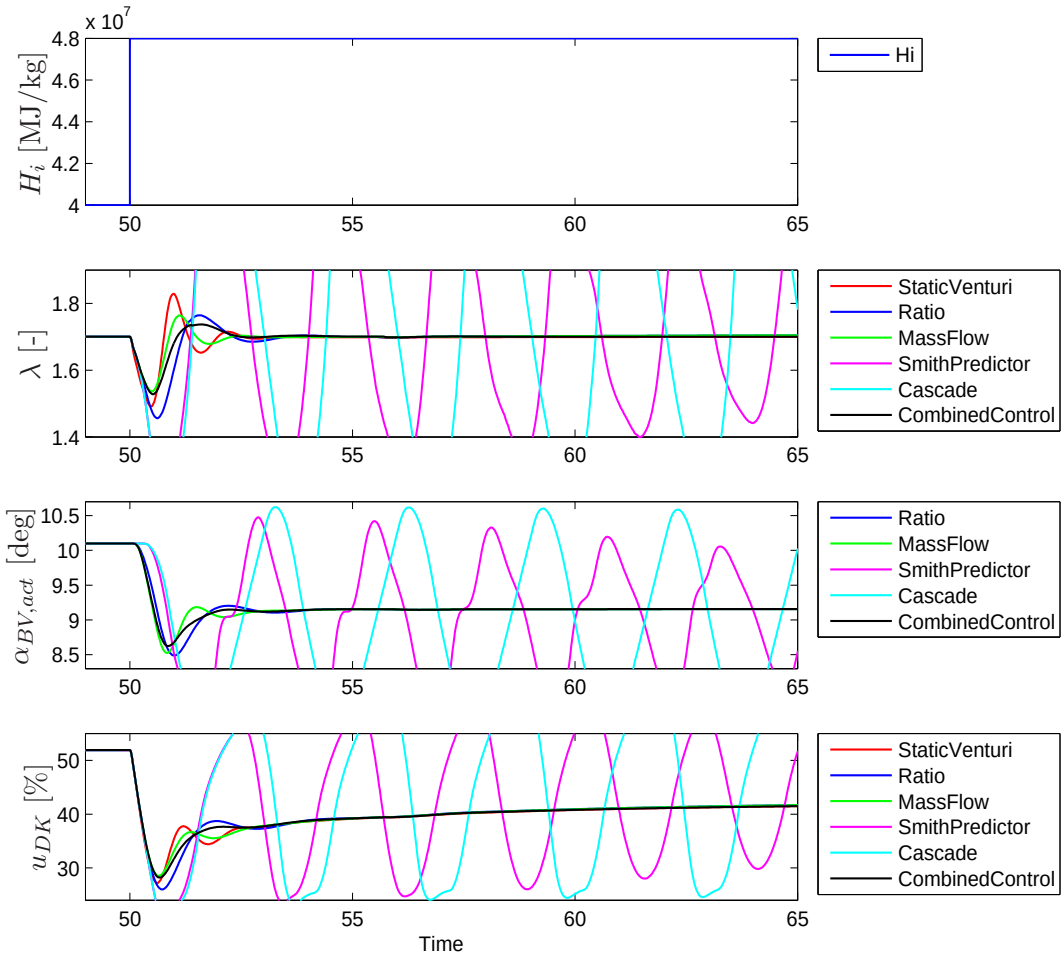

Figure 5.13: Result of a Calorific Value Disturbance of $\Delta H_i = 8MJ/kg$ at a Load of $P_{el} = 300kW$

In figure 5.13, the result of a calorific value step of $8MJ/kg$ at a load of $300kW$ is shown. In subplot two it can be seen that the cascade control as well as the smith predictor are almost unstable. Only a very low damping can be noticed. Furthermore, it can be noticed that the overshoot of the lambda value of the static venturi mixer is the biggest of all controllers, except for the rich side overshoot of the ratio controller. The comparison of the different controllers shows that almost all of them are able to compensate the calorific value disturbance within $2.5sec$. The overshoots in subplot three come from the influence of the speed controller, which closes the butterfly valve of the engine with an overshoot (subplot four). This overshoot has an influence on the mass flow across the engine, which in turn affects the gas mass flow. The compensation of this influence is not compatible with the required fast reaction time of the gas dosing system controller, because the controllers follow the mass flow across the gas dosing system. This overshoot must therefore be accepted.

Figure 5.14 shows a change of the calorific value of $-8MJ/kg$ at a load of $300kW$. In this figure, the influence of the variable calculation of the stoichiometric air requirement at the control strategies without a lambda feedback of the engine can be seen very clearly (subplot one). The ratio and the mass flow controller use the variable stoichiometric air requirement, which can be seen on the negative slope of the lambda value of both controllers in the second subplot. All other controllers are based on the lambda value of the engine, which does not change because of the effect of the fixed stoichiometric air requirement in the engine model (see section 3.7). In the case of the positive calorific value step, this effect is not as clearly observable as in this case, because the assumed stoichiometric air requirement difference between $40MJ/kg$ and $48MJ/kg$ is only 0.1 (see section 4.6). The negative change of the calorific value furthermore leads to a reduction of the load by the generator (subplot four) and a complete opening of the engine butterfly valve (subplot five). The second peak of all controllers at around 60 seconds is caused by the closing of the butterfly valve of the engine and opening of the recirculation system. It can be seen that the combined control has the best performance of the butterfly valve angle and also the best performance at the lambda value. At this point, the performance of the ratio and mass flow control is not comparable with the other control strategies.

Figure 5.15 shows the calorific value disturbance of $8MJ/kg$ at a load of $600kW$. The first thing which can be seen is that the combined control is not able to handle this disturbance and stays unstable. A step input of the calorific value disturbance of $8MJ/kg$ leads instantly to instability of the combined control. Load changes and increasing the calorific value in small steps can stabilize the system. The initial source of the instability is the rotational speed of the engine (subplot four). The oscillation of the rotational speed is transferred to the speed controller, which transfers the oscillation to the mass flow across the engine, which influences the gas dosing system controller. Thereby it comes to a stimulation of the controllers which ends in the unstable state. The main reason for this stimulation can be found in the linearized engine model. The increase of the calorific value

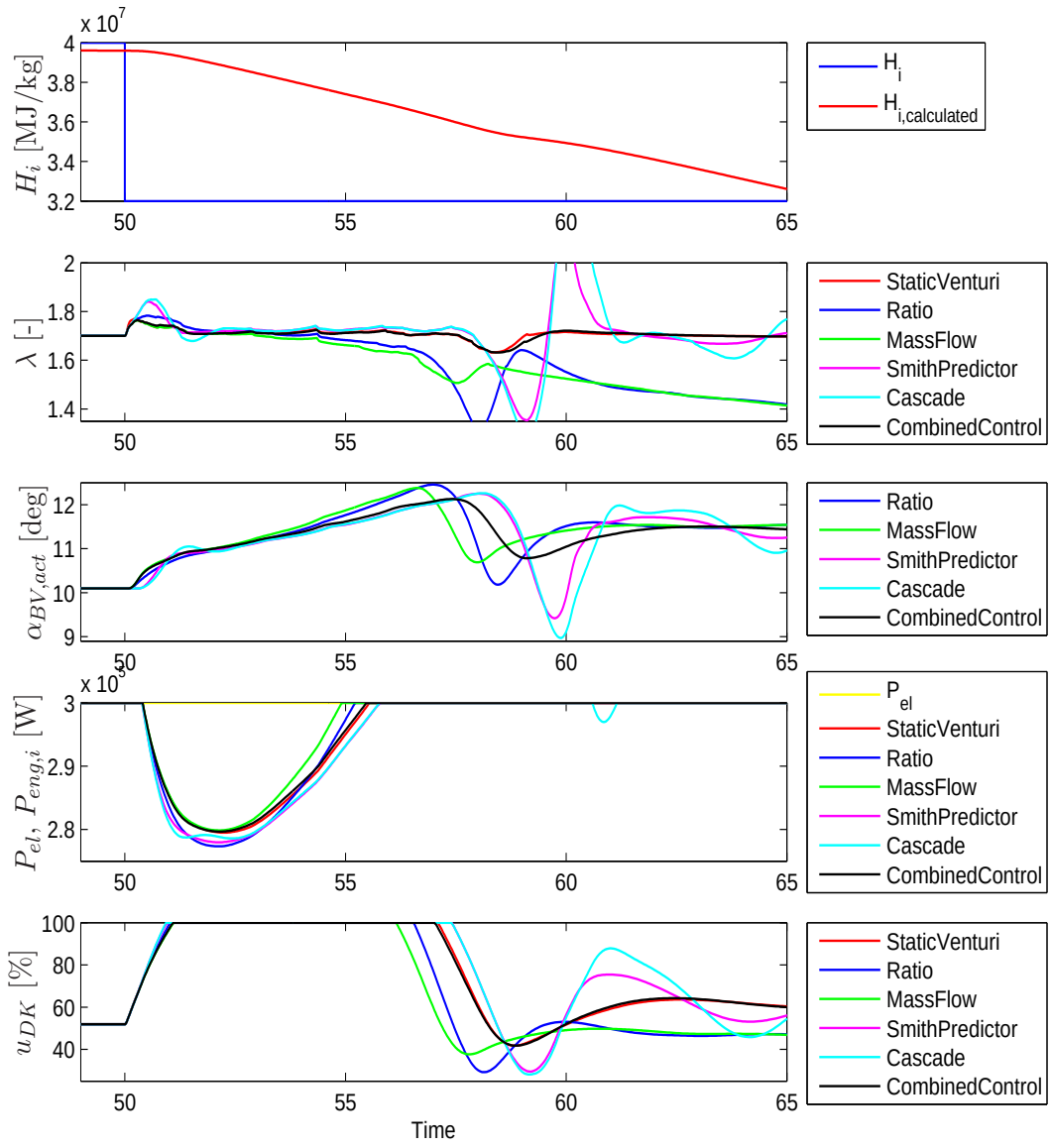

Figure 5.14: Result of a Calorific Value Disturbance of $\Delta H_i = -8MJ/kg$ at a Load of $P_{el} = 300kW$

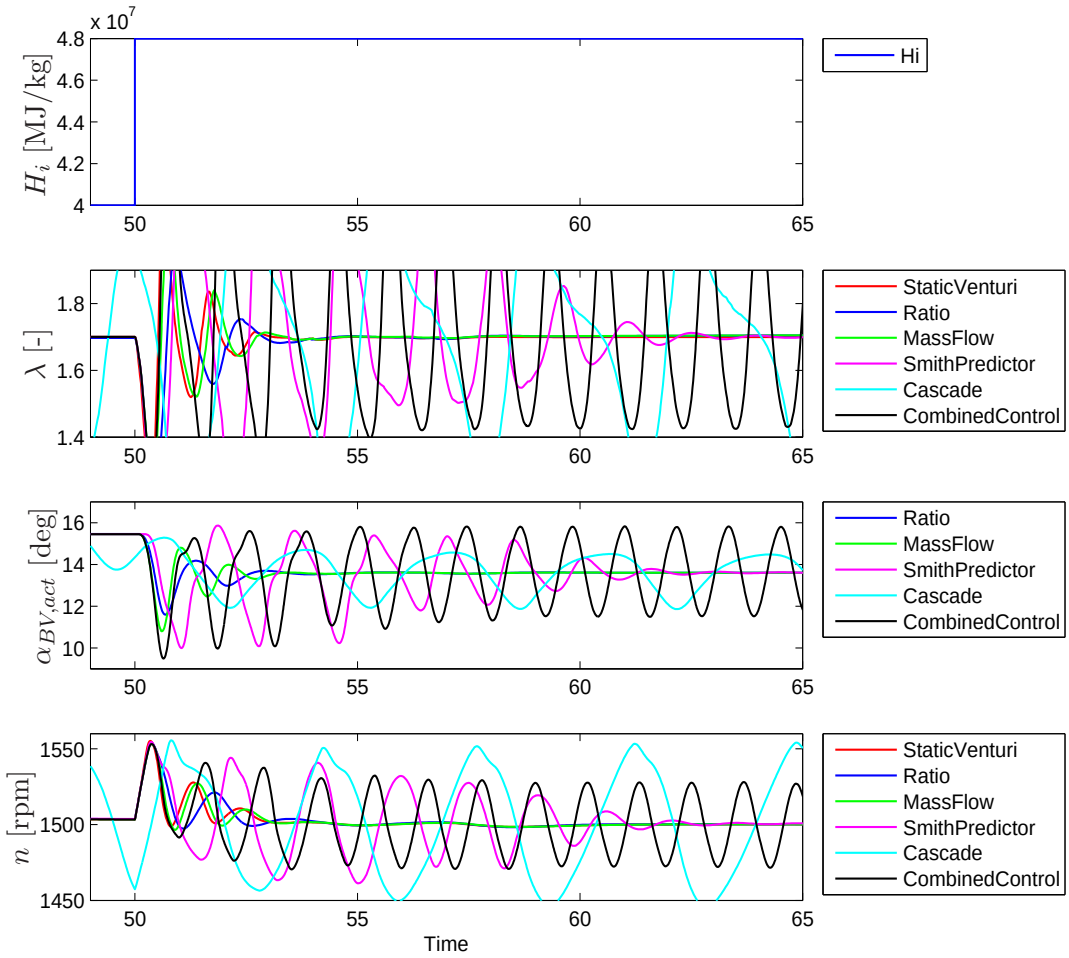

Figure 5.15: Result of a Calorific Value Disturbance of $\Delta H_i = 8MJ/kg$ at a Load of $P_{el} = 600kW$

leads to a smaller lambda value of the engine. The linearized engine model has only the angle of the shaft as input. Because of the higher energy content of the mixture, the engine butterfly valve closes which leads to a closing butterfly valve of the gas dosing system and this therefore to a higher lambda value of the linearized engine model rather than a lower lambda value. This influences the lambda control part of the combined controller, which ends in an unstable state. Here the limit of the combined control is shown very clearly. Furthermore the robustness of the ratio as well as the mass flow control is shown, too. The mass flow control is almost identical with the performance of the static venturi mixer reference.

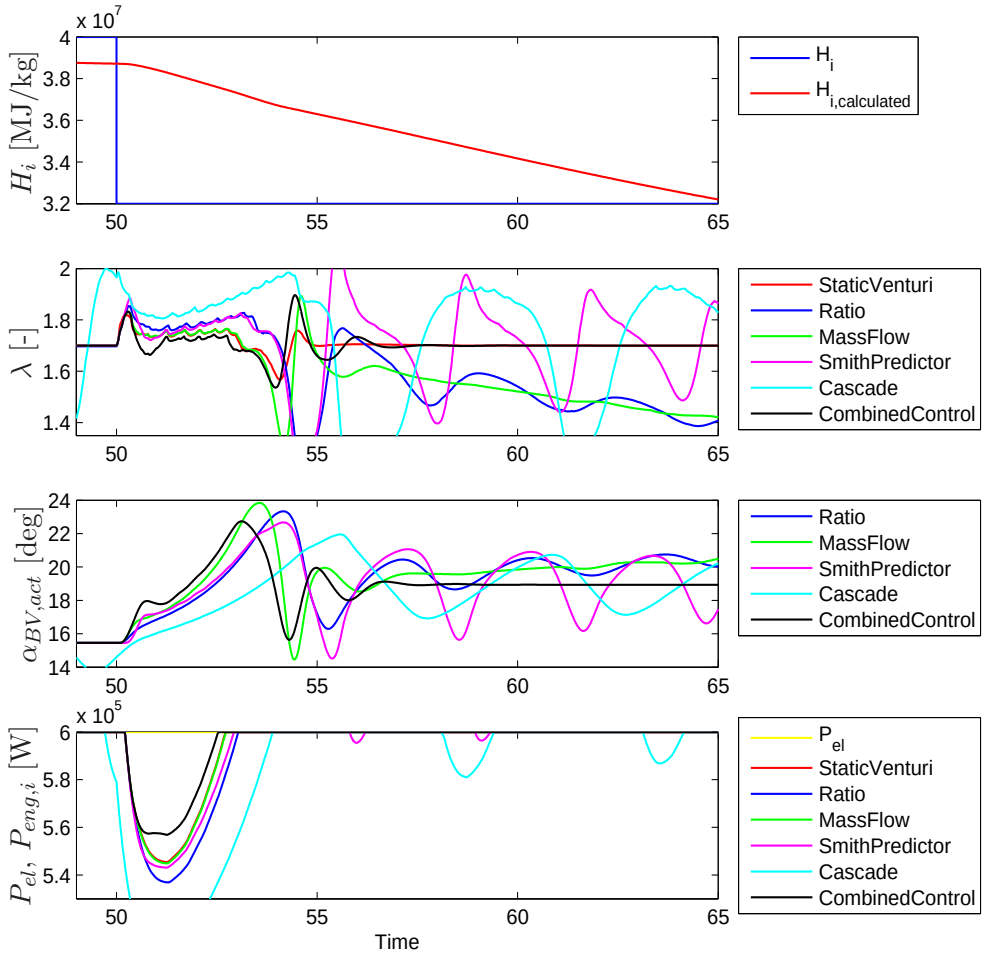

Figure 5.16: Result of a Calorific Value Disturbance of $\Delta H_i = -8MJ/kg$ at a Load of $P_{el} = 600kW$

Figure 5.16 shows a calorific value disturbance of $-8MJ/kg$ at a load of $600kW$. It can be seen that the ratio as well as the mass flow control in subplot two have again a negative slope, because of the fixed stoichiometric air requirement of the engine. Furthermore, it can be seen that the ratio controller has a longer post pulse oscillation. The cascade and the smith predictor controller are both unstable at this load and disturbance. The combined

control has more post pulse oscillations than at the lower load level. The rough behavior after the first peak in the second subplot comes from the engine model and is probably the result of some characteristic diagrams in the engine model. The implementation as an S-Function only allows this guess because the inner structure is not known. Basically it can be concluded that the performance of the mass flow and combined control are sufficient for this disturbance.

5.6 Influence of the Linearized Engine Model on the Controller

In this section, the influence of the linearized engine model, which is used in the combined control as well as in the smith predictor control, is discussed. The linearization of the engine model is not trivial, because the gas engine is not only dependent on the gas mass flow into the engine.

The difference between the engine and the linearized engine model is shown in figure 5.17 for the lower load level at a load change of $300kW$ to $360kW$ and in figure 5.18 for the higher load level at a load change of $540kW$ to $600kW$. Generally, the influence is only given for a positive load change. The load rejection is more influenced by the speed controller, as shown in section 5.7.

In figure 5.17 in the first subplot, the influence of the load change is clearly observable, followed by a rough behavior of the lambda value. The only input of the linearized model in subplot two is the angle of the shaft of the butterfly valve (shown in subplot four), which explains the smooth behavior of the value. In subplot three the difference between the lambda values can be seen. In figure 5.18 the lambda value of the engine (subplot one) is oscillating almost four times before it gets settled. A big difference to the lower load level case can be seen. The lambda value of the linearized engine model is already affected by the oscillation and is thus not as smooth as the lambda value of the lower load level case. Furthermore, it can be seen that the lambda value of the linearized engine model goes into the opposite direction from the engine. This combination leads therefore to the difference given in subplot three. The dead time also plays a role in this case. The dead time is shorter in the higher load level case, which gives the controller less time to react. Therefore, the influence of the linearized engine model is bigger at the higher load level than at the lower load level.

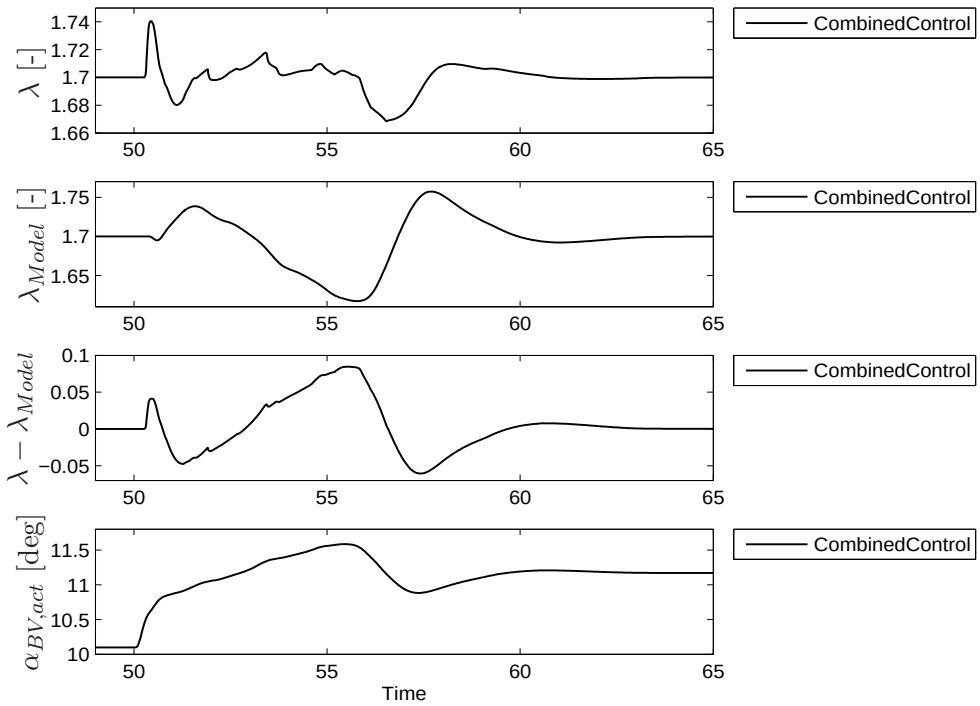

Figure 5.17: Influence of the Linearized Engine Model at a Load Change from $300kW$ to $360kW$

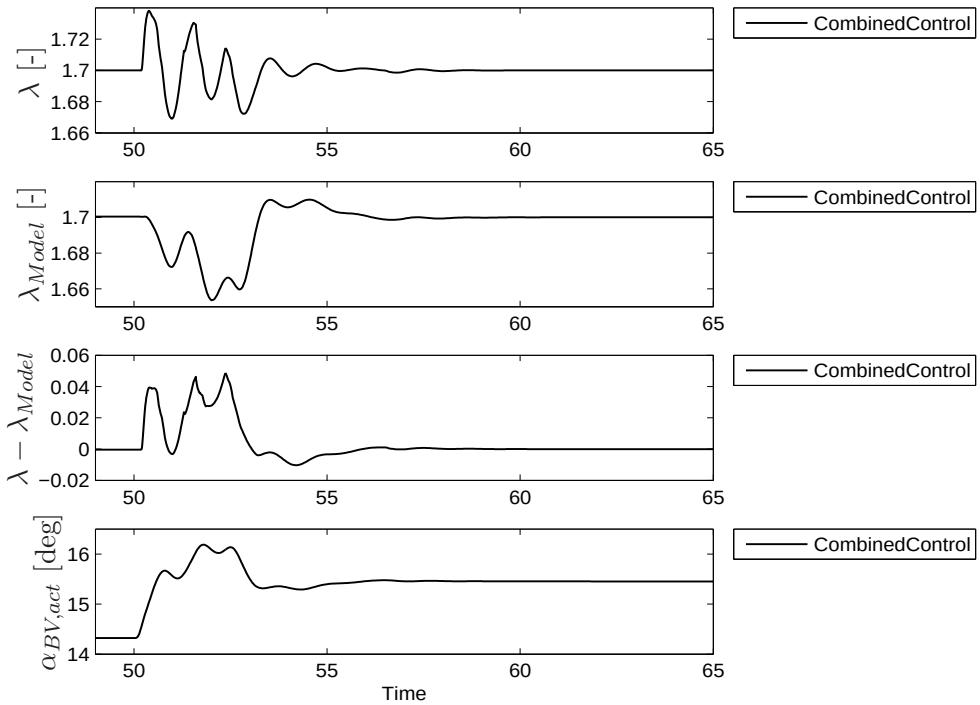

Figure 5.18: Influence of the Linearized Engine Model at a Load Change from $540kW$ to $600kW$

5.7 Influence of the Speed Controller on the Controller

In this section the influence of the speed controller is shown in more detail. As mentioned in the previous section, the speed controller has a stronger influence on the gas dosing system controller at a load rejection at the higher load level. Figure 5.19 shows the control variables of the speed controller at the higher load level, which are the aperture of the butterfly valve of the engine u_{DK} and the aperture of the recirculation valve u_{UV}. Both values are given in percentage of the completely opened valves. In the figure, the comparison between the ratio controller, the mass flow controller and the combined controller as well as the static venturi mixer is shown. Furthermore, the speed controller uses middle aperture values, which the controller tries to reach. This can be seen on the steady state value of the apertures and can be explained by the turbo charger. In subplot four the influence of the butterfly valve of the engine can be seen when looking at the combined control. The influence on the other controllers is not as strong as in the combined control case, because the other controllers do not consider the lambda value of the engine, which is the main transfer factor of the influence.

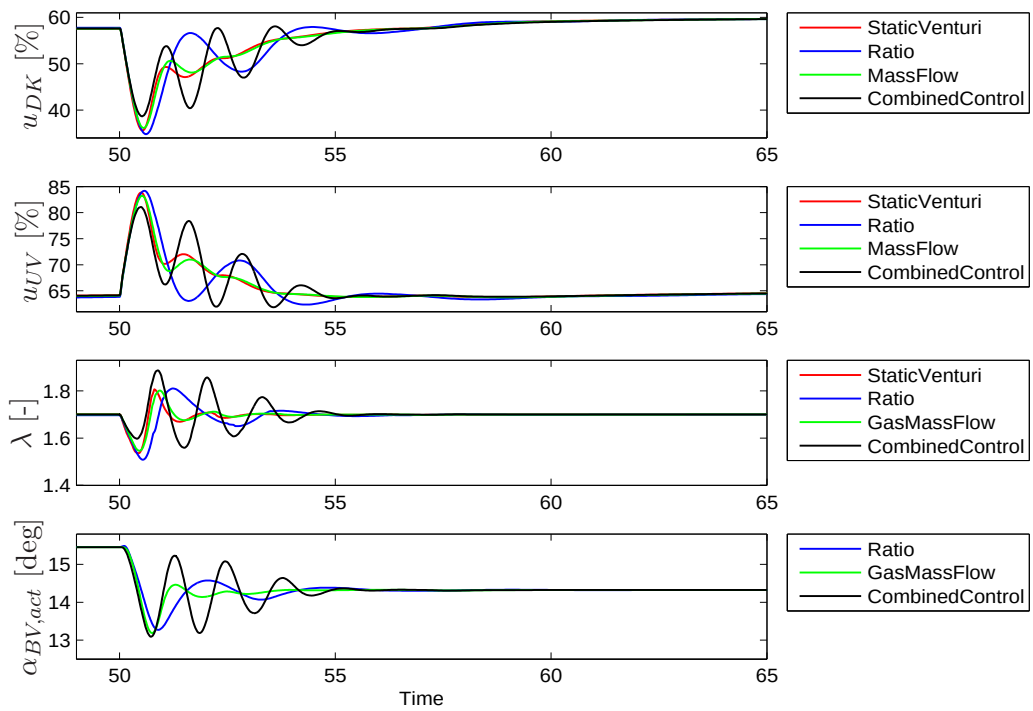

Figure 5.19: Speed Controller Influence of a Load Rejection at the Higher Load Level

5.8 Result and Performance at a Lambda Set Point Change

At the end of this chapter the case of a change of the lambda set point is discussed. The engine model limits the output lambda value, which leads to an unfavorable simulation result. The lambda value set point variations are also done at the lower and higher load level. The value is varied with $\lambda = 1.7 \pm 0.2$, which equals to $\pm 12\%$.

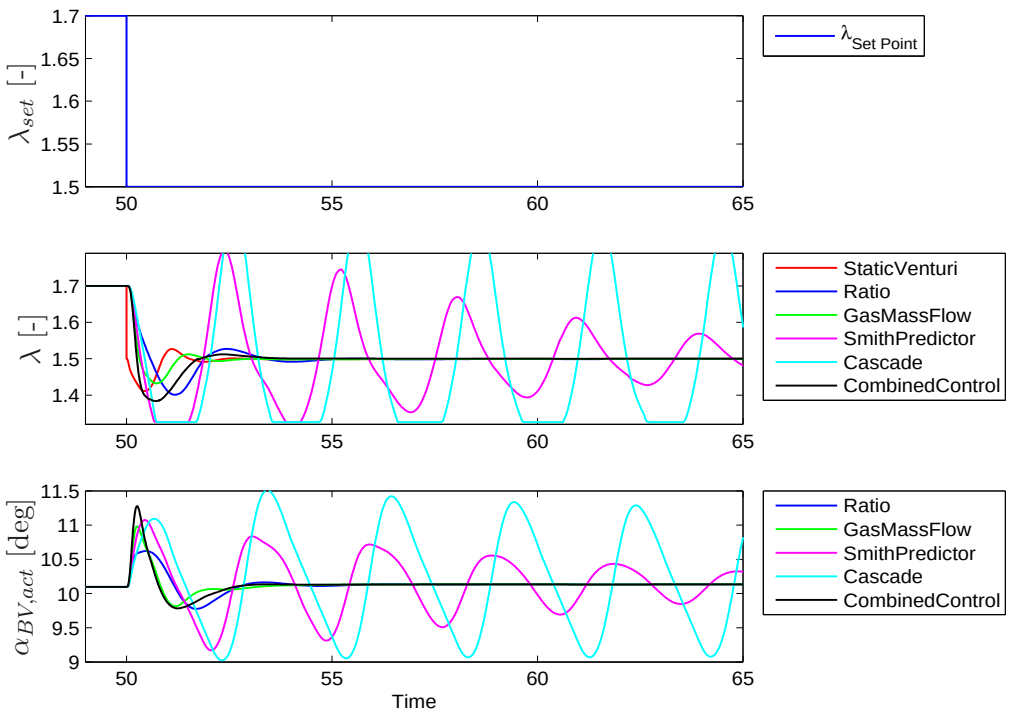

Figure 5.20: Result of a Lambda Set Point Change from 1.7 to 1.5 at a Load of $P_{el} = 300kW$

Figure 5.20 shows the case of a lambda value change to 1.5 at the load of $P_{el} = 300kW$. In subplot two it can be seen that the static venturi mixer reference directly shows the step input of the lambda value change. Therefore the static venturi mixer cannot be taken as a serious reference for the comparison of the performances, but it is still drawn in the following figures in order to show the form of the reference line which is actually a good reference. In subplot two, furthermore, the ratio control shows the slowest response to the step input. The combined control has the biggest overshoot, which can also be seen in subplot three. Although the mass flow control is included in the combined control, the performance of the mass flow control is better than the combined control. This can be explained with the direct influence of the engine lambda value on the control strategy.

Figure 5.21 shows the case of a lambda value change to 1.9 at the load of $P_{el} = 300kW$. All lambda value based control strategies shoot into the boundary of the lambda value, because of the limitations in the engine model. The overshoot of the mass flow control

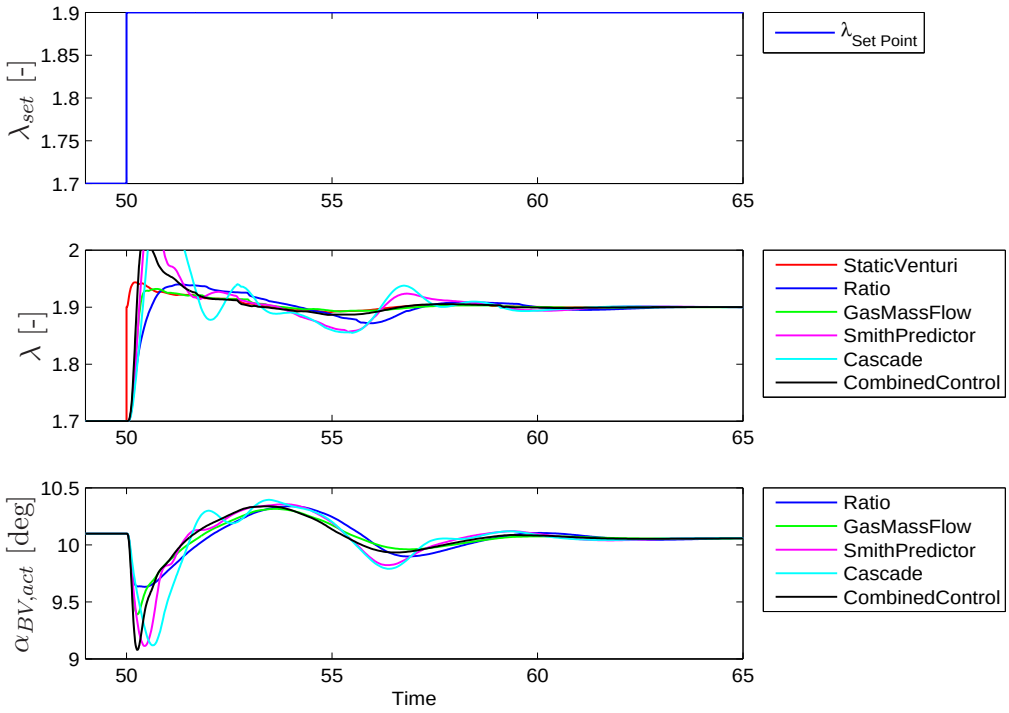

Figure 5.21: Result of a Lambda Set Point Change from 1.7 to 1.9 at a Load of $P_{el} = 300kW$

in subplot two is almost negligible. Smith predictor and cascade control strategy are also able to deal with the lambda set point change. The smallest overshoot of the angle of the shaft in the butterfly valve can be noticed in the ratio controller. After the peak almost all control strategies in subplot three are identical.

The case of a negative lambda value change in the higher load level is shown in figure 5.22. At the load of $P_{el} = 600kW$ it can be seen that all controllers go into the lower boundary at a lambda value set point change to 1.5. The combined controller shows an oscillating behavior, which is caused by the speed controller. In subplot three, it can be seen that the overshoot of the combined control is almost double the mass flow control, which again shows the best performance of all controllers. The smith predictor control has no higher overshoot than the mass flow control, but also oscillating behavior.

The rough behavior in subplot two in figure 5.23 is again caused by the engine model, but cannot be explained with the unknown construction of the engine model. The peak in subplot two at time 54, which appears before the steady state is reached, can again be explained by the overshoot of the engine valves. This effect cannot be compensated, as described before. The oscillation of the combined control in this case is caused by the difference of the linearized engine model. On the whole, the performance of the controllers is almost equal.

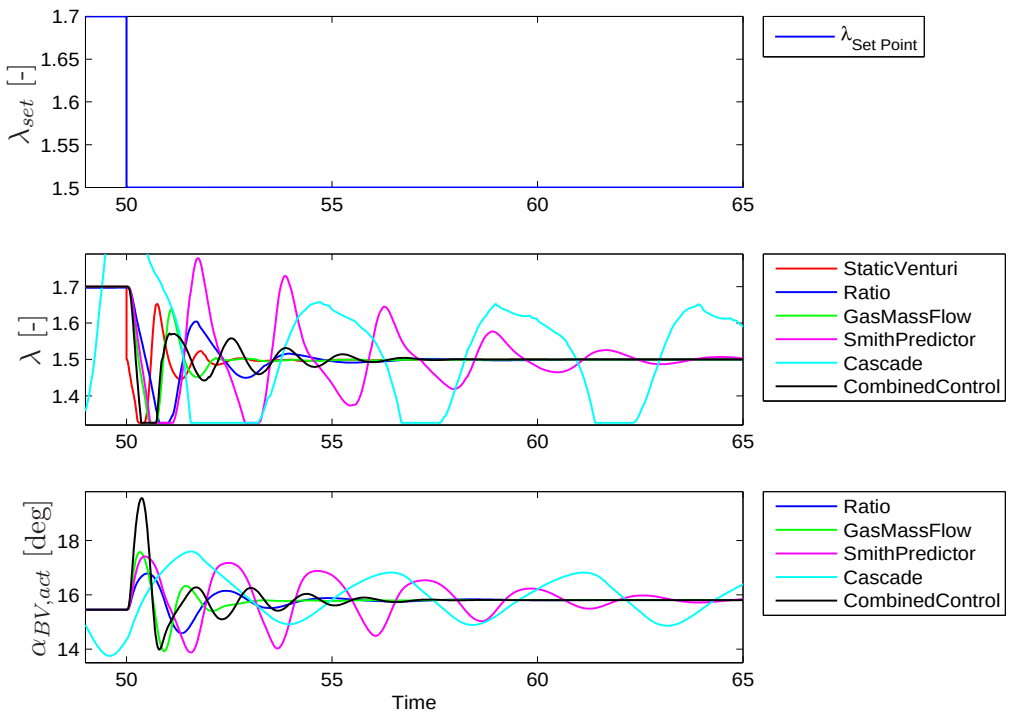

Figure 5.22: Result of a Lambda Set Point Change from 1.7 to 1.5 at a Load of $P_{el} = 600kW$

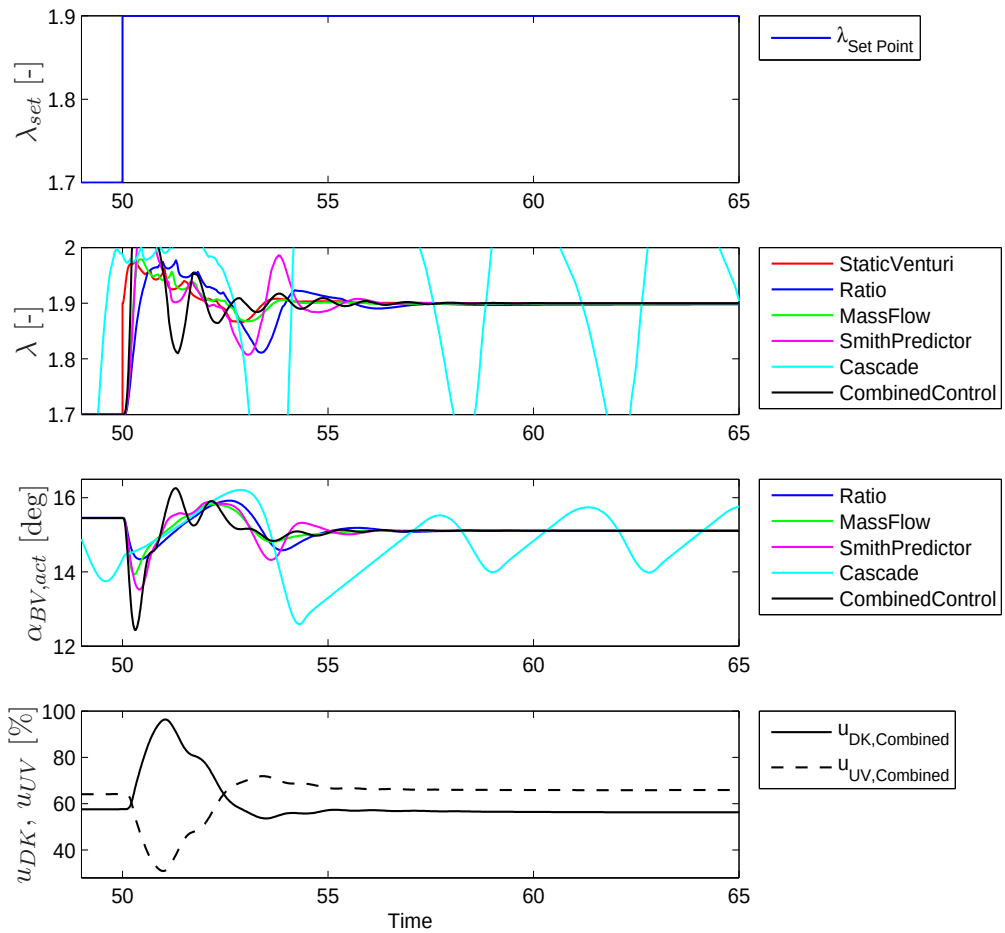

Figure 5.23: Result of a Lambda Set Point Change from 1.7 to 1.9 at a Load of $P_{el} = 600kW$

Chapter 6

Conclusion and Suggestions for Future Work

In this thesis a model of an active gas dosing system was developed and the behavior of different control strategies for this device was investigated. The main aims of the development were the disturbance compensation of the different disturbances as well as the improvement of the lambda control of an engine.

The first part of the work was the development of the model of an active gas dosing system. Resulting from the literature survey, the main model parts were chosen for a venturi mixer in combination with a butterfly valve. Between the venturi mixer and the butterfly valve a reservoir model was used in order to simulate the transport dynamics between these components. Additionally an air filter model was implemented to regard the dynamic of air filter losses at the air intake part. Furthermore, a mixture reservoir was modeled for the purpose of regarding the problem of emptying the intake manifold. The main difficulties with the implementation were the numerical stiffness which resulted from the dependence of the complete model on the engine mass flow. The model simulation time proved satisfactory.

The second part of the work dealt with the controller design as well as the comparison of different controller strategies. The linearization of the system was shown to be the key part of the controller design. The highly non-linear behavior of the model caused difficulties in the linearization of the model. It could be shown that using a model reduction as well as interpolation algorithms at the implementation of the controllers could improve the influences of the gain-scheduling. In addition the matrices of the controllers have been manipulated in order to compensate any remaining effects of the used gain-scheduling strategy.

The control strategies were divided into a part with and a part without a lambda value feed-back. It proved that the control strategies without lambda feed back can achieve a very good performance if the value of the stoichiometric air requirement is updated by

an update algorithm. Such an algorithm is also developed in this part of the work. The performances of all controllers were compared with a static venturi mixer approximation. In this approximation, the gas mass flow is calculated by the direct feedback of the engine mass flow. It could be shown that the performance of a combined control strategy is almost identical with the performance of the static venturi mixer approximation. Only the immeasurable disturbance of the calorific value led to a partly unstable behavior, when a step disturbance of 20% of the calorific value was applied to the system. All other disturbance ranges did not cause any instability.

Further investigations are needed for the linearized engine model, which is not satisfactory because it only depends on the angle of the shaft of the butterfly valve. The development of a characteristic diagram of the engine could result in a better performance as well as in a stabilization of the combined control in case of a calorific value change in the higher load level.

Because of the fact that this investigation was only theoretical, the system should be validated on a test bench. This will give further insights and can show which of the investigated strategies are also practical and useful for the implementation of a real system. Another case that was not investigated in this thesis are Bi-Fuel systems, which might be a topic for future research. Research in this field could pave the way for the development of new concepts for the gas market.

Bibliography

[1] *GTI*. Altronic Inc. http://www.gti-altronicinc.com/

[2] *GE J320 GS*. General Electrics. http://www.gejenbacher.com/

[3] *Air/Fuel Ratio Control for Stoichiometric and Lean-Burn Carbureted Engines*. Altronic Inc. http://www.altronicinc.com/

[4] *AF120*. Gill Instruments Ltd. http://www.gill.co.uk/

[5] *KRONOS 30*. Heinzmann GMBH&CoKG. http://www.heinzmann.com/

[6] *VM350*. Continental Controls Corporation. http://www.continentalcontrols.com/

[7] *PGC1000*. ABB Automation GmbH. http://www.abb.com/

[8] *BCP CH4*. Bluesens Gas Sensors GmbH. http://www.bluesens.com/

[9] *EnCal 3000*. Elster Instromet. http://www.elster-instromet.com/

[10] *Transmitter CC28*. GfG Gesellschaft für Gerätebau mbH. http://www.gasmessung.de/

[11] *TX6363*. Trolex. http://www.trolex.com/

[12] *Control Valve Handbook*. Emerson Process Management. http://www.emersonprocess.com/. Version: 4th edition

[13] *Valve Sizing - Technical Bulletin*. Swagelok Company. http://www.swagelok.com/

[14] *Q.Sonic*. Elster Instromet. http://www.elster-instromet.com/

[15] *RMG 980*. RMG Regel + Messtechnik GmbH. http://www.rmg.de/. Version: 1998

[16] *RMG 985*. RMG Regel + Messtechnik GmbH. http://www.rmg.de/. Version: 2001

[17] *ECV5*. Continental Controls Corporation. http://www.continentalcontrols.com/. Version: 2007

[18] *Data Sheet - Gasmischer*. Heinzmann GMBH&CoKG. http://www.heinzmann.de/. Version: 2007

[19] *Messprinzip Infrarot (IR).* GfG Gesellschaft für Gerätebau mbH. http://www.gasmessung.de/. Version: 2008

[20] *Product Catalog - Venturi Mixers.* Woodward Governor Company. http://www.woodward.com/. Version: Catalog 37404

[21] Eck, B.: *Technische Strömungslehre: Grundlagen.* Springer, 1988 (Technische Strömungslehre / Bruno Eck). – ISBN 978–3540187462

[22] Ganesan, V.: *Internal combustion engines.* McGraw-Hill, 1996. – ISBN 978–0074621226

[23] Guzzella, L. ; Onder, C.H.: *Introduction to modeling and control of internal combustion engine systems.* Springer, 2004. – ISBN 978–3540222743

[24] Hoinkis, J. ; Lindner, E.: *Chemie für Ingenieure.* 13th edition. Wiley-VCH Verlag GmbH, 2007. – ISBN 978–3527317981

[25] Papagiannakis R.G. ; Rakopoulos C.D. ; Hountalas D.T. ; Rakopoulos D.C.: Emission characteristics of high speed, dual fuel, compression ignition engine operating in a wide range of natural gas/diesel fuel proportions. In: *Fuel* 89 (2010), Nr. 7, S. 1397 – 1406. http://dx.doi.org/10.1016/j.fuel.2009.11.001. – DOI 10.1016/j.fuel.2009.11.001. – ISSN 0016–2361. – 17th International Symposium on Alcohol Fuels

[26] Papagiannakis R.G. ; Kotsiopoulos P.N. ; ZannisT.C. ; Yfantis E.A. ; Hountalas D.T. ; Rakopoulos C.D.: Theoretical study of the effects of engine parameters on performance and emissions of a pilot ignited natural gas diesel engine. In: *Energy* 35 (2010), Nr. 2, S. 1129 – 1138. http://dx.doi.org/10.1016/j.energy.2009.06.006. – DOI 10.1016/j.energy.2009.06.006. – ISSN 0360–5442. – ECOS 2008, 21st International Conference, on Efficiency, Cost, Optimization, Simulation and Environmental Impact of Energy Systems

[27] Stellwagen, K.: *Schwachgas Starkgas Mischung.* July 2000. – US Patent 6,092,364

[28] Adolf I.: *Fuel mixture control method for an internal combustion engine operated with gaseous fuel relies on an operating condition for mixing fuel in a gas-air Venturi mixer.* 2005. – Patent - DE10346983(A1)

[29] Ramaker, A.E.T.J. ; Wolters, L.: *Control system for supplying a gas flow to a gas consumption.* February 1995. – US Patent 5,388,607

[30] Daniel Rupp ; Lino Guzzella: Adaptive internal model control with application to fueling control. In: *Control Engineering Practice* (2010). http://dx.doi.org/10.1016/j.conengprac.2010.03.011. – DOI 10.1016/j.conengprac.2010.03.011. – ISSN 0967–0661

[31] Zhang, F. ; Grigoriadis, K.M. ; Franchek, M.A. ; Makki, I.H.: Linear Parameter-Varying Lean Burn Air-Fuel Ratio Control for a Spark Ignition Engine. In: *Journal of Dynamic Systems, Measurement, and Control* 129 (2007), Nr. 4, S. 404–414. http://dx.doi.org/10.1115/1.2745849. – DOI 10.1115/1.2745849

[32] Wiens, T. ; Burton, R. ; Schoenau, G. ; Sulatisky, M. ; Hill, S. ; Lung, B.: *Experimental Determination of Transport Delay in a Spark Ignition Engine.* Saskatchewan Research Council, Saskatoon, 2006. – Technical Report

[33] Yildiz, Y. ; Annaswamy, A. ; Yanakiev D. ; Kolmanovsky I.: Spark ignition engine fuel-to-air ratio control: An adaptive control approach. In: *Control Engineering Practice* 18 (2010), Nr. 12, S. 1369 – 1378. http://dx.doi.org/10.1016/j.conengprac.2010.06.011. – DOI 10.1016/j.conengprac.2010.06.011. – ISSN 0967–0661

[34] Gerber, Mandy: *Ganzheitliche stoffliche und energetische Modellierung des Biogasbildungsprozesses*, Ruhr-Universität Bochum, PhD Thesis, 2009

[35] Röth, Jens Adrian: *Untersuchung und Modellierung der optimalen Warmlaufstrategie eines monovalenten Erdgasmotors mit Turbolader*, ETH Zürich, PhD Thesis, 2009

[36] Anil, T.R. ; Ravi, S.D. ; Shashikanth, M. ; Tewari, P.G. ; Rajan, N.K.S.: CFD Analysis of a Mixture Flow in a Producer Gas Carburetor. In: *International Conference On Computational Fluid Dynamics, Acoustics, Heat Transfer and Electromagnetics CFEMATCON-06*, 2006

[37] Diego A. Arias ; Timothy A. Shedd: CFD Analysis of Compressible Flow Across a Complex Geometry Venturi. In: *Journal of Fluids Engineering* 129 (2007), Nr. 9, S. 1193–1202. http://dx.doi.org/10.1115/1.2754321. – DOI 10.1115/1.2754321

[38] Kenneth C. Cornelius ; Kartik Srinivas: Isentropic Compressible Flow for Non-Ideal Gas Models for a Venturi. In: *Journal of Fluids Engineering* 126 (2004), Nr. 2, S. 238–244. http://dx.doi.org/10.1115/1.1677499. – DOI 10.1115/1.1677499

[39] Friedemann Z. ; Weickel H.: *Venturi-Mischer zum Mischen von Gas und Luft-insbesondere fuer einen Verbrennungsmotor.* 1993. – Patent DE-4137573

[40] Vinayl, S.S. ; Ravi, S.D. ; PremaKumar, G. ; Rajan, N.K.S.: Numerical and Experimental Modeling of Producer Gas Carburettor. In: *Advances in Mechanical Engineering*, Proc. of the International Conference on, 2008

[41] Kastner, J.F. ; Halm, M.: Fachberichte-Echtzeit-Gasbeschaffenheitsmessung auf Basis von optischen und thermischen Gaseigenschaften. In: *Gas Wärme International* 55 (2006), Nr. 4, S. 251–254. – ISSN 0020–9384

[42] Puente, D. ; Gracia, F.J. ; Ayerdi, I.: Thermal conductivity microsensor to measure the methane number of natural gas. In: *Electron Devices, Spanish Conference*, 2005, S. 499 –502

[43] Udina S. ; Carmona M. ; Carles G.; Santander J. ; Fonseca L. ; Marco S.: A micromachined thermoelectric sensor for natural gas analysis: Thermal model and experimental results. In: *Sensors and Actuators B: Chemical* 134 (2008), Nr. 2, S. 551 – 558. `http://dx.doi.org/10.1016/j.snb.2008.05.043`. – DOI 10.1016/j.snb.2008.05.043. – ISSN 0925–4005

[44] Aono, T. ; Kowatari, T.: Throttle-control algorithm for improving engine response based on air-intake model and throttle-response model. In: *Industrial Electronics, IEEE Transactions on* 53 (2006), June, Nr. 3, S. 915 – 921. `http://dx.doi.org/10.1109/TIE.2006.874263`. – DOI 10.1109/TIE.2006.874263. – ISSN 0278–0046

[45] Gagner, J. ; Bondesson, R.: *Adaptive Realtime Control of a Nonlinear Throttle Unit*. Lund Institute of Technology, Department of Automatic Control, 2000 `http://www.control.lth.se/`. ISSN 0280–5316

[46] Horn, M. ; Schriebl, M. ; Unger, E. ; Dourdoumas, N.: Konzept zur digitalen Lageregelung von Drosselklappen bei Ottomotoren. In: *International Journal Automation Austria* 11 (2003), S. 90–103

[47] Hammer, E.A.: Flare gas metering and high pressure gas metering using ultrasonic sensors. In: *Ultrasound in the Process Industry, IEE Colloquium on*, 1993, S. 8/1 –8/4

[48] Kashiha, M.A. ; Jamshidi, D.: Developing a method for optical gas flow metering based on laser light scattering theory. In: *Power Electronics and Intelligent Transportation System (PEITS), 2009 2nd International Conference on* Bd. 1 IEEE, 2009, S. 116 –120

[49] Kawai, K.: *Butterfly valve having a function for measuring a flow rate and method of measuring a flow rate with a butterfly valve*. May 1990. – US Patent 4,926,903

[50] Idelchik, I.E.: *Handbook of hydraulic resistance*. Begell House, Redding, CT, USA, 1994. – ISBN 978–1567000740

[51] Kaidantzis, P. ; Rasmussen, P. ; Jensen, M. ; Vesterholm, T. ; Hendricks, E.: Robust, self-calibrating lambda feedback for SI engines. In: *SAE International* (1993). `http://dx.doi.org/10.4271/930860`. – DOI 10.4271/930860

[52] Lueptow, R.M. ; Phillips, S. ; Oczkowski, M.: Acoustic natural gas fuel quality sensor. In: *SAE International* (1995). `http://dx.doi.org/10.4271/950529`. – DOI 10.4271/950529

[53] Nakagawa, K. ; Okamoto, K. ; Shoji, F.: Development of an air/fuel ratio control system for lean burn gas engines. In: *SAE Special Publication* (1994). `http://dx.doi.org/10.4271/942041`. – DOI 10.4271/942041

[54] Schneider, W.: *Repetitorium Thermodynamik*. Oldenbourg, 2004. – ISBN 978–3486576146

[55] Skorjanz, Peter: *Physikalische Modellierung eines Großgasmotors und regelungstechnische Anwendungen*, Vienna University of Technology, PhD Thesis, 2001

[56] Sugiura, M. ; Okazaki, I. ; Saikalis, G.: Hot wire mass gas flow sensing device. In: *SAE International* (1994). `http://dx.doi.org/10.4271/940625`. – DOI 10.4271/940625

Appendix A

Nomenclature

a	Speed of Sound
$\boldsymbol{A}$	State-Stace Matrix A
A	General Cross Sectional Area Downstream
A_{AP}	Cross Sectional Area of the Annular Passage
A_{eff}	Effective Aperture of the Butterfly Valve
A_{filter}	Cross Sectional Area of the Air Filter
A_m	Cross Sectional Area at the Throat
A_u	General Cross Sectional Area Upstream
α_{AP}	Gap of the Annular Passage
α_{BV}	Set Angle of the Shaft of the Butterfly Valve
$\alpha_{BV,act}$	Actual Angle of the Shaft of the Butterfly Valve
$\boldsymbol{B}$	State-Stace Matrix B
$\beta\,(\Pi)$	Flow Rate Function
$\boldsymbol{C}$	State-Stace Matrix C
C	Element Carbon
CH_4	Chemical Structure of Methane
CO_2	Chemical Structure of Carbon Dioxide
$c_{p,air}$	Isobaric Specific Heat Capacity of Air
$c_{p,gas}$	Isobaric Specific Heat Capacity of Natural Gas

$c_{p,biogas}$	Isobaric Specific Heat Capacity of Biogas
c_p	General Isobaric Specific Heat Capacity
$c_{p,mix}$	Isobaric Specific Heat Capacity of the Mixture
$c_{v,R}$	Isochoric Specific Heat Capacity of the Wall
c_v	General Isochoric Specific Heat Capacity
$c_{v,air}$	Isochoric Specific Heat Capacity of Air
$c_{v,gas}$	Isochoric Specific Heat Capacity of Natural Gas
$c_{v,biogas}$	Isochoric Specific Heat Capacity of Biogas
c_{Wall}	Heat Capacity of the Wall
$\boldsymbol{D}$	State-Stace Matrix D
$\emptyset D_0$	Diameter of the Air Supply Pipe
$\emptyset D_G$	Diameter of the Gas Supply Pipe
$\emptyset D_{m0}$	Diameter of the Throat
$\emptyset D_z$	Diameter of the Zeppelin (Middle Venturi Part)
E	Control Error
E_{in}	General Energy Input
E_{out}	General Energy Output
η_{eng}	Efficiency of the Engine
$G(s)$	Transfer Function
H	Element Hydrogen
H_2O	Chemical Structure of Water
h_d	Enthalpy of a Fluid Downstream
h_u	Enthalpy of a Fluid Upstream
$H_{i,gas}$	Calorific Value of Natural Gas
$H_{i,biogas}$	Calorific Value of Biogas
κ	General Ratio of Specific Heats
κ_{air}	Ratio of Specific Heats of Air

κ_{biogas}	Ratio of Specific Heats of Biogas
κ_{gas}	Ratio of Specific Heats of Natural Gas
κ_{mix}	Ratio of Specific Heats of the Mixture
L_{st}	Variable Stoichiometric Air Requirement
$L_{st,eng}$	Stoichiometric Air Requirement assumed in the Engine
$L_{st,Methane}$	Stoichiometric Air Requirement of Methane
$L_{st,NG}$	Stoichiometric Air Requirement of Natural Gas
λ	Air/Fuel Ratio
λ_{BV}	Calculated Air/Fuel Ratio of the Ratio Control Strategy
M	Mach Number
$\dot{m}$	General Mass Flow
$\dot{m}_{air}$	Air Mass Flow
$\dot{m}_{air,st}$	Needed Air Mass Flow for a Stoichiometric Combustion
$\dot{m}_{air,venturi}$	Air Mass Flow Across the Venturi Mixer
$\dot{m}_d$	Mass Flow Downstream
$\dot{m}_{Exhaust}$	Exhaust Mass Flow
$\dot{m}_{gas}$	Gas Mass Flow Across the Butterfly Valve
$\dot{m}_{gas,set}$	Set Point of the Gas Mass Flow
$\dot{m}_{gas,venturi}$	Gas Mass Flow Across the Annular Passage
$\dot{m}_{GM}$	Mixture Mass Flow Across the Venturi Mixer
$\dot{m}_i$	Mass Flow of Fluid i
$\dot{m}_{IN}$	Input Mass Flow of the Reservoir
$\dot{m}_{OUT}$	Output Mass Flow of the Reservoir
$\dot{m}_u$	Mass Flow Upstream
m_R	Mass of the Fluid in the Reservoir
m_{Wall}	Mass of the Wall
$\frac{dm}{dt}$	Change Rate of the Mass

$\mathcal{M}_{air}$	Molar Mass of the Air
$\mathcal{M}_{CH_4}$	Molar Mass of Methane
$\mathcal{M}_{gas}$	Molar Mass of the Gas
$\mathcal{M}_{mix}$	Molar Mass of the Mixture
$\mathcal{M}_{O_2}$	Molar Mass of Dioxygen
n	Engine Speed
$\mathcal{N}_G$	Avogadro Constant
O	Element Oxygen
O_2	Chemical Structure of Dioxygen
p_t	Total Pressure of a Fluid
$p_{0,t}$	Total Pressure of the Air at State 0
p_1	Static Pressure at State 1
$p_{1,t}$	Total Pressure at State 1
p_2	Pressure at the State 2
p_d	Pressure Downstream
$p_{G,t}$	Total Pressure in the Gas Reservoir
p_R	Static Pressure in the Reservoir
P_t	General Power
p_u	Pressure Upstream
$p_{u,t}$	Total Pressure Upstream
Δp_{filter}	Pressure Difference at the Air Filter
$\Delta p_{venturi}$	Pressure Difference Across the Venturi Mixer
Π	Pressure Difference of the Flow Rate Function
$\dot{Q}$	General Heat Flow
$\mathcal{R}$	Universal Gas Constant
R_s	Specific Gas Constant
$R_{s,air}$	Specific Gas Constant of Air

$R_{s,biogas}$	Specific Gas Constant of Biogas
$R_{s,gas}$	Specific Gas Constant of Natural Gas
$R_{s,mix}$	Specific Gas Constant of the Mixture
ρ	General Density of the a Fluid
ρ_0	Density of the Air at the State 0
ρ_1	Density at the Air at the State 1
ρ_{air}	Density of Air
ρ_{biogas}	Density of Biogas
ρ_d	Density of the Fluid Downstream
$\rho_{Exhaust}$	Density of the Exhaust
ρ_{gas}	Density of Natural Gas
ρ_i	General Density of Fluid i
ρ_u	Density of the Fluid Upstream
T	General Temperature of the Fluid
T_t	General Total Temperature of a Fluid
$T_{0,t}$	Total Temperature of the Air at State 0
T_1	Temperature at the State 1
$T_{1,t}$	Total Temperature at the State 1
T_d	Temperature Downstream
T_{dead}	Dead Time of the Lambda Value
T_G	Temperature in the Gas Reservoir
$T_{G,t}$	Total Temperature in the Gas Reservoir
T_{G0}	Temperature in the Gas Supply Pipe
$T_{G0,t}$	Total Temperature in the Gas Supply Pipe
$T_{IN,t}$	Total Temperature of the Fluid into the Reservoir
$T_{m,air}$	Temperature of the Air at the Throat
$T_{m,gas}$	Temperature of the Gas at the Throat

$T_{m,mix}$	Temperature of the Mixture at the Throat
T_R	Static Temperature in the Reservoir
$T_{R,t}$	Total Temperature in the Reservoir
T_u	Temperature Upstream
$T_{u,t}$	Total Temperature Upstream
$\dot{T}_{R,t}$	Total Temperature Change in the Reservoir
$\tau_{Lambda-Sensor}$	Time Constant of the Lambda Sensor
u	Inner Energy
u_d	Inner Energy of the Fluid Downstream
u_u	Inner Energy of the Fluid Upstream
u	Atomic Mass - Exception valid for equation (2.17) and (2.18)
$\frac{dU}{dt}$	Change Rate of the Inner Energy
v	General Velocity of the Fluid
v_d	General Velocity of the Fluid Downstream
v_{filter}	Middle Velocity Across the Air Filter
v_m	Velocity of the Fluid at the Throat
v_u	General Velocity of the Fluid Upstream
$V_{Exhaust\ Manifold}$	Volume of the Exhaust Manifold
V_i	General Volume
$V_{Intake\ Manifold}$	Volume of the Intake Manifold
V_R	Volume of the Reservoir
x	Oxygen needed for a Complete Combustion of Methane
x_{gas}	Mass Fraction of Methane in the Gas
y_{air}	Molar Fraction of the Air
y_{gas}	Molar Fraction of the Gas
y_i	Molar Fraction of the Component i
Y_A	Auxiliary manipulated variable

Y_A^*	Auxiliary manipulated variable without dead time
ζ_{filter}	Variable Resistance Coefficient of the Air Filter
$\zeta_{venturi}$	Variable Resistance Coefficient of the Venturi Mixer

Shortcuts

AP	Annular Passage
BV	Butterfly Valve
CFD	Computational Fluid Dynamics
CNG	Compressed Natural Gas
CSA	Cross Sectional Area
FF	Feed Forward
FRF	Flow Rate Function
GC	Gas Mass Flow Calculation
LFG	Landfill Gas
LPV	Linear Parameter Varying
LTI	Linear Time Invariant
$MAT\ Sensor$	Manifold Temperature Sensor
MFG	Mass Flow Giving
MN	Mach Number
OP	Operation Point
PG	Pressure Giving
$PT1 - Element$	First-Order Lag Element
$PI - Structure$	Proportional-Integral Controller Structure
$PID - Structure$	Proportional–Integral–Derivative Controller Structure
$PIDT1 - Structure$	Proportional–Integral–Derivative Controller Structure with Additional Filter Structure
SB	Simulation Block

SC	Speed Controller
$SI - Units$	International System of Units
$SISOTOOL$	Toolbox in Matlab for the Design of Single Input Single Output Controllers
SO	State-Observer
SS	State-Space
$UEGO\ Sensor$	Universal Exhaust Gas Oxygen Sensor

Appendix B

Simulink Model

In the following, the screenshots of the Simulink model are depicted. This should support the understanding of the tutorials as well as the file list.

The first four figures are the overview of the model. The part of the model can be identified with the grey boxes in the left upper corner of the figure. Figures five and six show the submodels of the gas dosing system block in the overview. The figures are signed with the small gas dosing system symbol in the grey boxes. The last figure shows the submodels of the venturi mixer, which can be identified by the venturi mixer symbol in the grey box.

Figure Overview

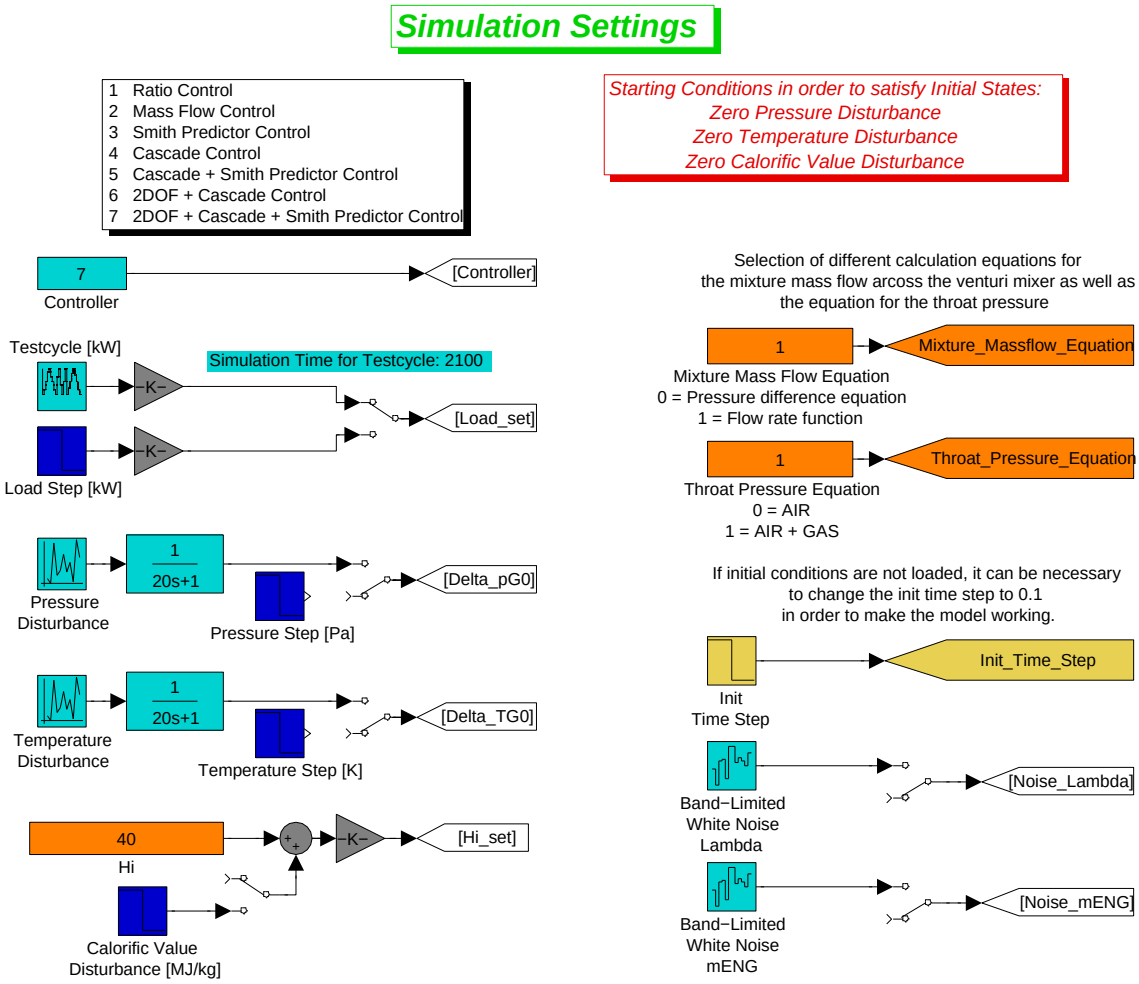

Figure B.1: Simulink Model Overview - Part 1

Figure Overview

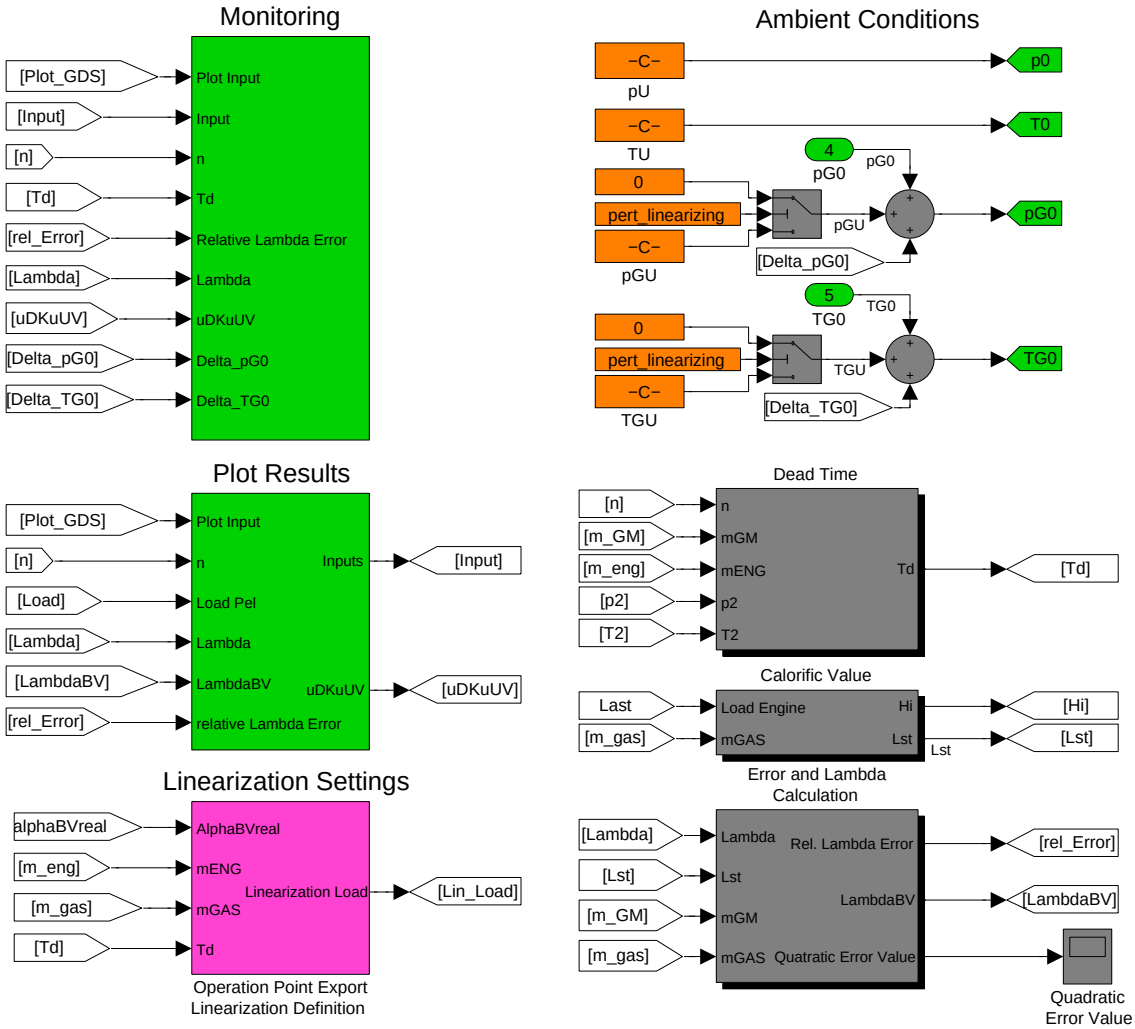

Figure B.2: Simulink Model Overview - Part 2

Figure Overview

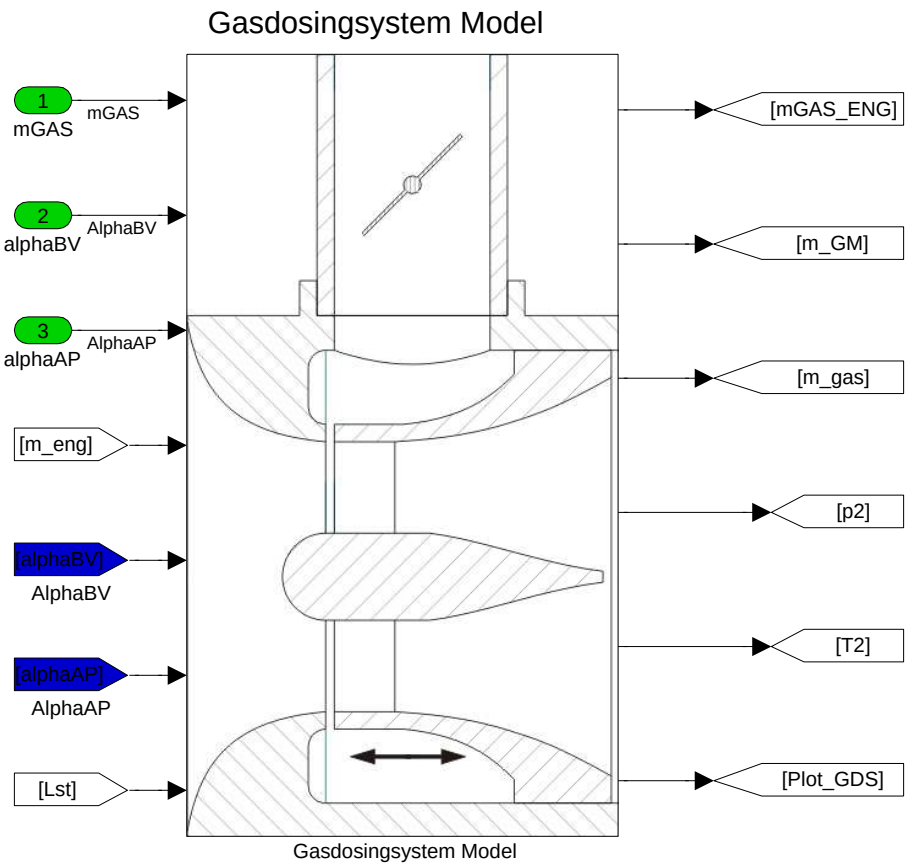

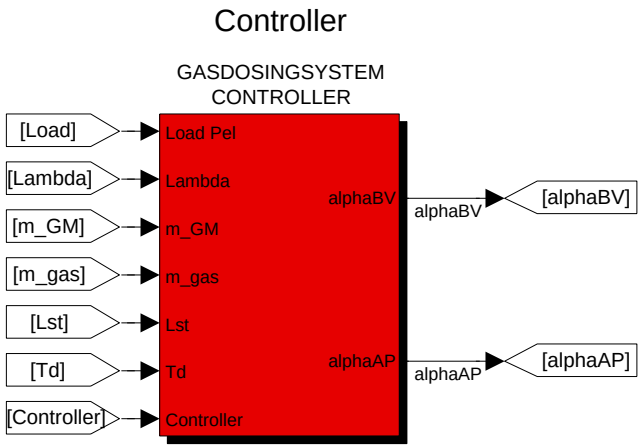

Figure B.3: Simulink Model Overview - Part 3

Figure Overview

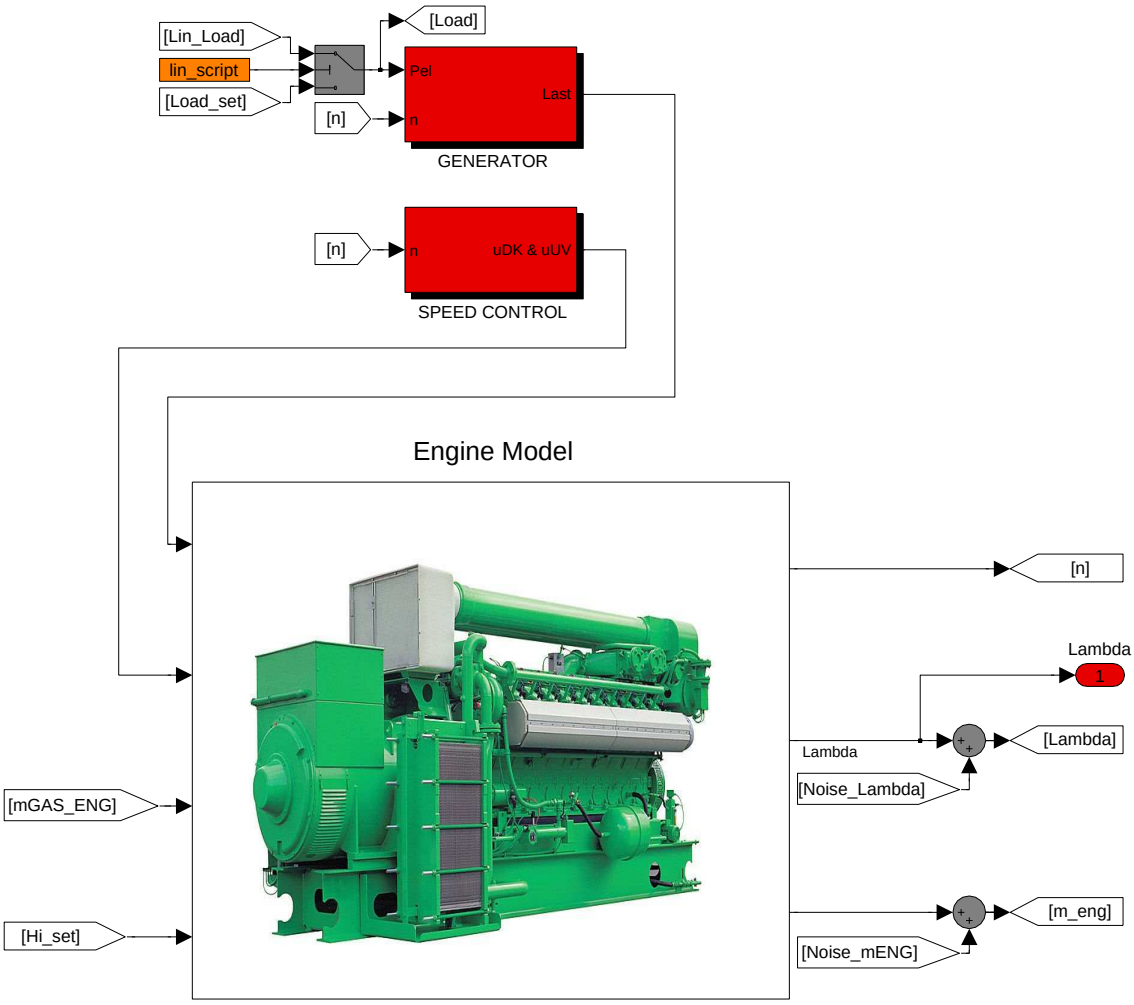

Figure B.4: Simulink Model Overview - Part 4

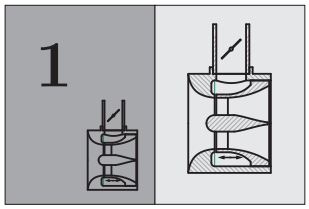

Figure Overview

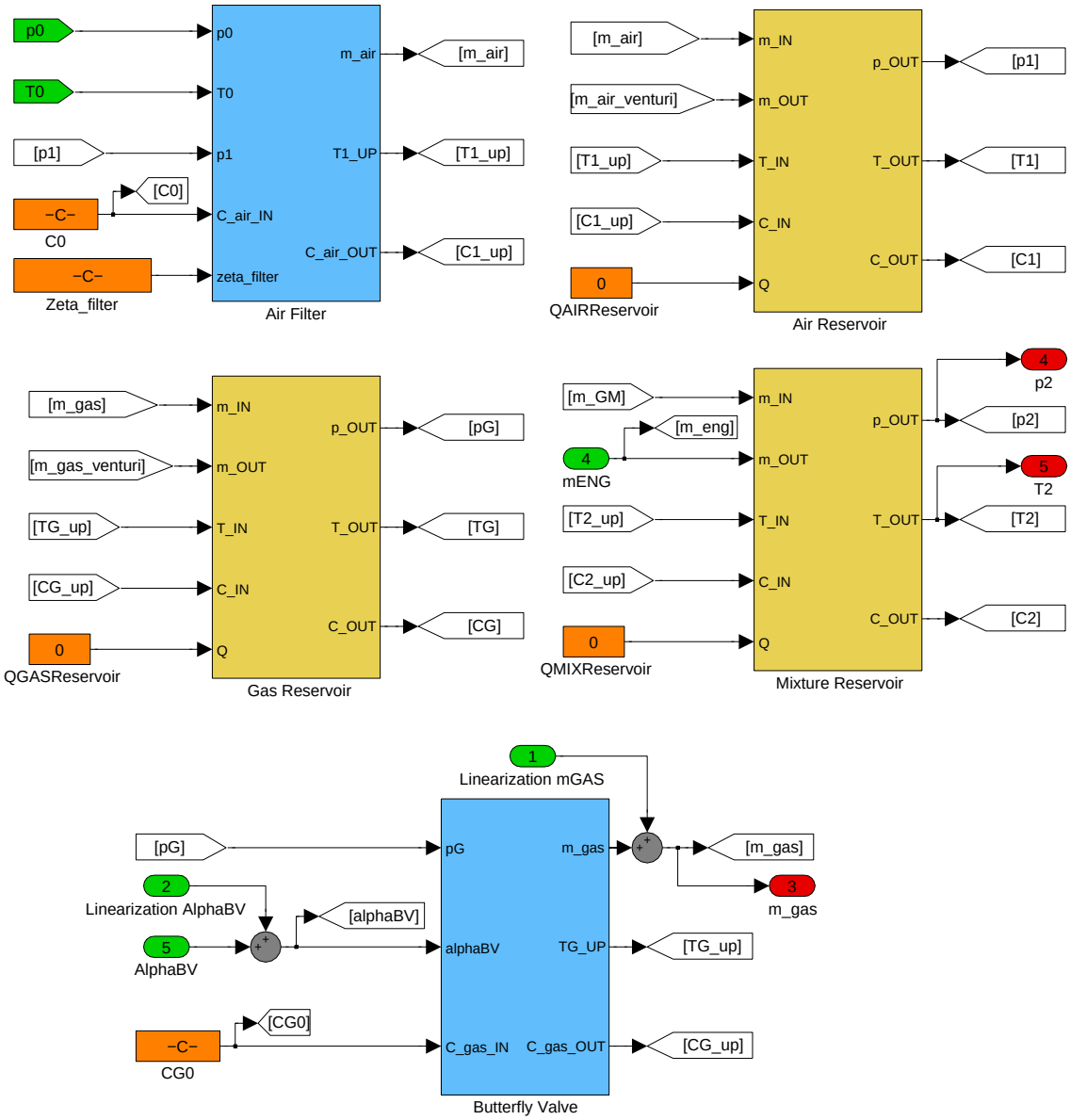

Figure B.5: Gas Dosing System Model Block - Part 1

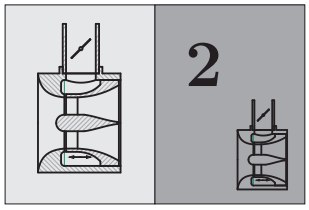

Figure Overview

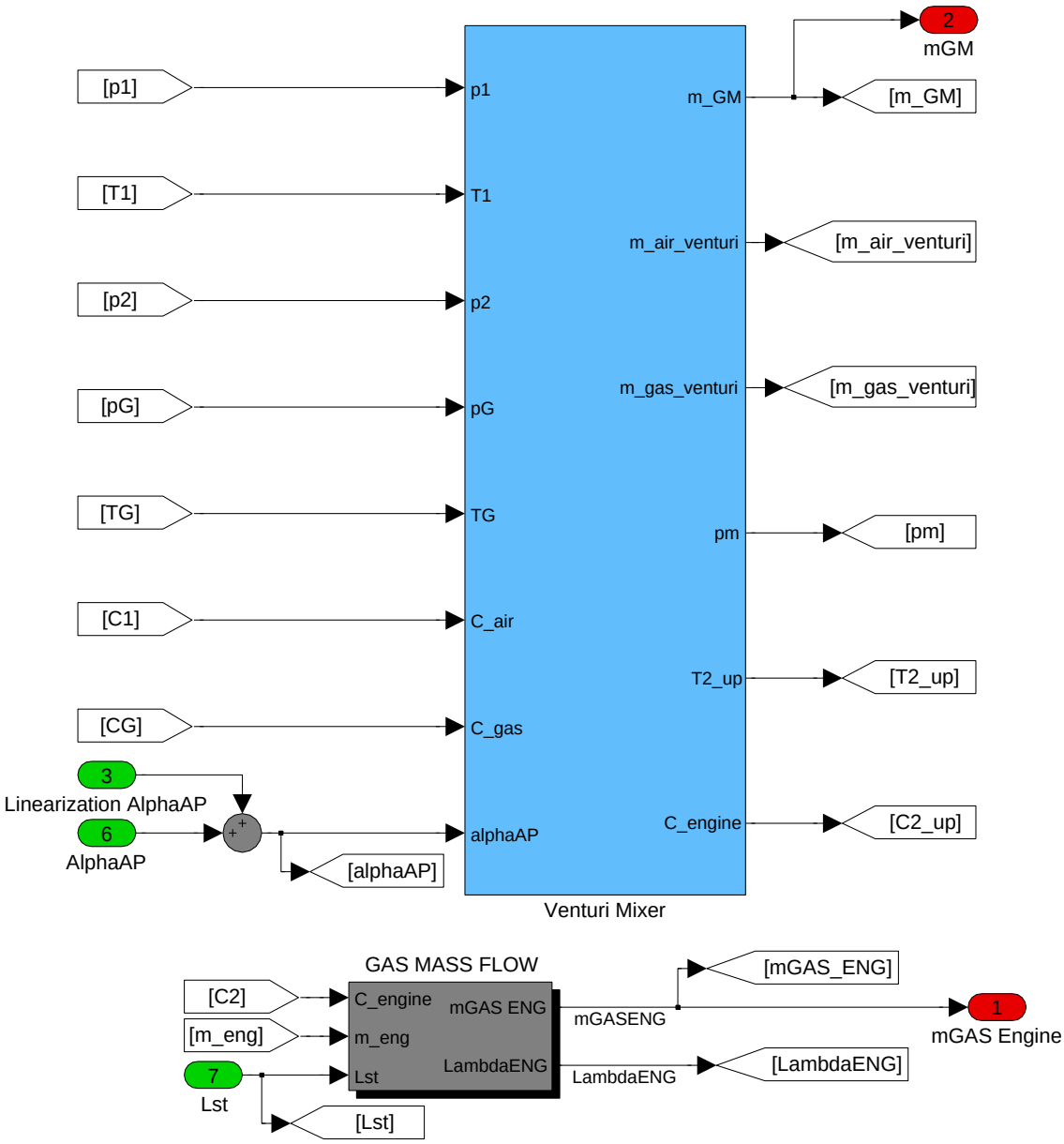

Figure B.6: Gas Dosing System Model Block - Part 2

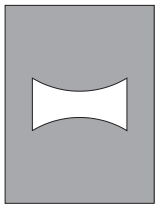

Figure Overview

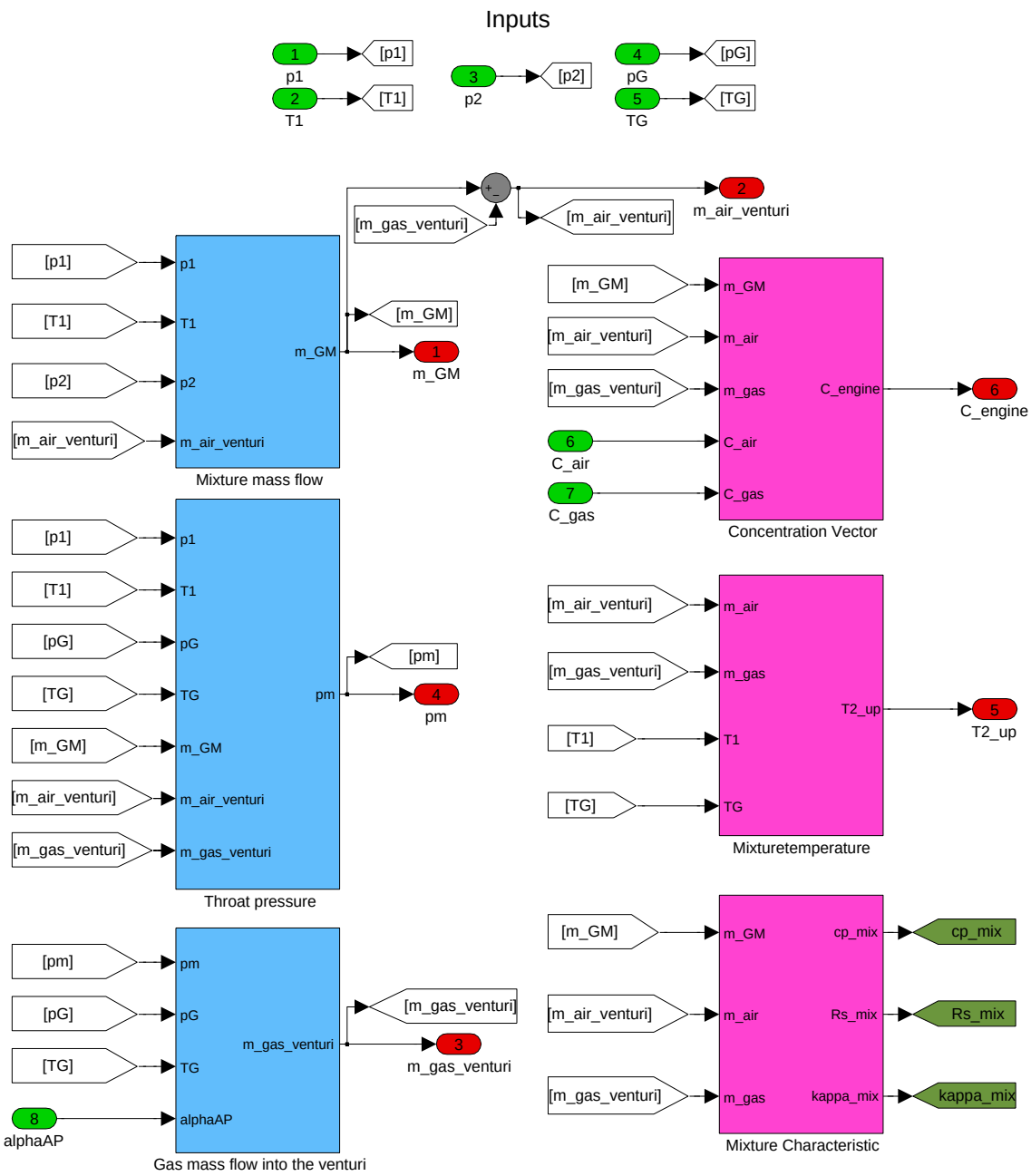

Figure B.7: Venturi Mixer Simulink Model Block